INSTABILITY AND RETREAT OF A LAKE-CALVING TERMINUS, MENDENHALL GLACIER, SOUTHEAST ALASKA

By

Eleanor Boyce

RECOMMENDED:

_____

_____

_____

Advisory Committee Chair

_____

Chair, Department of Geology and Geophysics

APPROVED:

_____

Dean, College of Natural Science and Mathematics

_____

Dean of the Graduate School

_____

Date

INSTABILITY AND RETREAT OF A LAKE-CALVING TERMINUS, MENDENHALL GLACIER, SOUTHEAST ALASKA

A

THESIS

Presented to the Faculty

of the University of Alaska Fairbanks

in Partial Fulfillment of the Requirements

for the Degree of

MASTER OF SCIENCE

By

Eleanor Boyce, B.A.

Fairbanks, Alaska

May 2006

Abstract

Mendenhall Glacier is a lake-calving glacier in southeastern Alaska that is experiencing substantial thinning and increasingly rapid recession. Long-term mass wastage linked to climatic trends is responsible for thinning of the lower glacier and leaving the terminus vulnerable to buoyancy-driven calving and accelerated retreat. Bedrock topography may play a role in stabilizing the terminus between periods of rapid calving and retreat. Lake-terminating glaciers form a population distinct from both tidewater glaciers and polar ice tongues, with some similarities to both groups. Lacustrine termini experience fewer perturbations (e.g. tidal flexure, high subaqueous melt rates) and are therefore inherently more stable than tidewater termini. At Mendenhall, rapid thinning and simultaneous retreat into a deeper basin led to floatation conditions along approximately 50% of the calving front. This unstable terminus geometry lasted for $\sim$ 2 years and culminated in large-scale calving and terminus collapse during summer 2004. We used a 1-dimensional viscoelastic model to investigate the transient response of a floating glacier tongue to buoyant forcing. Results suggest that creep may be capable of accommodating buoyant torque if it is applied gradually. As unresolved bending stresses approach the tensile strength of ice, small rapidly applied perturbations may cause buoyancy-driven calving.

Table of Contents

List of Figures

List of Tables

List of Other Materials

List of Appendices

Acknowledgements

Not everyone is given a chance to research fascinating things in their backyard, so I feel lucky to have had the opportunity to work on Mendenhall Glacier for the past three years. This research was inspired by my graduate advisor, Roman Motyka, who deserves credit for providing support and constructive criticism throughout the study (after convincing me there was more to look at on Mendenhall than mass balance). I thank him also for opportunities to haul batteries around in some amazing parts of Alaska. Martin Truffer and Keith Echelmeyer have been an excellent advisory committee, although they could have warned me about the slippery slope of modeling. Martin shared not only his experience but his view of the Alaska Range during my first year here.

This project owes a great deal to Ed Bueler, who spent extra time helping with my numerical analysis project to try and turn it into a useful model. Somewhere there is an ideal lake-calving glacier that will suit that model. Others at the Geophysical Institute who have contributed to this research are Sandy Zirnheld, By Valentine, Chris Larsen, Anupma Prakash, and Miho Aoki. Thanks to Larry Musarra, the Mendenhall Glacier Visitor Center, and Northstar Trekking for sharing their glacier observations and assisting fieldwork. A group of people at the University of Alaska Southeast has been involved in Mendenhall Glacier fieldwork, some for longer than I have. Thanks to Cathy Connor, Matt Heavner, Mike Hekkers, Eran Hood, Adam Bucki and the Geology 315 class in spring 2004 for help with fieldwork and sharing the experience of magnetometer surveys.

Thanks to friends, fellow grad students and glaciers lab crowd for entertainment and encouragement along the way: Anthony, Jason, Elsbeth, Sandy, Brent, Dana, Inari, Tinu, Leslie, Tanja, Sharon, Lars and the Belfairians. Special thanks to Andy for sharing my belief that somehow things usually work out well; I'm looking forward to some fun adventures together. Finally, I feel I should thank my dad for his memorable advice on finishing a thesis (although I haven't taken it, obviously): "The problem with computer files is they just don't burn well."

Chapter 1
Introduction

1.1 Background

It is not uncommon for proglacial lakes to form at the termini of glaciers as they retreat into overdeepened channels formed by glacier erosion. The number of lake-calving glaciers is in constant flux as glaciers transition from land- to lake-terminating and back. A study measuring the recent thinning of 65 Alaskan Glaciers included 5 lake-calving and 15 tidewater calving glaciers [Arendt et al., 2002]. Of the calving glaciers of Patagonia, there are more than twice as many lacustrine termini as tidewater termini [Warren and Aniya, 1999]. Tidewater-calving glaciers have received much attention since they may undergo rapid calving retreat. Lake-calving glaciers have been far less studied, although their behavior is in some ways quite different than that of tidewater glaciers. On a scale from land-terminating glaciers to tidewater glaciers, lake-calving glaciers fall somewhere in the middle. Exactly where in the middle depends on the role that calving plays for the particular glacier. Calving glaciers are sensitive to many factors including ice flux into the terminus, water depth, ice thickness, channel geometry, subaqueous melting, and the presence of a moraine shoal in front of the calving front. Because it is difficult to make generalizations about the behavior of calving glaciers, Warren and Aniya [1999] stress the importance of conducting detailed case studies. This is essential since the link between glacier thinning/retreat and climate is complicated for glaciers that lose mass through calving [Arendt et al., 2006; Larsen et al., to be submitted]. Accelerated retreat and thinning of lacustrine termini is not necessarily representative of other (calving and non-calving) glaciers nearby.

This thesis presents a detailed case study of lake-calving Mendenhall Glacier, a maritime valley glacier located in southeastern Alaska. Since the end of the Little Ice Age, this glacier has undergone dramatic retreat. In the early 20^{th} century, Mendenhall Lake began to form in conjunction with terminus retreat. Such a transition can have huge implications for the rate of retreat, since calving can be a much more efficient mechanism than surface ablation for removing ice at the terminus. Periods of rapid retreat during the last century have indeed been linked to periods of increased calving. However, the glacier has also experienced substantial thinning which is attributed to negative mass balances due to climate change. When compared to the volume of ice lost by ablation, calving is a minor

fraction of the total mass loss.

1.2 Research Questions and Motivation

The focus of this study has been the terminus dynamics of Mendenhall Glacier, within the larger context of glacier-wide behavior, between the years 2000 and 2005. Of particular interest are change in terminus geometry, ice flow and calving rate. Mass balance, velocity and terminus position data have been collected at Mendenhall Glacier since completion of a study by Motyka et al. [2002]. The motivation for this current study began between 2000 and 2003 when R. J. Motyka observed significant changes in the geometry of the lake-calving terminus, including upwarping of the ice tongue. Earlier work concluded that the terminus was particularly vulnerable to calving as ice thicknesses approached floatation and the terminus retreated into an overdeepening [Motyka et al., 2002].

In 2004, the terminus of Mendenhall Glacier retreated over 200 m in a series of large calving events. The nature of the events suggested a buoyancy-driven calving mechanism, such as the theory developed by Warren et al. [2001]. Thinning of the terminus to floatation thickness subjects ice to buoyant (upward) forces. If bending stresses are not accommodated by deformation (ice creep), calving may occur. Bending stresses may also result in upwarping of a floating ice tongue, which was observed at Mendenhall in the two years prior to eventual breakup. This is somewhat surprising, since it is thought that temperate (0 °C) tidewater glaciers are unable to sustain floating termini [Meier and Post, 1987]. Despite apparent vulnerability, the glacier was temporarily stable between 2002 and 2004.

These observations motivate another research question: under what circumstances is a temperate lake-calving glacier able to sustain a floating tongue? Also, what factors trigger its eventual breakup? These questions will be answered by modeling how a viscoelastic glacier tongue deforms under buoyant load. A 1-dimensional viscoelastic model is used to determine the deflection and bending stress in a floating glacier tongue. The model is simplified and its goal is to investigate the underlying mechanism that could allow a floating temperate terminus to be sustained. Different perturbations to the floating ice are considered, including annual cycles in water level and ice thickness.

Mendenhall Glacier has provided a slow-motion picture of the factors affecting a calv-

ing front, including accumulated stresses leading to deformation of the terminus, and eventual failure through large-scale (relative to the size of the glacier) calving events. This story is synthesized from a diverse assortment of data, which includes (often incomplete) records of surface mass balance, velocity, aerial and ground-based photography, remote sensing, lake level and temperature, local weather conditions at the glacier terminus, glacier surface surveys, lake bathymetry and more.

1.3 Content of Thesis

Chapter 2 is a paper co-authored with Roman Motyka and Martin Truffer (UAF Geophysical Institute) that will be submitted to the Journal of Glaciology. Ed Bueler (UAF Department of Mathematics and Statistics) assisted in developing the numerical model which is summarized in this paper and is the subject of Chapter 3). Chapter 2 concentrates on the recent terminus dynamics of Mendenhall Glacier. In particular, we focus on changes in the eastern lake-calving terminus leading to its breakup in summer 2004. We determine how various factors control terminus behavior, and how glacier-wide changes are affecting the terminus. A conceptual model discusses how buoyant upwarping of a partially floating terminus may be temporarily stable but gradually approach the point of instability. We speculate on specific triggers for large-scale calving events during summer 2004.

Chapter 3 contains unpublished work developed with Ed Bueler, initially for a Continuum Numerical Analysis course project. The original goal of the project was to reproduce the 1-dimensional viscoelastic tidal flexure model developed by Reeh et al. [2003], using a different numerical model. Ed Bueler developed this working numerical method to solve the tidal flexure case, which looks at a transverse profile of a floating glacier tongue. We use the same bending beam equations and ice rheology as Reeh et al. [2003] to evaluate the response of a floating ice tongue in the longitudinal direction. The goal is to investigate the mechanism of buoyant upwarping for a hypothetical floating ice tongue, ignoring the effect of bed and margins. We wish to determine how quickly bending stresses are relaxed by ice creep, and when they exceed the tensile strength of ice. We find that two factors are of particular importance: first, the rheology of the ice at a particular temperature and stress state, and second, the rate at which buoyant stresses are applied. Buoyant stresses are caused by perturbations from hydrostatic equilibrium, including changes in

ice thickness and changes in water depth.

The appendices contain supplementary material which could not be incorporated into Chapters 2 or 3 for space considerations, but may be useful for future studies. Appendix A contains survey data collected on Mendenhall Glacier between 2000 and 2005. Appendix B contains scripts used to solve the numerical model in Chapter 3. Appendix C describes the data contained on the enclosed CD.

1.4 References

Arendt, A., K. Echelmeyer, W. Harrison, C. Lingle, and V. Valentine (2002), Rapid wastage of Alaska glaciers and their contribution to rising sea level, Science, 297, 382–386.

Arendt, A. A., K. A. Echelmeyer, W. Harrison, C. Lingle, S. Zirnheld, V. Valentine, B. Ritchie, and M. Druckenmiller (2006), Updated estimates of glacier volume changes in the western chugach Mountains, Alaska, USA and a comparison of regional extrapolation methods, Journal of Geophysical Research, in press.

Larsen, C. F., R. J. Motyka, A. A. Arendt, K. A. Echelmeyer, and P. E. Geissler (to be submitted), Glacier changes in southeast Alaska and contribution to sea level rise, Journal of Geophysical Research, Earth Surface Processes.

Meier, M. F., and A. Post (1987), Fast tidewater glaciers, Journal of Geophysical Research, 92(B9), 9051–9058.

Motyka, R., S. O'Neel, C. Connor, and K. Echelmeyer (2002), Twentieth century thinning of Mendenhall Glacier, Alaska, and its relationship to climate, lake calving, and glacier run-off, Global and Planetary Change, 35, 93–112.

Reeh, N., E. Christensen, C. Mayer, and O. Olesen (2003), Tidal bending of glaciers: a linear viscoelastic approach, Annals of Glaciology, 37, 83–89.

Warren, C., and M. Aniya (1999), The calving glaciers of southern South America, Global and Planetary Change, 22, 59–77.

Warren, C., D. Benn, V. Winchester, and S. Harrison (2001), Buoyancy-driven lacustrine calving, Glaciar Nef, Chilean Patagonia, Journal of Glaciology, 47(156), 135–146.

Chapter 2
Floatation and Retreat of a Lake-Calving Terminus, Mendenhall Glacier, Southeast Alaska[1]

2.1 Abstract

Mendenhall Glacier is a lake-calving glacier in southeastern Alaska that is experiencing substantial thinning and increasingly rapid recession. Long-term mass wastage linked to climatic trends is responsible for thinning of the lower glacier and leaving the terminus vulnerable to buoyancy-driven calving and accelerated retreat. Bedrock topography may play a role in stabilizing the terminus between periods of rapid calving and retreat. Lake-terminating glaciers form a population distinct from both tidewater glaciers and polar ice tongues, with some similarities to both groups. Lacustrine termini experience fewer perturbations (e.g. tidal flexure, high subaqueous melt rates) and are therefore inherently more stable than tidewater termini. At Mendenhall, rapid thinning and simultaneous retreat into a deeper basin led to floatation conditions along approximately 50% of the calving front. This unstable terminus geometry lasted for $\sim$ 2 years and culminated in large-scale calving and terminus collapse during summer 2004. We used a 1-dimensional viscoelastic model to investigate the transient response of a floating glacier tongue to buoyant forcing. Results suggest that creep may be capable of accommodating buoyant torque if it is applied gradually. As unresolved bending stresses approach the tensile strength of ice, small rapidly applied perturbations may cause buoyancy-driven calving.

2.2 Introduction

The rapid thinning of many glaciers in Alaska since the Little Ice Age has significantly contributed to rising sea level and is linked to climate change [Arendt et al., 2002]. However, the link between glacier thinning/retreat and climate is complicated for glaciers that lose mass through calving [Arendt et al., 2006; Larsen et al., to be submitted]. Calving is an important ice-loss mechanism, and can result in larger volumes of ice lost to the glacier than would be possible through surface ablation alone [Van der Veen, 2002]. The advance/retreat cycle of a tidewater glacier may oscillate independently of climate change,

[1]Boyce, E., R. J. Motyka, and M. Truffer, (2006), Floatation and Retreat of a Lake-Calving Terminus, Mendenhall Glacier, Southeast Alaska. Prepared for submission to Journal of Glaciology.

due to the inherent instability of calving termini and their sensitivity to subglacial topography [Meier and Post, 1987; Post and Motyka, 1995]. Calving can also play a significant role in lacustrine situations at many spatial scales, from small Alpine glaciers terminating in cirque basins to large lake calving glaciers in Patagonia [e.g. Warren et al., 1995; Warren and Aniya, 1999; Naruse and Skvarca, 2000; Warren et al., 2001] to lakes surrounding the Laurentide Ice Sheet at the end of the Last Glacial Maximum [e.g. Cutler et al., 2001]. It is not uncommon for proglacial lakes to form at the termini of glaciers as they retreat through overdeepened channels formed by glacier erosion [Warren and Aniya, 1999]. These proglacial lakes can then modify glacier behavior by increasing calving and either initiating or accelerating terminus retreat [e.g. Funk and Röthlisberger, 1989; Warren and Aniya, 1999]. Fluctuations of lacustrine termini are influenced by bed topography [Warren et al., 1995, 2001; Naruse and Skvarca, 2000] and conditions in proglacial lakes which affect melting of the calving face. Mendenhall Glacier provides an opportunity to study the terminus dynamics of a rapidly receding glacier as it approaches the probable end of its lake calving phase.

The calving dynamics of tidewater glaciers have received much attention, because the stability of these glaciers is important for sea level rise [e.g. Arendt et al., 2002; O'Neel et al., 2003; Rignot et al., 2004]. Much less is known about lacustrine calving systems, even though the number of such systems is increasing as glaciers world-wide continue to shrink. On a scale from land-terminating glaciers to tidewater glaciers, lake-calving glaciers often fall somewhere in between in terms of their dominant ablation mechanism. Some lake-calving glaciers lose mass mostly through surface ablation; calving affects mainly terminus geometry and retreat rate on sub-decadal time scales. Others, for example some large lake-calving glaciers in Patagonia terminating in deep water, lose more mass through calving, similar to many tidewater glaciers [Venteris, 1999].

Investigations of calving behavior at stable tidewater glaciers have shown that there is a linear correlation between annual calving rate and water depth at the terminus [Brown et al., 1982], although the reasons for this relationship are not well understood. In general, a similar relationship holds for large lacustrine termini, but lacustrine calving rates are typically an order of magnitude lower than at tidewater termini [Funk and Röthlisberger, 1989; Warren et al., 1995; Warren and Aniya, 1999]. Van der Veen [1996] suggests that

for retreating calving glaciers the calving rate is not simply related to water depth, but also to ice approaching floatation thickness. He proposed a buoyancy-driven mechanism for calving in which ice thickness and water depth control the terminus position. Here, if surface melting and/or longitudinal extension of the glacier sufficiently thins the ice, the terminus calves back until it achieves a critical thickness, which may be up to 50 m in excess of floatation for some temperate tidewater glaciers. An increase in the calving rate results from thinning of the glacier and does not necessarily require retreat into even deeper water.

Meier and Post [1987] state that, "no temperate tidewater glaciers have floating termini, except perhaps locally and temporarily." When parts of a tidewater terminus do reach floatation it is not sustained and calving results. However, some retreating lake-terminating glaciers apparently may achieve buoyancy for longer periods [Naruse and Skvarca, 2000; Warren et al., 2001]. Van der Veen [2002] argued that lacustrine glaciers may become locally buoyant but not achieve floatation, if surrounding ice has the tensile strength to accommodate the buoyant forces. This has led to the following theory of buoyancy-driven lacustrine calving proposed by Warren et al. [2001]. Thinning of the terminus subjects ice to buoyant (upward) forces. If bending stresses are not accommodated by deformation, tensile stress at the base of the grounded ice tongue may form basal crevasses. Their calculations assume the ice tongue remains grounded, although they suggest that in some cases the buoyant stresses may be partially accommodated by ice creep. If so, this could allow a floating terminus to be sustained despite its apparent instability. A situation such as this appears to have developed at Mendenhall Glacier between 2002 and 2004. The evidence for this condition and its causes are the subject of this paper, as well as a discussion of how a floating terminus in a temperate lacustrine situation can be sustained for extended periods.

2.3 Glacier Setting, Description, and History

Mendenhall Glacier lies on the western (maritime) side of the northern Coast Mountains (Fig. 2.1), in southeastern Alaska. It is 22 km long, flowing from an ice divide at 1600 msl (meters above sea level) to its terminus in Mendenhall Lake at 20 msl. The glacier has been in recession since the end of the Little Ice Age (LIA) in the late 18^{th} century. The

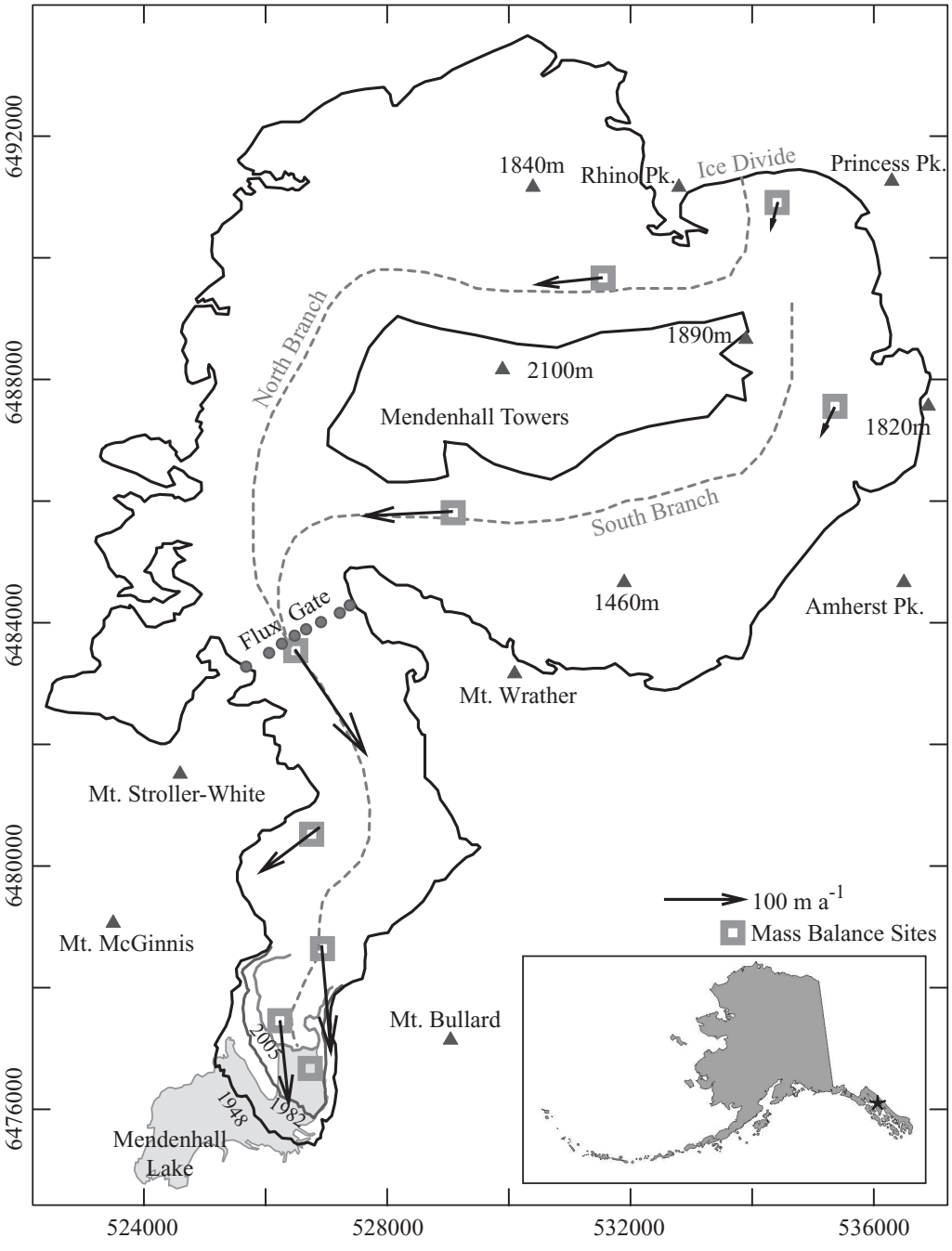

Figure 2.1. Map of Mendenhall Glacier showing locations of study sites. The 1948 outline, 1982 terminus, and locations of nearby peaks are taken from USGS topographic maps. The grey squares indicate mass balance sites, and dark circles indicate velocity measurements across the "Flux Gate" profile. The grey dashed line shows the approximate centerline of the main branches.

proglacial lake began forming in the early 1930s. Motyka et al. [2002] have documented substantial mass wastage and negative mass balances at Mendenhall during the past ∼50 years, with an estimated volume loss of 5.5 km^3 since 1948. The lower glacier has thinned by more than 200 m since 1909, with thinning accelerating to over 2 m a^{-1} in the late 20^{th} century. Likewise, since 1909 the terminus has retreated ∼3 km, with the most rapid recession occurring during two periods, one in the mid-1940s and the second from the late 1990s to present [Motyka et al., 2002]. Motyka et al. [2002] have linked 20^{th} century recession to a ∼1.6 °C increase in mean annual air temperature since 1943. However, the rapid wastage of Mendenhall is attributed to two factors: negative mass balances due to climate change and lacustrine calving enhancing retreat rates - periods of rapid recession have corresponded to periods of increased lacustrine calving.

During the late 20^{th} century, the western side of Mendenhall Glacier retreated past a prominent bedrock outcropping (Fig. 2.2). As ice thinned, the majority of the ice flow was diverted eastward into the lacustrine terminus area by the bedrock topography. (Hereafter we will use 'terminus' to refer only to the lacustrine part.) Bathymetric surveys conducted by Motyka et al. [2002] revealed submerged ridges extending eastward in front of the terminus, lying in front of two ∼70-90 m deep basins adjacent to the 2000 terminus position. Radio echo sounding (RES) profiles near the 2000 terminus position located glacier bed elevations below sea level and an overdeepening behind the eastern side of the lacustrine terminus. Motyka et al. [2002] suggested that retreat into deeper water would leave the lacustrine terminus increasingly vulnerable to calving, possibly accelerating the rate of retreat. In 2000, the terminus was estimated to be within 85% of floatation thickness. Motyka et al. [2002] predicted that Mendenhall Glacier could retreat onto land within one to two decades. Since their study, which was carried out between 1997 and 2000, continued observation of Mendenhall Glacier noted evidence for increasing instability of the lacustrine terminus. We have focused on the terminus dynamics of Mendenhall Glacier, within the larger context of glacier-wide behavior. In particular, we have focused on changes in terminus geometry, ice flow, and calving rate beginning in 2000 and culminating in summer 2005. Mendenhall Glacier has given us a slow-motion picture of dynamic and hydrological factors affecting a calving front, including accumulated stresses leading to deformation of the terminus, and eventual failure through large-scale (relative to the size of the glacier)

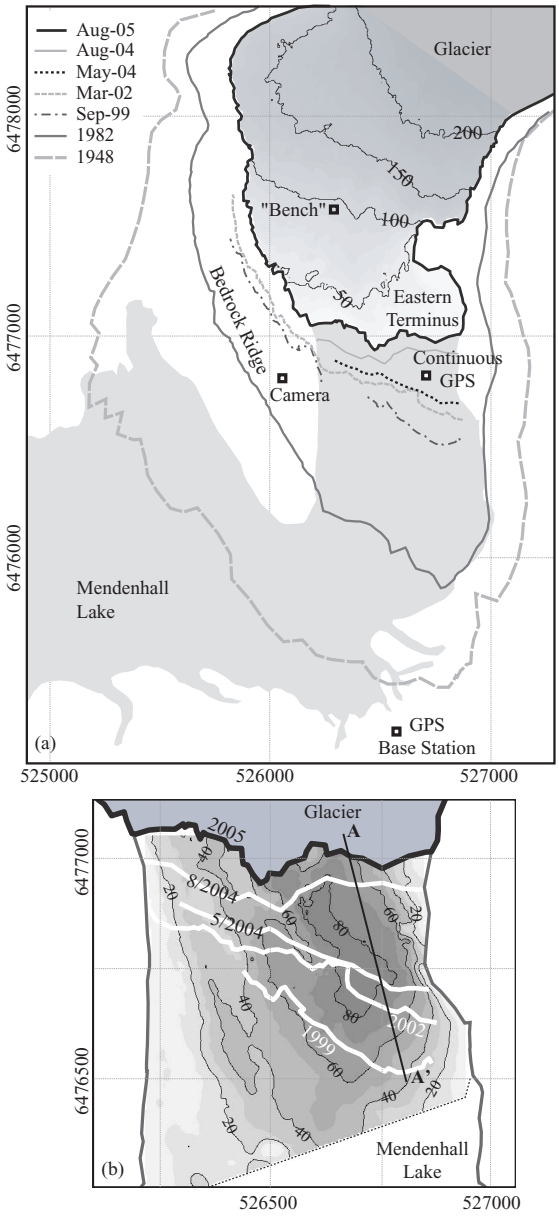

Figure 2.2. Glacial topography and proglacial lake bathymetry near the calving terminus. (a) Terminus positions from 1948 and 1982 are shown as references, while recent terminus positions (derived from ground-based surveys and aerial photography) show the rapid retreat of the calving terminus between 1999 and 2005. More than half of the recent retreat has occurred since May 2004. The 2004 semi-permanent GPS, base station, time-lapse camera, and "Bench" site are marked by black squares. (b) Post-retreat bathymetry shows the former bed geometry beneath the eastern terminus. The transect A-A' marks the location of the cross-section shown in Fig. 2.9. Data are in UTM 8N, WGS84, height above ellipsoid. Depths are referenced to 0 m on the USGS lake gauge.

calving events.

2.4 Methods

2.4.1 Terminus Positions and Geometry

Aerial photographs covering the lower part of Mendenhall Glacier (below ∼250 msl), including the lake calving terminus, were acquired on August 24, 2004 and September 9, 2005. The stereoscopic coverage allowed a digital terrain model (DTM) to be generated using the photogrammetric package SOCET SET®. Ground control was obtained from surveyed bedrock sites near the terminus using DGPS with an accuracy of 1 m or less. The orthorectification models generated by SOCET SET® have RMS values of 1 m or better in both horizontal and vertical coordinates. Elevation accuracy is estimated to be ±2 m for the 10×10 m gridded DTMs. This error is determined by comparing surveyed bedrock and glacier points (the latter corrected for ablation) to the digital elevation model. Ground-based surveys using DGPS provided more accurate terminus positions and could be acquired at the same time as bathymetry surveys. While the DGPS positions are accurate to within about 1 m, the boat could only follow the calving front to within about 15 m. Recent surveyed terminus positions are from September 9, 1999, August 27, 2000, March 24, 2002, May 5, 2004, August 24, 2004, and August 23, 2005. Terminus position data were used to calculate the rate of retreat by averaging the change in terminus position across the width of the glacier.

Between February 29 and August 8, 2004, oblique photographs were acquired by a time-lapse camera stationed on bedrock adjacent to the glacier terminus (Fig. 2.2). The camera automatically obtained one photo per day and held up to 400 frames. The film was periodically retrieved, developed, and digitized at high resolution. Using bedrock control points, each image is two-dimensionally orthorectified according to the method described by Krimmel and Rasmussen [1986]. Scion Image, an image processing software, and MATLAB® scripts were used to analyze the 2004 photos and obtain daily terminus positions which are accurate to ±5 m (Appendix C.7). The oblique photos provide information on terminus retreat, timing and style of calving events, and changes in the ice cliff. Additionally, the digitized time-lapse images were assembled to make a movie of glacier movement and terminus change.

Since day-to-day changes are typically minor, we mainly use the daily terminus positions to calculate the change in area during large, discrete calving events. Terminus position data, ice velocities and post-retreat bathymetry data were used to estimate the calving flux.

We also used kinematic GPS to survey the surface topography of the eastern side of the terminus on August 27, 2002 and January 10, 2004. The surveys cover the area from near the calving front to 150 m upglacier. These ice surface data are accurate to about 1 m and were used to construct a cross-section of the terminus. Additionally, centerline profiles of the glacier were acquired by an airborne laser altimetry system [as described in Echelmeyer et al., 1996] on 31 August 2000. Elevations are determined every 1.5 m along the profiles with an accuracy of 0.1-0.3 m.

Together with the DEM created from the 2005 photogrammetry, these data are used to quantify the amount of thinning that has occurred over the lower glacier between 2000 and 2005. Three methods are used to quantify thinning. First we differenced the 2005 and 2004 DTMs to determine surface elevation change on a 10 m grid of the lower glacier (below about 250 msl as discussed above). Second, the 2004 and 2005 DTMs were used to determine surface elevations at the 2000 altimetry profile points. Finally, we show DGPS ice surface data between August 2002 and May 2004 to indicate changes very close to the calving front. This final method yields only a rough approximation of thinning, since the surveyed areas and points do not overlap in all cases. Since the area of interest is completely within the ablation area, we are looking at changes in the ice surface.

2.4.2 Surface Mass Balance

Between 2000 and 2003, mass balance was intermittently measured at eleven locations (Fig. 2.1) originally established by Motyka et al. [2002], following the glaciological method described by Østrem and Brugman [1991]. During the 2004 melt season, ten markers were drilled in early May to measure summer ablation, and re-measured in late August. The balance year is taken to be from September 1 to August 31. Six of these markers in the ablation area were re-measured in 2005. The equilibrium line altitude (ELA) was also estimated for balance years 2003 and 2004. Wires were drilled into the glacier for lower elevation sites within the ablation area. Poles were placed at most sites in the accumula-

tion area. For the three sites located highest on the glacier, magnets were used to mark the summer surface. The depths of the magnets were measured in subsequent years using a magnetometer. In 2003 and 2004, snow pits were dug at a few sites in the accumulation area to measure snow density profiles and these data were extrapolated to other sites where only snow thicknesses were available. An ablation meter, which measures surface melt by means of a pressure transducer drilled into the glacier [Bøggild et al., 2004], was installed near a mass balance marker called "Bench," at 120 msl (Fig. 2.2). Surface melt was recorded at three-hour intervals over a two month period in summer 2004.

2.4.3 Ice Thickness and Bathymetry

Ground-based radio echo sounding was used to determine ice thickness. Soundings were obtained along several transverse profiles located in the eastern terminus area as well as one profile near "Bench," located $\sim$750 m upglacier. The 5 MHz radar is capable of sounding approximately 600 m in temperate ice, with an accuracy of $\sim$10 m [Motyka et al., 2002]. Most near-terminus RES data were made obsolete once post-retreat bathymetric data with higher resolution and better accuracy was acquired. Furthermore, radio echo soundings made near the terminus may reflect from the terminal cliff (ice/water interface) and not the bed. There is also a strong possibility of obtaining reflections from shallower bedrock that is not directly below the sounder.

Lake bathymetry was measured using an acoustic depth sounder, with a transducer mounted on a small boat. We used a 1 kW transducer with a narrow beam (6 °). The system was calibrated in-situ against known water depths. The estimated accuracy of raw water depth measurements is on the order of 0.5 m. The bathymetry data were co-registered and logged with GPS data at 5 s intervals. Post processing against a local base station provided positional accuracy of $\pm$1 m or better. Raw water depth data were then referenced to the zero height level on the USGS Mendenhall Lake gauging staff (http://nwis.waterdata.usgs.gov/ak/nwis/dv/?site_no=15052500&agency_cd=USGS).

Previous work had mapped lake bathymetry up to the 2000 terminus position [Motyka et al., 2002]. Soundings obtained in 2002 and 2004 concentrated on the new proglacial lake area created by glacier recession. Bathymetry acquired soon after retreat is assumed to measure the former glacier bed.

2.4.4 Ice Motion

We measured surface velocities at mass balance and motion markers (Figs. 2.1 and 2.2) using repeat surveys with differential GPS (DGPS) having positional accuracy of ± 1 cm. Mass balance markers were surveyed in the early and late melt season. In 2002, additional markers were placed on the ice to measure horizontal velocities near the calving front. These markers were surveyed spring and fall between 2002 and early 2004. Nine additional velocity markers were placed on the lower glacier in May 2004. Three bolts were drilled into supraglacial boulders near the RES profile "Bench," and six bolts were affixed to rocks between the center of the lacustrine terminus and the eastern margin. All bolts in the terminus area and at "Bench" were surveyed two or three times in early May and resurveyed in mid-June 2004. Only one terminus bolt remained to be resurveyed in late August. The bolts yielded horizontal velocities only. Velocities are accurate to ± 0.2 m a^{-1} at mass balance markers and to ± 0.5 m a^{-1} at surface motion markers and bolts placed in supraglacial boulders.

A semi-permanent GPS receiver was established on the eastern terminus in January 2004 (Fig. 2.2). The GPS antenna was mounted on three poles drilled into the ice. The station was positioned approximately 100 m behind the calving front. The GPS recorded satellite data at 30 second intervals, with gaps from periodic equipment failures. A base station located across Mendenhall Lake was simultaneously operating. These data were post-processed in 30-minute bins to obtain differentially-corrected positions. The error in each 30-minute position is estimated at $\pm$ 1 cm or better horizontal and $\pm$ 2 cm or better vertical. We will only use 12 and 24 hour mean positions, since the difference between 30-minute positions is within the error.

2.4.5 Ice Flux

In 2000, a "flux gate" (Fig. 2.1) was established $\sim$7 km from the terminus by Motyka et al. [2002]. The cross-section of the transverse profile was determined by RES and surface GPS. Velocity markers were placed across the profile between May and August 2004. Ice flux through a known cross-section can be estimated from surface measurements [Nye, 1965] since the mean surface velocity is approximately equal to the mean cross-sectional

velocity. Paterson [1994, p. 272] notes that this estimate may be improved by an adding a 10% correction factor. From the corrected values, we assume an error of $\pm 10\%$ in the estimation of mean cross-sectional velocity by measurement of mean surface velocity. Additionally there may be an error of ± 10 m in ice depths acquired by radio echo sounding. These independent errors may be combined to give an estimate of the error in a single ice flux calculation. However, since both errors are systematic the error in change in ice flux between 2000 and 2004 is correspondingly much smaller.

Ice flux through the terminus is calculated by the same method, using bathymetry to constrain the glacier cross-section. An estimated average ice surface of 10 m above lake level is added to the bathymetry to obtain the cross-sectional area of the terminus. Water depths (obtained by post-retreat bathymetry) are integrated over the change in terminus area to determine the volume of ice lost by terminus retreat.

2.4.6 Temperatures and Water Levels

A weather station was placed within 300 m of the terminus and recorded air temperature at hourly intervals $\sim$1.5 m from the ice surface. Precipitation events were recorded at the same site by a tipping bucket rain gauge. Water temperatures in Mendenhall Lake were measured at a mooring near the eastern side of the terminus, in $\sim$90 m water. Sensors fixed at 40 m, 60 m, and 80 m depths recorded hourly temperatures between May and August 2004. Temperatures are accurate to ± 0.2 °C.

Daily mean water level in Mendenhall Lake is recorded by the USGS at a permanent gauging station (Site ID 15052500) in Mendenhall Lake. Lake level is recorded at 15-minute intervals and used to calculate daily means. Provisional data are available from USGS Water Resources of Alaska. We will use the notation "LGR" to denote heights measured with respect to the "Lake Gauge Reference" throughout the paper. The datum of gauge is 14.836 m referenced to Geoid96 (Alaska), measured by differential GPS survey.

2.5 Results

2.5.1 Mendenhall Lake Bathymetry and Water Levels

Post-retreat bathymetry (Fig. 2.2) shows that the sublacustrine basin identified by Motyka et al. [2002] extends upglacier as a 80-90 m deep trough. This channel trended southeast to northwest beneath the eastern side of the terminus. Water depths along the western half of the terminus are relatively shallow, while the bed rises quickly from the trough to the eastern margin.

The lake undergoes seasonal fluctuations in water level, with minimum lake levels occurring between January and April, rising through May and June to maximum levels from June to September, and dropping from October to December (Fig. 2.3). The annual range of water levels is typically 1.5-2 m. Increases of up to 0.5 m over several days are common from January to July. During late summer and autumn, rapid rises in lake level of up to 1 m may occur. Short-term changes in lake level in summer 2004 will be discussed in Section 2.5.4.

2.5.2 Observations of the Calving Front

Between 2000 and 2003, we observed significant changes in the terminus geometry of Mendenhall Glacier. In 2000, the surface of the glacier was relatively flat for several hundred meters upglacier from the calving front. Thermo-erosional notches $\sim$1.5 m above lake level were noted along the eastern half of the terminus on June 24, 2002. Due to calving and surface ablation of the face, these notches were discontinuous along the calving front. All were parallel to the lake surface.

Subsequent observations on August 31, 2003 again found horizontal thermal notches $\sim$1.5 m above lake level. Along the eastern side of the terminus, the height of the calving front was at more than 10 m above lake level by late 2003. Behind the uplifted ice cliffs, the glacier surface sloped backward into a deep depression upglacier from the terminus. A survey of the terminus in August 2003 determined that the base of the depression was close to lake level at the time of observation. A few large transverse crevasses, some water-filled, were observed in the uplifted area, although the surface was relatively smooth and easily navigable.

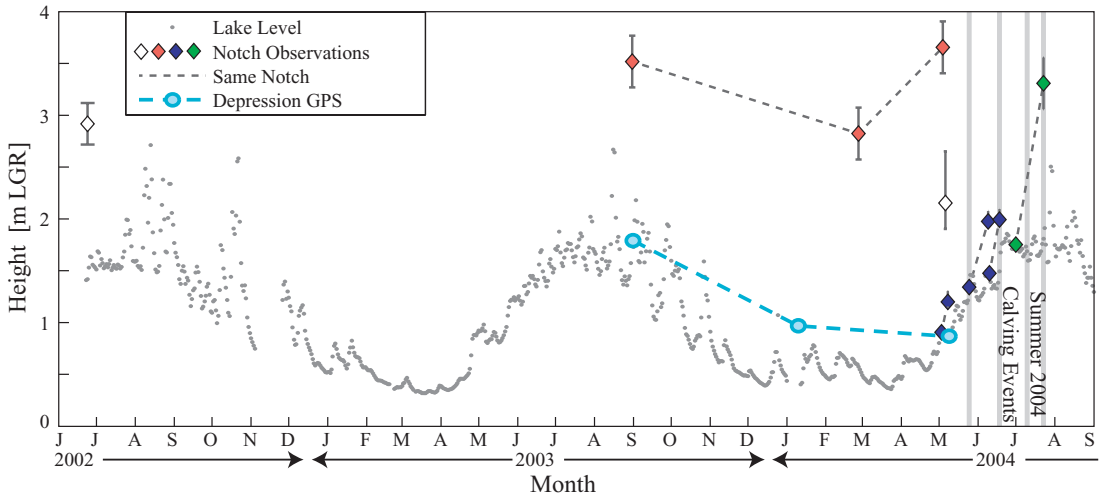

Figure 2.3. Comparison of lake levels to heights of thermal notches, 2002-2004. Water levels (grey dots), estimated heights of thermo-erosional notches (diamonds), and surveyed ice surface height in the terminus depression (circles) are all shown relative to a fixed vertical reference, LGR. Dashed lines indicate consecutive observations of the same melt feature.

Figure 2.4. Oblique view of the eastern terminus of Mendenhall Glacier in May 2004. The calving front is ∼12 m above lake level and the large depression lies 100-200 m behind the calving front. Arched thermo-erosional notches are visible on the ice cliff.

By spring 2004, the maximum height of the ice cliff was 12.5 m above lake level, located over the deepest part of the proglacial lake. Cliff height sloped down to less than 4 m along the eastern face and similarly toward the central part of the terminus. The ice cliff in Fig. 2.4 obscures the large depression, which by May 2004 had dropped to lake level. Silty ponds in the depression appeared to be hydraulically connected to the lake. The depression and reversed slopes behind the calving front can be clearly seen in Fig. 2.4. By May 4, 2004, thermo-erosional notches had now risen up to 3 m above the lake surface near the highest part of the ice cliff (Fig. 2.3, red diamonds). These former water lines were arcuate in shape and sloped down to the lake surface in both directions (Fig. 2.4), which indicates deformation. Near the center of the terminus, a series of 3-4 thermal notches paralleling the lake surface was observed on May 6, 2004. The highest of these was $\sim$1.25 m above lake level.

In order to place thermal notch and ice surface depression heights within a fixed vertical reference frame, we use daily mean lake level records to determine the elevation of each feature relative to 0 m on the lake gauge (LGR). Fig. 2.3 shows actual elevations of thermal notches substantially greater than lake level from late 2003 through summer 2004. The elevation of the highest notch changes through the period of observation. Three small thermal notches observed during May - July 2004 (marked by blue diamonds) are elevated relative to a fixed reference, at a greater rate than concurrent rise in lake level. During July 2004, one series of observed notches is uplifted by $\sim$1.5 m (marked by green diamonds).

2.5.3 Terminus Breakup

Breakup of the eastern terminus began in May 2004. The terminus behavior between February and August 2004 is depicted in the movie created from time-lapse photographs (Appendix C.7) and in Fig. 2.5. In the weeks preceding terminus breakup, the photographs show transverse crevasses opening up where failure eventually occurred. Between May 25 and July 23, four large calving events caused the eastern terminus to retreat more than 200 m, roughly twice the maximum annual retreat previously observed at Mendenhall Glacier. The largest two calving events produced tabular icebergs roughly 70 m$\times$200 m in size. The first event on May 25 removed a large section of the ice cliff at the eastern side of the terminus (Fig. 2.5b), reducing lateral support from the remaining

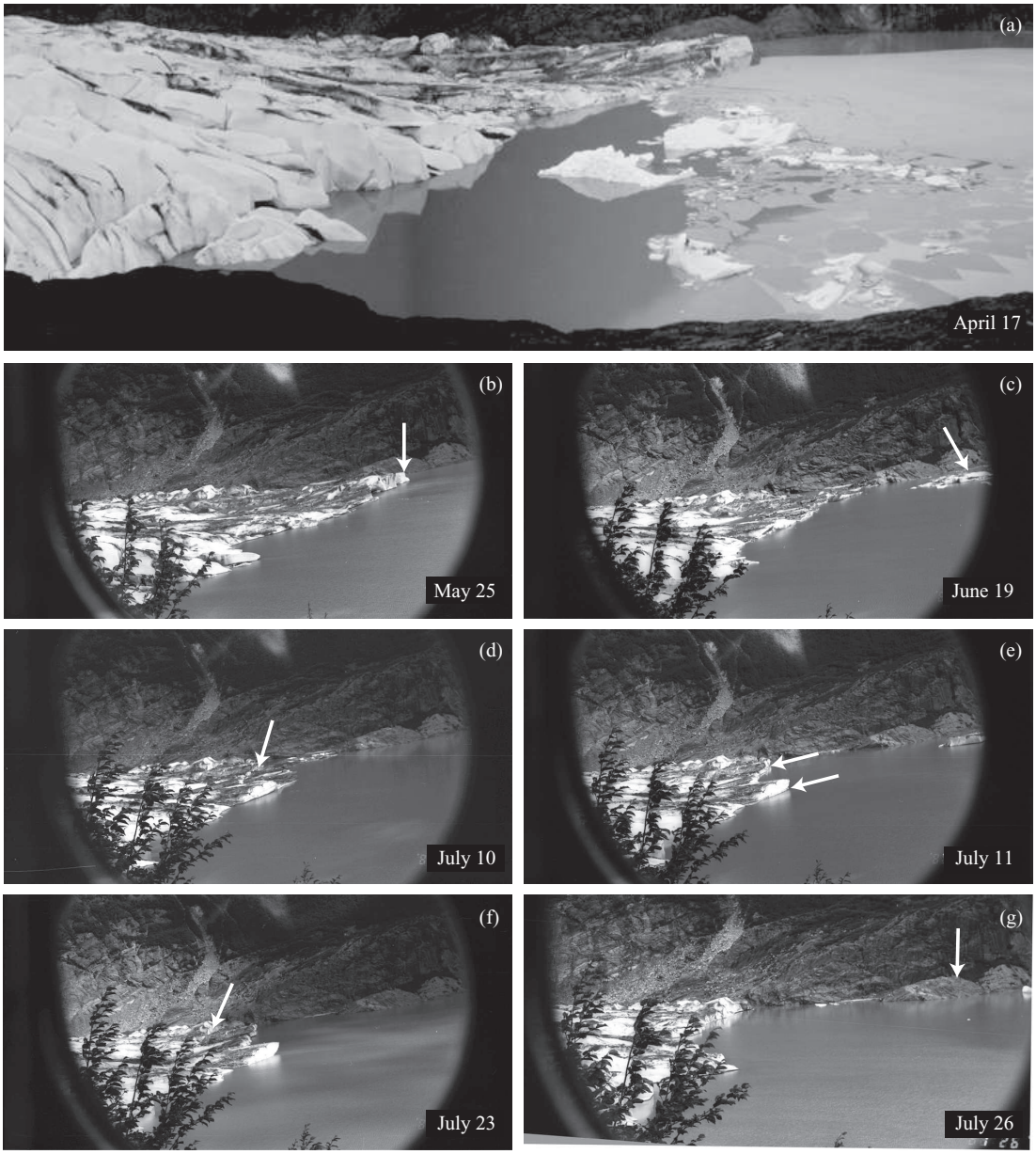

Figure 2.5. Time-lapse photographs acquired at Mendenhall Glacier during spring and summer 2004. View is from the camera marked in Fig. 2.2, opposite from Fig. 2.4. (a) April 17. Note depression and reversed slopes behind calving front. (b) May 25. Arrow marks location of first large calving event. (c) June 19. Arrow marks the iceberg from June 18. (d) July 10. Arrow marks preexisting crevasse where failure occurs. (e) July 11. Arrows mark upwarping sections of the calving front. (f) July 23. Arrow marks hinge line where failure occurs. (g) July 26. Arrow marks the January 2004 terminus position.

elevated calving front. Removal of this section of the ice cliff allowed the lake to inundate the ice depression behind the calving front, partially filling it with lake water. Most crevasses in the terminus area filled with silty lake water, as did the supraglacial ponds in the central part of the depression. The second (and largest) event on June 18 removed the remaining uplifted area, producing icebergs which floated at approximately the same height as the former ice cliff, ∼12 m freeboard (Fig. 2.5c). The terminus retreated almost halfway through the depression, which remained partially flooded. The remainder of this low-lying area calved in a third event on July 10, resulting in the terminus retreating to the upglacier side of the former depression (Fig. 2.5d). Following this event, we observed local uplift along the central and eastern parts of the terminus (Fig. 2.5e). The rate of uplift, measured by the rise of the thermo-erosional notches marked in Fig. 2.3 (green diamonds), was at least 7 cm d^{-1}. The newly uplifted area broke off on July 23 as a large tabular iceberg floating higher than the remaining eastern side of the calving front (Fig. 2.5f and g).

2.5.4 Terminus Environment

Lake temperatures show an overall cooling trend during the summer of 2004 (Fig. 2.6). Water temperatures in the proglacial lake are cooler and show an opposite trend than those recorded in front of LeConte Glacier, a nearby temperate tidewater glacier [Motyka et al., 2003] (Fig. 2.6). Fig. 2.7 shows the water temperature record from Mendenhall Lake during summer 2004, compared to water level as measured by the USGS lake gauge, air temperature and precipitation recorded at the glacier terminus weather station, and daily ablation recorded at "Bench". Between early May and August, water temperatures dropped from above 3 °C to ∼1.5 °C. Temperatures at 40, 60, and 80 meters depth typically fluctuate in unison, with swings of 1-2 °C occurring within one or two days. Strong negative excursions in water temperature generally coincide with increases in lake level, which in some cases (but not all) occur during large precipitation events. High precipitation on May 24-26 may have contributed to the rise in lake level and drop in water temperature during the same period. There was moderate precipitation (around 10 mm d^{-1} or less) throughout the first two weeks of June, and this may have contributed to rising lake level in mid-June. The greatest short-term rise in lake level occurs in late July, following three consecutive days of more than 35 mm d^{-1} precipitation.

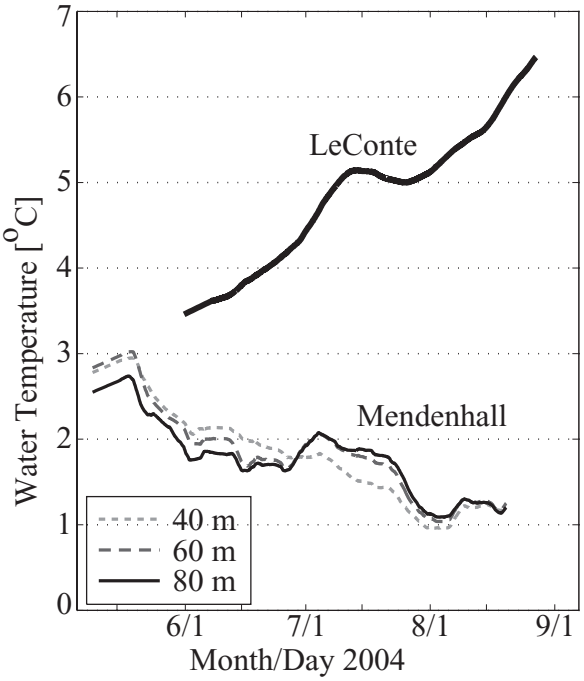

Figure 2.6. Summer water temperatures in proglacial Mendenhall Lake and LeConte fjord, two-week running means. Ocean water adjacent to LeConte Glacier at 40 m depth exhibits a warming trend, while lake water near Mendenhall Glacier cools over the melt season.

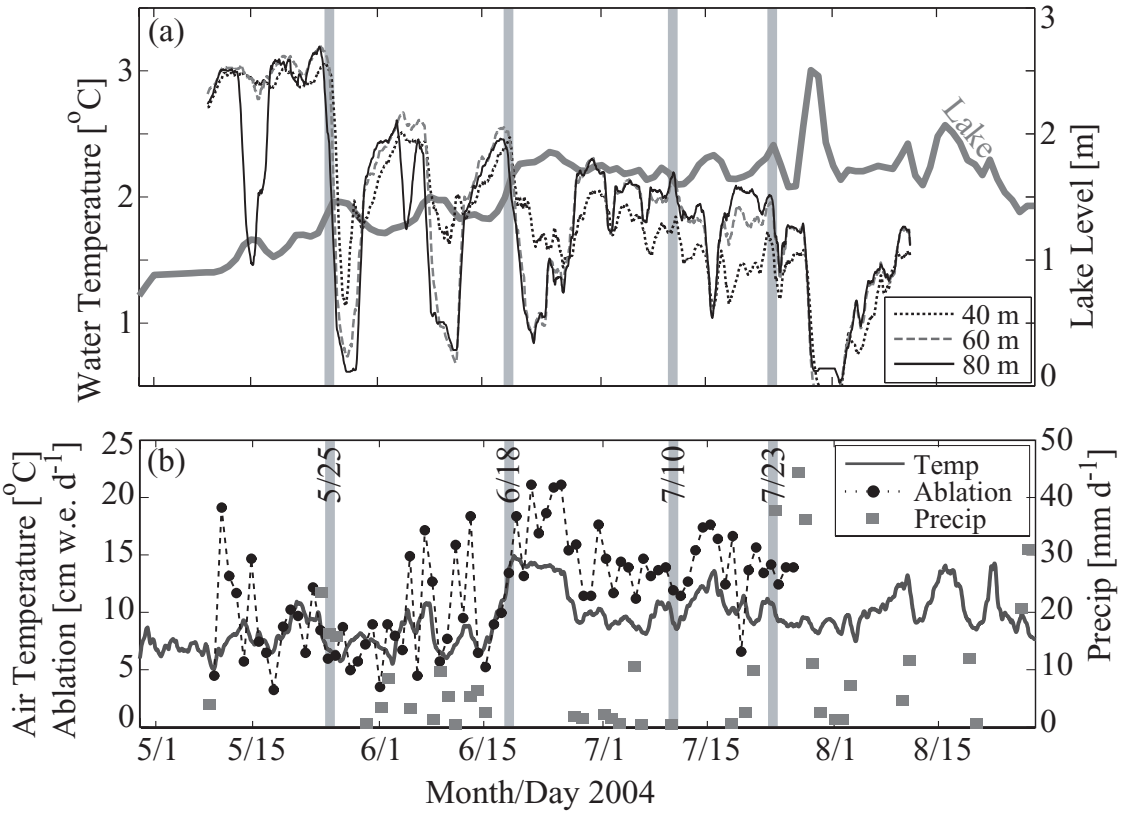

Figure 2.7. Environmental variables recorded near the terminus of Mendenhall Glacier during summer 2004. The four largest calving events (responsible for much of the 2004 retreat) are indicated by grey shaded days. (a)Lake level (solid grey line) is highly variable but generally rises through the melt season. Daily water temperatures also show strong negative excursions and an overall cooling trend (note Fig. 2.6). (b) Air temperature (°C, solid line), daily ablation (cm, black dots) and precipitation (mm, grey squares) over the same time period.

Drainage events from several marginal lakes along Mendenhall Glacier may also be a possible cause of cold water pulses into Mendenhall Lake. Between downward spikes, the 40 m temperature is fractionally cooler than the 80 m temperature. Since the density minimum is at 4 °C, this is compatible with stable stratification. During four large downward spikes recorded during May and June, the coldest water temperatures are recorded at the deepest depths. This is consistent with meltwater entering the lake near the glacier bed and undergoing some mixing in the lake. The final downward spike in temperature, recorded in late July, shows more uniform temperatures at depth - in fact, the coldest temperatures remain at 40 m throughout the cold pulse.

The four large calving events during summer 2004 are marked for reference (the calving events are discussed in 2.5.3). The first two events, which occur on May 25 and June 18, coincide with small (less than 0.5 m) increases in lake level and also with strong negative excursions in water temperature. The correlation may be coincidence, or may suggest some hydrological connection to the timing of these two events. The third large calving event (July 10) exhibits no correlation to any abrupt changes in water temperature, lake level, or precipitation. The fourth calving event again coincides with an increase in lake level and a slight dip in water temperature. The largest short-term change in lake level and water temperature occurs in late July, after the breakup of the eastern terminus was largely complete.

2.5.5 Surface Mass Balance

Results of the 2003, 2004, and 2005 mass balance measurements are shown in Fig. 2.8. For comparison, mass balance measurements collected by Motyka et al. [2002] are shown for balance years 1998 and 2000. The ELA was estimated from airborne and ground-based observations to be around 1370 msl in 2003 and 1250 msl in 2004, $\pm$50 m. Few mass balance data were collected in 1999 or 2001, so no data are presented for those years. Most mass balance measurements were collected at the end of the melt season, therefore only annual balances are shown. As noted by Motyka et al. [2002], the 2000 balance year had exceptionally high accumulation. 2003, 2004 and 2005 show similar patterns of accumulation and ablation at central and higher elevations. Accumulation measured in 1998 is comparable to the most recent three years. Over the lower glacier, data are more variable

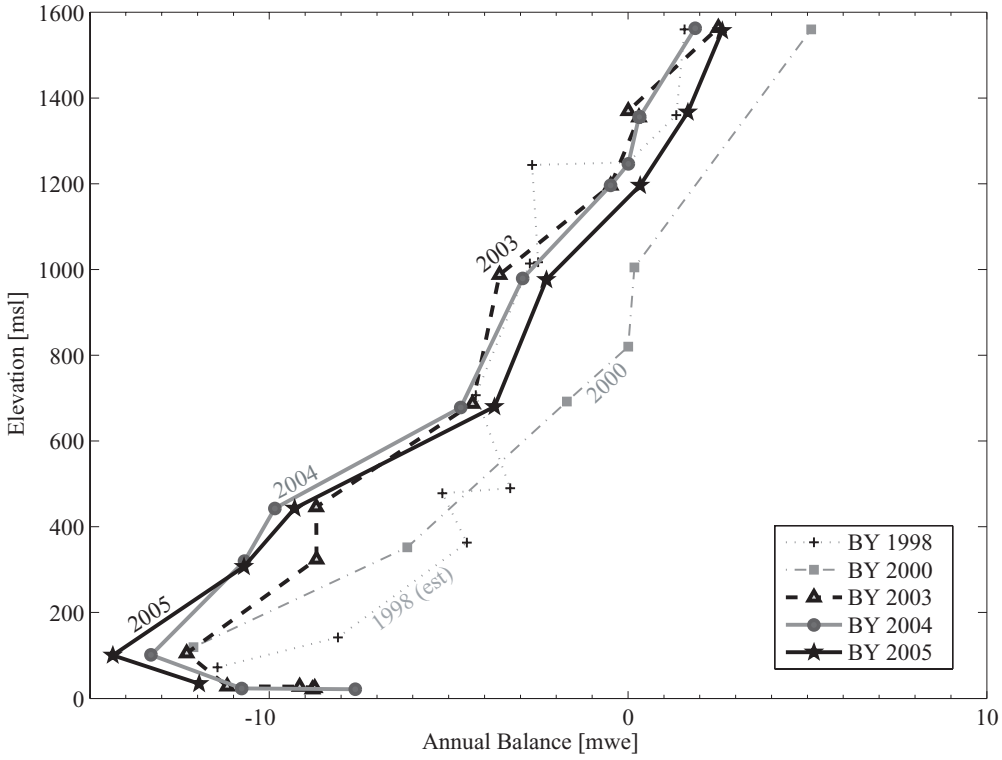

Figure 2.8. Annual specific mass balance versus elevation for Mendenhall Glacier. 1998 (crosses, dotted line) and 2000 (grey squares, dashed line) balance years are modified from Motyka et al. [2002]; 2003 (triangles, black dashed line), 2004 (grey circles, solid line) and 2005 (black stars, solid line) balance years are unpublished data. Visual estimates of ELAs are plotted as points with 0 m balance.

although 1998 is much less negative than 2003-2005. All balance curves from 2000-2005 have reversed slopes at the lowest elevations, indicating that maximum ablation does not occur in the eastern terminus but near "Bench," perhaps because of shading and debris cover lower on the glacier. The pattern of thinning between 2004 and 2005 (Fig. 2.10) also indicates higher ice loss at "Bench." Maximum ablation rates were -12.3, -13.3 and -14.4 mwe a^{-1} (meters water equivalent) for balance years 2003, 2004 and 2005 respectively, all measured at 100 msl. Maximum summer ablation (between May 1 and August 31) was also recorded at 100 msl and measured -9.3, -11.5 and -11.3 mwe for balance years 2003, 2004 and 2005 respectively.

Estimates of glacier-wide annual surface mass balance are given in Table 2.1. With the exception of 2000, all are strongly negative. The values given are reference surface balances, calculated using the area-altitude distribution from the 1948 USGS 1:63,360 scale map as a "reference-surface" [Elsberg et al., 2001], which is the more climatically relevant mass balance. These values do not include the fraction of ice loss due to calving. The estimated error in glacier-wide balances is ± 0.3 mwe a^{-1}.

Table 2.1. Glacier-wide surface mass balance $\dot{B}$ (mwe a^{-1}) and volume loss ΔV (m^3we a^{-1}). 1998 and 2000 calculations are based on field data from Motyka et al. [2002].

Balance Year	$\Delta V \cdot 10^7$	$\dot{B}$
1998	-17	-1.4
2000	+16	+1.4
2003	-20	-1.8
2004	-14	-1.2
2005	-11	-0.9

2.5.6 Terminus Geometry and Thinning

The longitudinal cross-section in Fig. 2.9 shows the former geometry of the lacustrine terminus along the profile A-A' (Fig.2.2), which runs along the eastern side of the deep subglacial trough. It was chosen to maximize the density of ice surface data for the cross-section. All elevations are referenced to LGR. Note that terminus positions only indicate

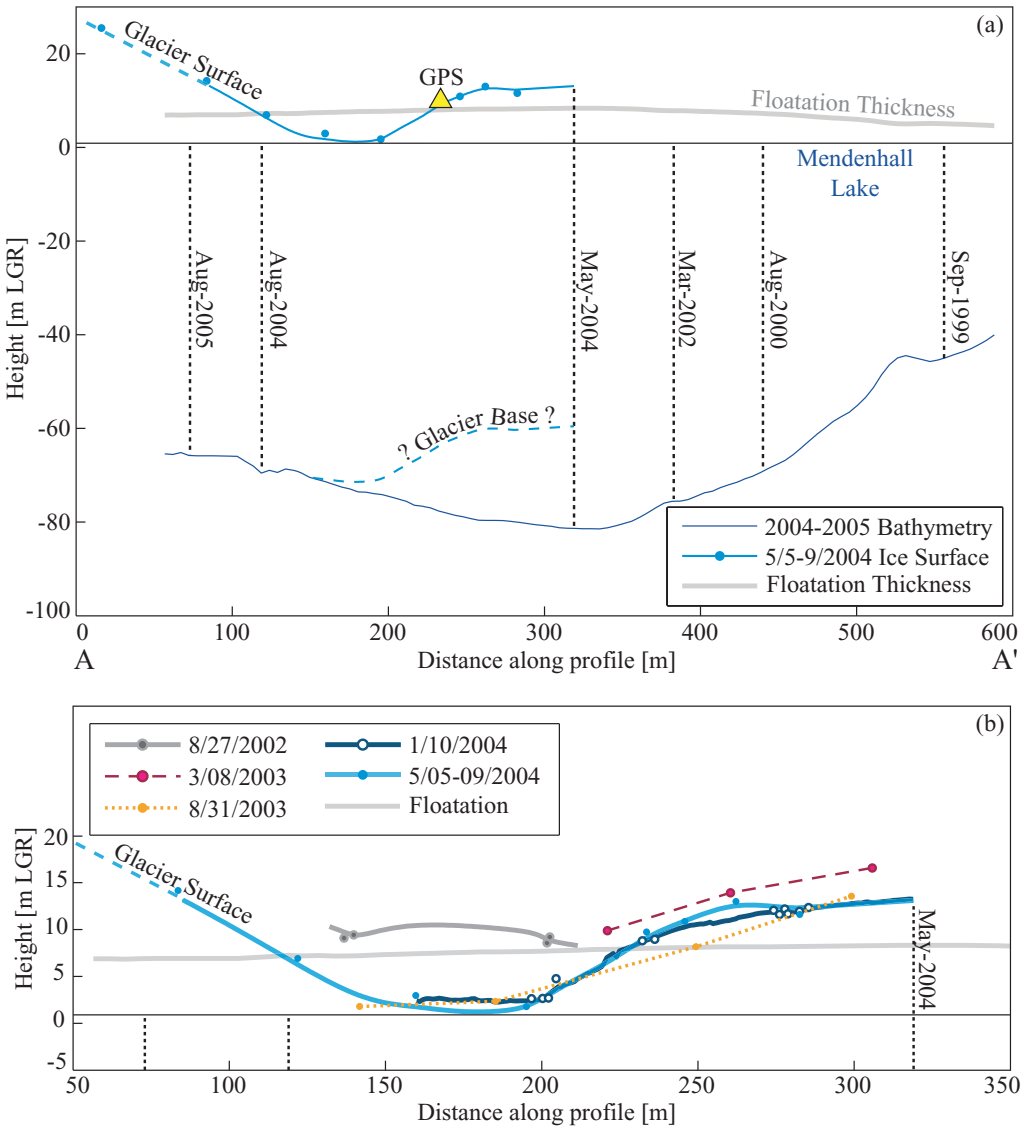

Figure 2.9. Cross-section AA' (Fig. 2.2)of the lacustrine terminus of Mendenhall Glacier. Vertical exaggeration is 3x. Vertical reference is LGR, horizontal reference is UTM NAD83. The May 9, 2004 lake level of 0.9 m is plotted. (a) Location of the semi-permanent GPS on May 5, 2004 (triangle), bed profile from 2004-2005 bathymetry, floatation thickness (thick grey line) based on May 9, 2004 water levels. The ice surface from May 2004 depicts the large depression behind the uplifted calving front. (b) Ice surface data from ground-based surveys 2002-2004. Solid lines (8/2002, 1/2004, 5/2004) are surface profiles obtained from gridded GPS survey data. Dashed lines are interpolated ice surfaces between sparse point data (3/2003, 8/2003). Terminus coverage is patchy for 2002 and 2003.

the position of the calving front on A-A′. Between September 1999 and May 2004 the eastern terminus extended further than the western side.

We define floatation thickness, h_f, to express how close ice is to achieving floatation. d is water depth, ρ_w is water density (1000 kg m^{-3}) and ρ_i is the density of glacier ice (917 kg m^{-3}).

$$h_f = \frac{\rho_w}{\rho_i} d \tag{2.1}$$

Only a few ice surface data are available from August 2002, but they show ice slightly in excess of floatation thickness at 8-10 m LGR. March 2003 data show the beginning of a depression behind the calving front, which deepens an additional 5 m by August 2003. August 2003 surveys show the ice surface through the depression at lake level (also in Fig. 2.3), the first indication of ice surface falling below the floatation thickness. A profile from the January 2004 kinematic GPS survey indicates slight thickening through the depression, although this may be a seasonal effect due to snow accumulation. The May 2004 surface lies below the floatation thickness through the area of the depression, 120-225 m along the profile A-A′. The calving front is locally several meters higher than the expected freeboard height (floatation thickness), drops to floatation height to each side of the profile A-A′, and again exceeds floatation height near the eastern margin (Fig. 2.4). Upglacier, the August 2004 terminus position is close to the point where May 2004 ice thicknesses again exceed floatation thickness.

The minimum ice thickness (between measured ice surface and bed) occurs through the depression, at about 150 m distance along the profile A-A′. There is no evidence for ice thickening between the depression and the calving front, therefore we assume ice at the calving front is no greater than the thickness under the depression. Measured ice surface elevations therefore require that the final ∼100 m of ice behind the May 2004 calving front was not grounded. Measured depression and ice cliff heights indicate that this situation may have begun in summer 2002.

Comparison of 2004 and 2005 DTMs, with 2000 altimetry profiles, shows significant thinning of the lower glacier over this period (Fig. 2.10). Between 2004 and 2005, the annual volume change below 250 msl due to surface lowering was -1.0·10^7 m^3we a^{-1} ice, or an average thinning of 11.5 m a^{-1} ice. Up to 10-25 m a^{-1} of surface lowering was measured between 150 msl and the terminus, except in the far eastern part of the terminus which is

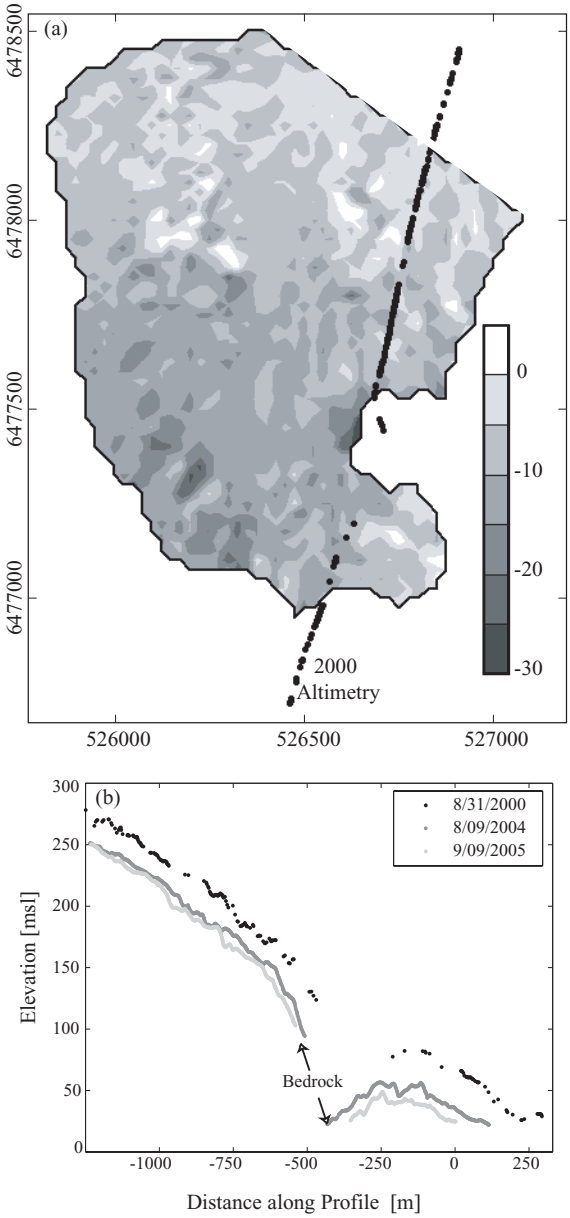

Figure 2.10. Recent thinning of lower Mendenhall Glacier. (a) 25×25 m gridded isopach map derived from comparison of 2004 and 2005 DTMs. The greyscale bar shows surface change in meters of ice. Thinning is extensive, particularly on the lower western side of the glacier. Black dots mark points measured by laser altimetry in 2000. (b) Surface profiles along the altimetry track show the glacier surface in autumn 2000 (black), 2004 (grey) and 2005 (light grey). The overall pattern of thinning shown in (a) is not well represented by the profiles shown in (b).

extensively debris-covered (Fig.2.10a) and may be affected by topographic shading. The altimetry profile skims the eastern edge of the terminus, crossing an outcrop of bedrock which was exposed in early 2004. Between 2000 and 2005, the average change in surface height along the altimetry profile was -5.8 m a^{-1} ice. Thinning along the altimetry profile between 2004 and 2005 is likewise -5.8 m a^{-1} ice, which is half of the average thinning estimated by differencing two DTMs over the entire lower glacier.

2.5.7 Ice Flow at the Terminus

Surface velocities in the eastern part of the terminus range from 30-50 m a^{-1} in winter to 60-70 m a^{-1} in summer. Speeds are higher at the center of the terminus, reaching 110 m a^{-1} in summer. Velocities in the eastern terminus area were measured at least six times between the summers of 2002 and 2004, with no apparent trends (except seasonal variations) in the magnitude of the velocities. Therefore in all terminus flux calculations, a surface velocity of 55 m a^{-1} is taken as a mean across the cross-sectional area of the terminus. We focus on velocity measurements made near the terminus between 2002 and 2004, the period of interest during which the calving front was apparently being uplifted (flow-field shown in Fig. 2.11a). The change in the velocity field over the two-year period is shown in Fig. 2.11b. The overall direction of flow is toward the eastern margin. Most velocity vectors are roughly parallel to contours in the subglacial topography rather than exhibiting a strong relationship to surface slopes (as would be expected for deformational ice flow). Over the two-year period, there is a trend toward more easterly motion, as the orientation of flow vectors approaches the strike of the bedrock trough ($\sim$145 $^{\circ}$).

The semi-permanent DGPS station has yielded a high-resolution record of ice motion near the calving terminus in spring and early summer 2004 (Fig. 2.12). The record is intermittent due to equipment failure or melt-out of the station. Motion was divided into a vertical component and a longitudinal component. The overall trend is an increase in along-flowline velocity through the spring of 2004, from an average of 0.14 m d^{-1} in January to 0.19 m d^{-1} averaged over May. The overall vertical motion is upward and vertical velocities are also highest in May. Also shown are daily lake levels during the same period, which follow the same general trends as the ice motion data. Ice motion and lake level trends are most similar during May, when vertical ice motion appears to correlate

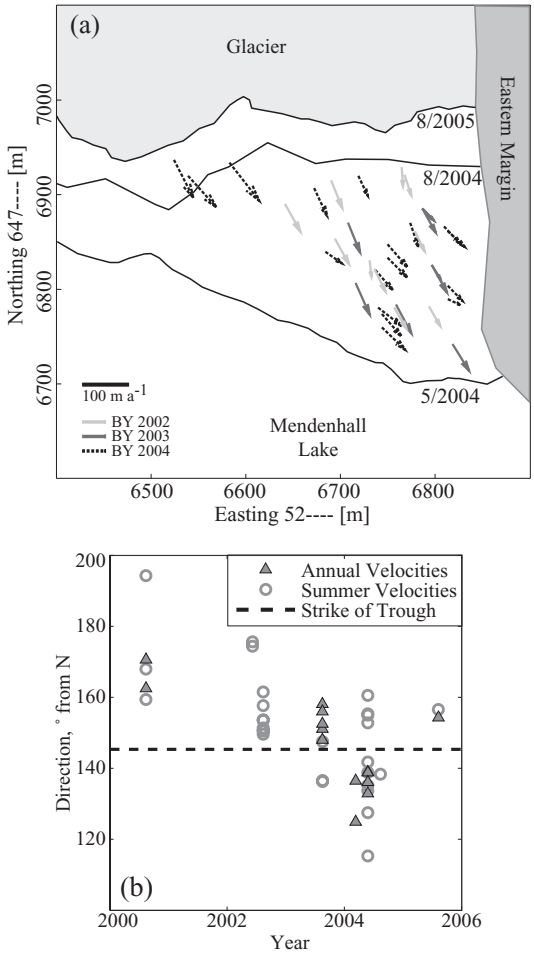

Figure 2.11. Changes in ice flow at the eastern terminus of Mendenhall Glacier, 2002-2004. (a) Flow field shown in relation to terminus positions. Summer velocities are distinguished by balance year for easier comparison. (b) Points mark the orientation of velocity vectors with respect to the strike of the deep bedrock trough (dashed line). Circles are summer velocities, triangles are annual velocities. The bedrock trough axis is $\sim$145 $^\circ$ and the calving front generally strikes east-west.

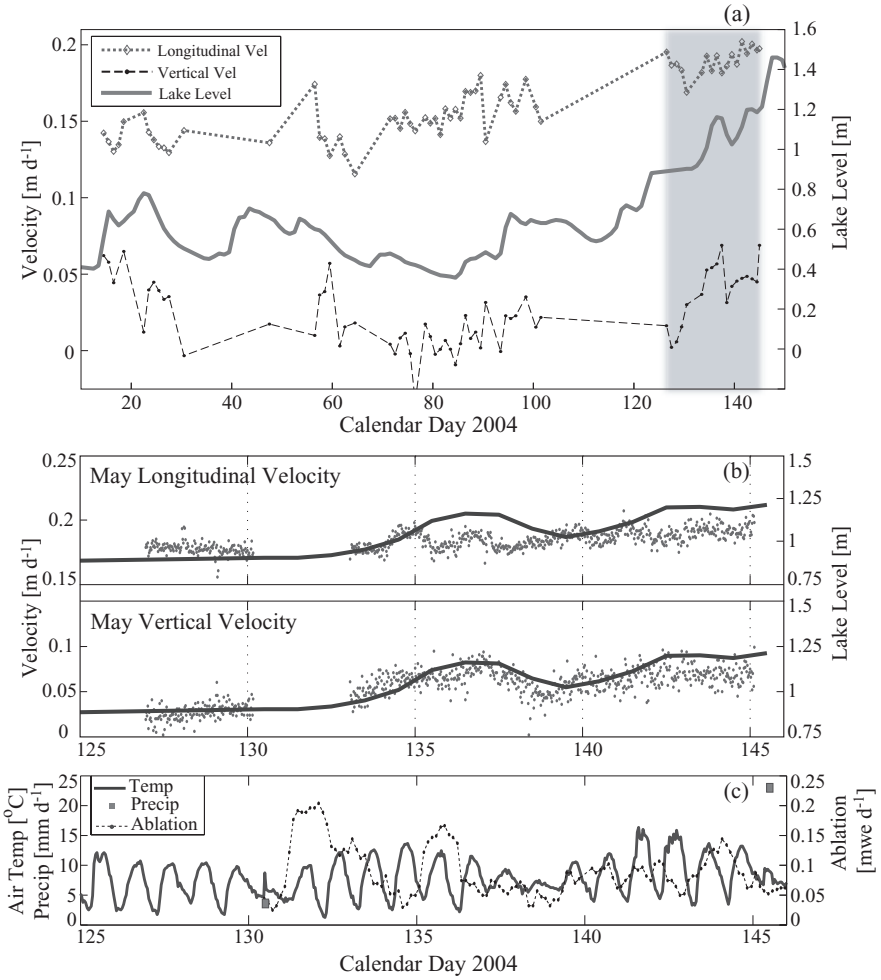

Figure 2.12. Ice motion at the eastern terminus of Mendenhall Glacier compared to environmental factors. (a) A comparison of lake level and ice motion (measured intermittently) between January and May 2004. Daily mean velocities are shown for days on which the GPS was operational for more than 12 hours. Longer segments of dashed line represent interpolation over data gaps. Mean daily longitudinal and vertical velocity are marked by diamonds and black dots, respectively. Daily mean lake level in Mendenhall Lake (thick solid line) rises over the spring. Short time-scale variations during May (shaded area) are shown in (b). (b) Longitudinal and vertical velocities (grey dots) and lake level (solid line) over a 20-day period in May 2004. Velocity data are 12-hr running means. (c) Air temperature (°C, solid line), daily ablation (mwe a^{-1}, dashed line) and daily precipitation (mm, squares). Only two precipitation events were recorded during this period.

to lake level. Short-term fluctuations in lake level and velocity are shown for a 20-day interval in May 2004. There is a slight increase in mean daily lake level around Day 133-134, and a corresponding increase in vertical velocity which appears to track the lake level curve. A slight increase in longitudinal velocity also occurs around the same time, but is more variable and less strong than the change in vertical velocity. Air temperature and daily ablation, measured over the same time period, show no obvious correspondence to short-term ice motion. We note that lake ice adjacent to the terminus breaks up around Day 105, a period for which there is no GPS data.

The ratio between vertical and longitudinal motion also changes throughout the season (Fig. 2.13). This change is more clearly depicted in the net displacement of the GPS station than in the velocity. The ratio of vertical to horizontal motion is initially high in January, 26%. Vertical motion drops through February, March and April, when it is typically less than 20% of horizontal motion. May data show an increase in vertical motion to 34% of the horizontal motion. This change is shown in Fig. 2.13 as an abrupt change in the slope of the vertical displacement curve, with no equivalent change in the slope of horizontal displacement data.

2.5.8 Rates of Retreat and Calving

Terminus positions between fall 1999 and spring 2004 (Fig. 2.2) show that the eastern side of the calving front extended out into the lake up to 250 m further than the western half, and retreat was relatively uniform across the glacier until summer 2004. Rates of terminus retreat (averaged across the width of the calving front) are derived from comparison of surveyed terminus positions, which are accurate to $\pm$15 m. Table 2.2 shows the changes in rate of terminus retreat of Mendenhall Glacier, compared to the 1999-2000 data from Motyka et al. [2002]. The average rate of retreat between 1997 and 2000, -66 m a^{-1} [Motyka et al., 2002], is comparable to the average rate of retreat between 2000 and 2005. When short time periods are considered the terminus has experienced quite rapid rates of retreat, up to 366 m a^{-1} between May and August 2004. The terminus has also experienced periods of low retreat rate, and was almost stable between March 2002 and May 2004.

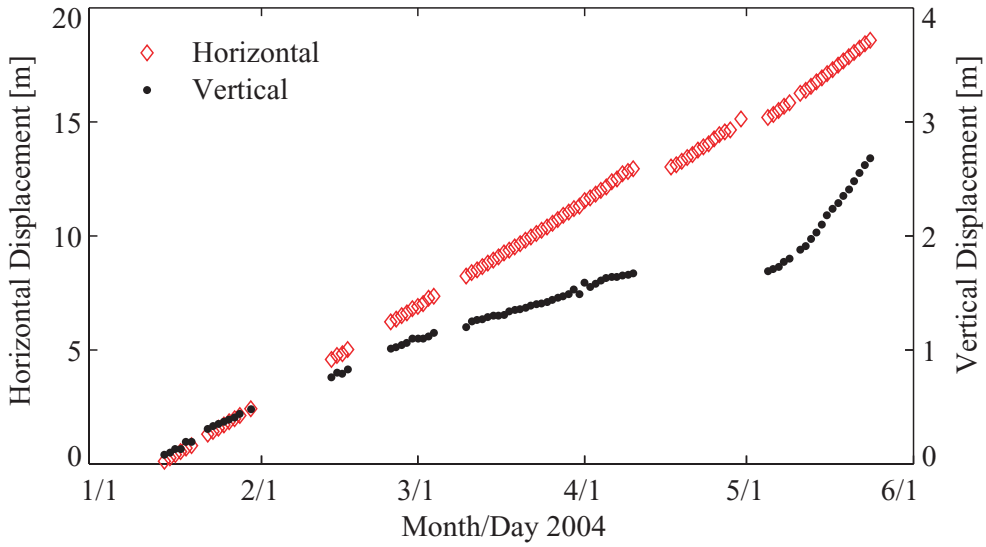

Figure 2.13. Total displacement of the continuous GPS. Daily horizontal (red diamonds) and vertical (black dots) displacement are shown for spring 2004. The long gap in vertical data in April represents a period when the GPS antenna was not drilled into the ice. The station was reset in early April and again in early May.

Table 2.2. Recent rates of retreat, in m a^{-1}, at Mendenhall Glacier. The first column is the average retreat over the eastern half of the terminus (Fig. 2.2), and the second column gives the retreat averaged across the entire width of the calving front.

Time Period	Eastern Half	Entire Terminus
Sep99-Aug00	57	31
Aug00-Mar02	60	59
Mar02-May04	8	12
May04-Aug04	528	366
Aug04-Aug05	57	60
2000-2005	65	58

'Calving rate' is defined as the difference between rate of change of terminus position and ice velocity at the terminus, and melting at the calving face is generally included implicitly in calculations of the calving rate. A mean cross-sectional velocity of 55 m a^{-1} is used to estimate ice flux into the calving front. The amount of ice calved is expressed as a calving flux, Q_C, and calculated as the difference between ice flux into the calving front, Q_i, and the volume flux expressing the rate of terminus advance, Q_L [O'Neel et al., 2001]:

$$Q_C = -(Q_i + Q_L) \tag{2.2}$$

Calving fluxes were recalculated for the 1999-2000 data using more recently measured bathymetry. Table 2.3 shows the calving flux between September 1999 and August 2004. There is very little change in the mean water depth in front of the terminus, and significant variation in the calving flux. Maximum calving flux occurs during the summer of 2004. We estimate the error in calving flux in the same way "flux gate" error is estimated (2.4.5). Although lake depth is known to within $\pm$0.5 m, the error in the mean surface height is $\pm$5 m. Again there is a $\pm$10% error in the estimation of mean cross-sectional velocity by measurement of surface velocities. Calculation of Q_L requires terminus positions, which are only surveyed to within 15 m due to safety constraints. Since some of the error in terminus position is systematic between repeated surveys of the calving front, we estimate the error in terminus retreat to be $\pm$15 m. The resulting error in calving flux is $\pm 0.06 \cdot 10^7$ m^3we a^{-1}.

Table 2.3. Calving flux, and mean water depth $\bar{d}$. Flux is given in $m^3we\ a^{-1}$ ice and water depths in m LGR.

Time Period	$Q_C \cdot 10^7$	$\bar{d}$
Sep99-Aug00	-0.35	47
Aug00-Mar02	-0.32	50
Mar02-May04	-0.25	52
May04-Aug04	-1.7	48
Aug04-Aug05	-0.29	30
Aug00-Aug05	-0.64	45

2.5.9 Upper Glacier Ice Flow and Flux

Surface velocities increase going upglacier from the terminus to the "flux gate" profile. Table 2.4 presents annual velocity data from velocity markers near the glacier centerline (CL_1, CL_2, Bench) and the eastern terminus (LakeWest, LakeEast, LakeUpper, Term), surveyed in late summer of each year. At "Bench", 120 msl, centerline annual velocity in 2004 was 106 m a^{-1} with a seasonal range of 95 m a^{-1} in winter to over 120 m a^{-1} in early summer 2004. The highest surface ice velocity measured during summer 2004, 166 m a^{-1}, was on the centerline at "flux gate". The velocity profiles across the flux gate in 2000 and 2004 are almost identical, with only a slight decrease of $\sim$3 m a^{-1} in the mean surface velocity between 2000 and 2004.

Ice flux through the "flux gate" decreased by $\sim 5.9 \pm 0.1\%$ between 2000 and 2004 from $8.2{\cdot}10^7$ $m^3we\ a^{-1}$ to $7.7{\cdot}10^7$ $m^3we\ a^{-1}$. During the same interval the "flux gate" profile thinned by an average of 3.1 m a^{-1}, reducing the cross-sectional area of the glacier with a concurrent decrease in mean velocity. The estimated error in ice flux through the "flux gate" is $1.0{\cdot}10^7$ $m^3we\ a^{-1}$. Most of this error is systematic, so the estimated error in the change in ice flux between 2000 and 2004 ($-0.48{\cdot}10^7$ $m^3we\ a^{-1}$) is only $-0.05{\cdot}10^7$ $m^3we\ a^{-1}$.

As a check on thinning and calving flux estimates, we calculate the balance flux of ice for the lower glacier.

$$Q_F - Q_B - Q_C = \Delta V \tag{2.3}$$

Table 2.4. Surface velocities on lower Mendenhall Glacier, 2002-2005. The elevation of each marker is referenced to Geoid96 (Alaska). Velocities are distinguished by balance year since repeat surveys occurred in late August, with the exception of the final surveys of LakeEast, LakeWest, and LakeUpper in June 2004. Velocities are given in m a^{-1} and degrees from true north.

Marker	MSL	BY	Speed	Azimuth
LakeWest	17	2003	48	158
LakeWest	17	2004	62	139
LakeEast	22	2003	47	151
LakeEast	17	2004	43	136
LakeUpper	24	2003	41	151
LakeUpper	19	2004	47	133
Term	27	2005	34	154
Bench	97	2003	104	174
Bench	105	2004	106	181
Bench	95	2005	100	186
CL_2	316	2003	141	177
CL_2	312	2004	134	175
CL_2	306	2005	128	176
CL_1	682	2003	158	146
CL_1	673	2004	155	147
CL_1	687	2005	156	145

Q_F is the flux through "flux gate," as estimated above. An average of surface mass balance data from balance years 2003-2005 provides Q_B, the average mass lost due to surface ablation below the flux gate. Q_C is taken as the mean calving flux between March 2002 and August 2004. The remainder, ΔV, is the change in mass due to thinning of the glacier. These fluxes are shown in Table 2.5.

Table 2.5. Ice flux through lower Mendenhall Glacier. The volume change is divided by the surface area of the lower glacier to estimate an average thickness change Δh below the "flux gate."

Fluxes	$\cdot 10^7$ m^{3}we a^{-1}
Q_F	+7.70
Q_B	-12.5
Q_C	-0.41
ΔV	-4.35
Surface Change	m a^{-1} ice
Δh	-8.8

Thinning of the lower glacier calculated by the balance flux method is consistent with measured thinning rates of -11.5 m a^{-1} between the terminus and 150 msl, and -3.1 m a^{-1} at "flux gate."

2.6 Discussion

Earlier work on Mendenhall Glacier concluded that the terminus was particularly vulnerable to calving as ice thicknesses approached buoyancy and the terminus retreated into an overdeepening [Motyka et al., 2002]. Without shoals or bedrock rises to exert backpressure on the calving front, the terminus was in an inherently unstable position given current rates of thinning and ice flux to the terminus area. However, the position of the terminus changed very little between 2002 and its dramatic breakup in summer 2004, suggesting that despite apparent vulnerability the glacier was temporarily stable. We discuss the various factors affecting the eastern terminus during the two years prior to its disintegration and the accompanying changes in ice flow and terminus geometry.

2.6.1 Effects of Volume Loss and Thinning

The total volume loss at Mendenhall consists of surface ablation and calving flux. The average calving flux between 2002 and 2005 was -0.75·10^7 m^3we a^{-1}, compared to an average annual volume lost to surface melt of -15·10^7 m^3we a^{-1} over the same period. Thus calving represented about 2.6% of the ice lost by surface melting between 2002 and 2005. As a fraction of the longterm mean annual volume change measured since 1948 by Motyka et al. [2002], calving is around 4%. Although calving has been relatively minor when compared to total volume loss, it has still played a key role in affecting terminus dynamics. Changes in the annual mass balance at Mendenhall Glacier do not appear to impact terminus behavior over short time scales, yet long term negative mass balances have led to the long-term downwasting of the glacier and left the terminus susceptible to large-scale calving events. The low CAR (calving to surface ablation ratio) of only 0.026 is an indication of how different Mendenhall Glacier is from tidewater calving glaciers, which may have values of CAR more than two orders of magnitude higher [Echelmeyer et al., 1992].

Motyka et al. [2002] measured a thinning rate of 8 m a^{-1} on the lower glacier between 1995 and 2000, a trend that persisted between 2000 and 2005. Surface lowering of the lower glacier is consistent with predictions of volume change obtained from balance flux calculations. The terminus has simultaneously narrowed and downwasted, leaving a smaller lacustrine terminus increasingly close to floatation. Recent thinning of the terminus was accompanied by a change in ice flow driven by the underlying basin geometry. Gudmundsson et al. [2003] observed that ice may become more sensitive to the subglacial topography when the ratio of basal sliding to internal deformation increases. As the terminus approached floatation and the surface slope became almost flat, we would expect the component of ice flow due to internal deformation to drop. At the same time, thinning of the ice could lead to an decrease in effective pressure at the bed and an increase in basal sliding.

As terminus ice was pushed in a more easterly direction, the margin may have provided more “back-pressure” to stabilize the eastern terminus. In the case of Mendenhall Glacier, there is no obvious topographic rise in front of the glacier, but sufficient lateral stability may have been provided by the eastern bedrock margin. It is interesting to note that at Mendenhall, large-scale calving during June and July 2004 followed the removal of

a small section of the ice cliff closest to the eastern margin (May 25 calving event).

2.6.2 Uplift and Floatation of the Calving Front

Thermo-erosional notches are formed by melting of ice at the waterline. Therefore notches observed above the lake level may have formed in two ways. First, the calving front may remain stationary while lake levels drop, leaving notches exposed on the cliff face. Second, lake level may remain stationary while the calving front is uplifted. In this case, notches are formed at lake level and then elevated to their observed positions. Thermal notching is only observed where the ice cliff is stable and experiences no small calving events before being uplifted. A comparison of notch height and lake level relative to a fixed reference frame clearly shows that the second process is responsible (Fig. 2.3). The most extensive thermal notch (marked by red diamonds) is higher than any water levels reached during the preceding year. Also, its height appears to track lake level between August 2003 and May 2004. The formation of smaller notches (marked by blue diamonds) was observed during summer 2004. These notches rise along with lake level during May and June 2004. We interpret this to be an uplift of the entire eastern calving front as water levels rise. The final series of notches forms on a part of the calving front that was previously held below floatation height (marked by green diamonds). The magnitude of the notch rise in this case exceeds a concurrent rise in lake level. The warping of notches in the transverse direction indicates support from the margins.

The next evidence for an uplifted, floating calving front comes from combining ice surface and bathymetry data. The reversed slopes behind the terminus and uplifted ice cliff suggest two possible causal mechanisms:

1. Ice flowing through an overdeepening (below the depression) could be forced upward by subglacial topography, locally elevating the terminus. However, bathymetric surveys conducted post-retreat show that the area of maximum upward displacement along the calving front is directly over a deep trough.

2. The lower glacier had simultaneously thinned and retreated into a deep basin, where it eventually reached floatation. Buoyant forces caused upwarping of the glacier tongue.

The second mechanism is consistent with post-retreat bathymetry, terminus geometry and thermal notch uplift.

Observations suggest that the eastern calving front had locally reached floatation by 2002. Comparison of ice surfaces with post-retreat bathymetry indicates that between 2003 and 2004 the eastern terminus reached floatation between the depression and the calving front. The sensitivity of ice flow to lake level suggests that during spring 2004, the eastern terminus was ungrounded 100-150 m behind the calving front. It is likely that some seasonal variation in the extent of the floating area occurred as buoyant forces increased during the summer and decreased again in the winter.

The surface depression behind the calving front had thinned to below floatation thickness by January 2004. Although ice thickness there approached lake level, ice was held below floatation by ice to the front and sides, and possibly due to the tensile strength of grounded ice upglacier [Van der Veen, 2002]. Without the surrounding ice to balance buoyant forces, the new calving front was upwarping at a relatively rapid rate, lifting thermo-erosional notches up to 1 m over a two week period. We suggest that although the floating terminus may have been capable of withstanding seasonal variations in lake level of 1.5-2 m (as well as 11.5 m a^{-1} thinning), by 2004 it could no longer withstand relatively small increases in lake level occurring over short periods.

2.6.3 Effect of Mendenhall Lake on Ice Motion and Calving

The trend in longitudinal velocities measured at the continuous GPS can be attributed to increased basal sliding throughout the spring, possibly indicating an increase in subglacial water pressure. The increase in vertical velocity as ice approached the calving front is not attributed to compressional flow, since there is no indication of longitudinal compression in the terminus velocity field, rather the opposite. Also, there is no change in basal topography which could increase drag near the terminus. The increase in vertical velocity and also in the ratio of vertical:horizontal motion is interpreted to be further evidence of floatation as ice approaches the calving front. Qualitatively, changes in the ice motion seem to track fluctuations in lake level (Fig. 2.12).

It has been suggested that subaqueous melting of the ice face is important in the calving of tidewater glaciers [Motyka et al., 2003], where warmer ocean water and thermoha-

line convection near the terminus leads to substantial melting of ice. Water temperatures at Mendenhall Lake suggest that the lake is thermally stratified through the summer, and that pulses of meltwater or runoff entering from the glacier do not greatly disturb the water column. No evidence for thermal convection was found. Sublacustrine shelves extending several meters from the ice cliff were commonly observed, suggesting that subaerial ablation rates may be higher than sublacustrine melting. Due to the cooler temperatures and lack of convection, we conclude that sublacustrine melting is not an important process at Mendenhall Glacier. Lacustrine glaciers may be quite unlike tidewater glaciers with regard to the importance of subaqueous melting Motyka et al. [2003].

Calving events are infrequent, and most calving losses during Summer 2004 were in large tabular bergs released in discrete calving events. Fluctuations in water level, water temperature, and precipitation may be linked to the timing of some calving events at Mendenhall Glacier. We will speculate about the possible triggers for each of the four large calving events. The May 25 calving may be a result of a $\sim$30 cm rise in lake level over May 24-26, due to a large drainage or runoff event. Although this calving event was relatively small in terms of ice volume, it may have been significant in removing a large amount of lateral stability from the floating part of the terminus. The uplifted area was no longer connected to the eastern margin.

Without the added stability to hold the floating ice in position, another increase in lake level may have been sufficient to cause the large calving event on June 18. Again the lake level exceeded previous water levels for the season, following two weeks of moderate precipitation, high ablation rates and a large pulse of cold water entering the lake. The third large-scale calving event does not have a strong correlation to rising lake level or water temperature fluctuations. This event may be a result of the terminus continuing to adjust to a decrease in backpressure following the removal of the uplifted front. In the two weeks prior to the fourth event, we can clearly see upward bending of the calving front. The calving coincides with a relative maximum in lake level. Thus three out of the four calving events responsible for rapid retreat during 2004 are related to short time-scale increases in lake level, which are in turn related to increased subglacial discharge or runoff from precipitation or marginal lake drainage events.

2.6.4 A Viscoelastic Model of Buoyant Upwarping

We see evidence for upward deformation during a period of relative stability (low retreat rates) between 2002 and May 2004. To investigate the circumstances under which upwarping can occur without leading to immediate calving, we use a simple model based on published work by Reeh et al. [2003]. We consider a glacier tongue which is at floatation between its grounding line and the terminus. Buoyant forces exert a torque, resulting in vertical deflection of the terminus. If the bending stress exceeds the tensile strength of ice, failure (calving) occurs. Elastic beam theory can be used to estimate the deflection and maximum stress and its location in the ice tongue. Warren et al. [2001] calculated the basal tensile stresses due to buoyant torque using a static model in which ice was not allowed to deform upward. However, ice creep will accommodate some buoyant stresses if they increase gradually. Modeling this behavior requires a viscoelastic rheology for ice, such as the one-dimensional viscoelastic bending beam model used by Reeh et al. [2003] to evaluate the tidal flexure across a floating ice tongue. We use the same linear viscoelastic model to evaluate the response of a floating ice tongue to buoyant forcing (Chapter 3). The model is summarized below.

For a floating ice beam (e.g. a glacier terminus), the load on the beam depends on its deflection from hydrostatic equilibrium, u, and some external forcing, f. External forcing may include variations in water level (such as tides or seasonal variations, short-term fluctuations in lake level) or changes in ice thickness (constant thinning or seasonal balance). The balance of forces and torques acting on an element of the bending beam is used to derive an equation relating the load on the beam to the bending moment. Partial derivatives are denoted by subscripts in Eqs. 2.4 and 2.5. Notation: x is the longitudinal coordinate (+ downglacier), M is the bending moment, ρ_w is the density of ice (917 kg m^{-3}), g is the acceleration due to gravity.

$$M_{xx} = \rho_w g(f - u) \tag{2.4}$$

For a linear viscoelastic material and assuming plain strain, there is a relationship between the beam curvature u_{xx} and the bending moment M [Reeh et al., 2003]. Notation: t is time, I is the moment of inertia, E_M is Young's modulus, E_v and μ_v are elastic modulus and viscosity associated with primary creep, and μ_M is viscosity associated with steady creep

(see 3.2 for values of constants).

$$I\left(\frac{3\mu_v}{E_v}u_{xxtt}+u_{xxt}\right)=\frac{2.25\mu_v}{E_vE_m}M_{tt}+0.75\left(\frac{1}{E_v}+\frac{1}{E_m}+\frac{\mu_v}{\mu_mE_v}\right)M_t+\frac{0.25}{\mu_m}M \tag{2.5}$$

Equations 2.4 and 2.5 are solved numerically, using appropriate boundary conditions for a beam with one end pinned (the grounding line) and one end free (the calving front). The technique used is a semi-discretization in time by centered finite difference approximations, and a Chebyshev spectral method in space [Trefethen, 2000, pg.51]. From a known initial condition (typically zero deflection) the system of equations is solved at each time step using MATLAB® built-in matrix inversion. The result is deflection $u(x,t)$ and bending moment $M(x,t)$. Warren et al. [2001] use the torque, or bending moment M, to calculate tensile stress at the base of the bending beam of ice. Notation: h is ice thickness, I is moment of inertia.

$$\sigma_{xmax}=\frac{hM}{2I}. \tag{2.6}$$

The driving forces in the model are changes in water level or changes in ice thickness, both of which result in buoyant torque acting on the glacier tongue. Unlike the high-frequency variations of a tidally-forced system, forces in a lacustrine environment vary seasonally. Lake levels rise during the melt season and fall during the winter months over a range of 1.5-2 m at Mendenhall Glacier. Survey and mass balance data indicate that the terminus of Mendenhall Glacier undergoes seasonal fluctuations in its thinning rate. Balance rates are strongly negative during the summer, often ranging from 10-20 cm d^{-1} near the terminus. Winter accumulation results in positive balance rates and slight thickening. We use a simple forcing function that is consistent with lake level, ablation rate, and thinning data.

For perturbations occurring over seasonal time scales, model results show that during the first "summer" of elevated lake levels and thinning rates - upward forcing in the model - the calving front may be uplifted to hydrostatic equilibrium, while ice near the grounding line is held below floatation thickness since we require ice at the grounding line to be pinned. Maximum basal tensile stresses occur at the grounding line, but may be insufficient to cause calving. Over the following "winter" water levels drop and accumulation occurs - downward forcing - leads to downward deflections which are of lower magnitude than upward deflections previously achieved. The maximum stresses are still

found at the grounding line, but negative deflections correspond to basal compressive stresses and surface tensile stresses. In this scenario, subsequent cycles of upward forcing and deflection (during the "summers") result in higher basal tensile stresses (still at the grounding line) than those reached during the first melt season. Eventually these unresolved tensile stresses may result in calving. It should be noted that this theoretical model allows the glacier tongue to experience negative deflections. In the case of ice only barely at floatation, these downward deflections could not occur because the ice would simply become grounded. Therefore a real glacier tongue would not experience the downward deflections and corresponding stresses suggested by the model. In fact, the length of the glacier tongue affected by buoyant forces would become shorter during the winter.

A critical factor in buoyancy-driven lacustrine calving is the time scale of perturbations. In reality, glacier tongues are not forced by simple oscillatory functions or constant thinning rates. So far, we have only considered seasonally varying perturbations, applied in a continuous fashion. If the same amount of deformation were achieved instantly (elastically), stresses would be much higher - probably resulting in breakup of the glacier tongue. However, this cyclic deformation may still result in damage to the ice, but on a smaller scale. Accumulated damage could lower the tensile strength. Our model indicates that high amplitude perturbations may not lead to terminus breakup if they occur on annual or seasonal time scales. Thus a lacustrine glacier tongue could remain locally at floatation for a much longer period than previously supposed. We propose that after two years of partial floatation, unresolved basal tensile stresses at the grounding line were approaching a critical level during the 2004 melt season, making the terminus of Mendenhall Glacier susceptible to short-term perturbations. Such short-term perturbations could be small increases in lake level over a period of several days to several weeks, or an abrupt removal of adjacent ice thereby decreasing the lateral stability of the glacier tongue. We believe such a mechanism may have triggered the calving events observed at Mendenhall Glacier during summer 2004.

The stability or failure point of a floating terminus is further complicated by preexisting zones of weakness (crevasses) and channel geometry. Margins may provide backpressure, as in the case of the eastern side of Mendenhall Glacier. Grounded ice at the margins (where water depths are shallower) may prevent floating ice (over a deep trough) from

calving.

2.7 Conclusions

The terminus of Mendenhall Glacier has experienced periods of both rapid retreat and relative stability during the past five years. Retreat during a three-year period between 1999 and 2002 was approximately equal to the retreat that occurred during a three-month period in Summer 2004. The episodic nature of the retreat suggests that bedrock rises or positive basal slopes may exert sufficient back-pressure to temporarily stabilize the terminus. This may have occurred between 1999 and early 2004, as the glacier terminus slowly pulled back from a bedrock rise. During this period of relative stability the eastern half of the terminus thinned until it reached floatation.

In considering what drives the retreat of a glacier such as Mendenhall, we identify factors on three time scales (there may be more):

First, we consider long-term changes in the lower glacier. Dramatic post-LIA thinning of the lower glacier has been attributed to negative mass balances linked to climate change [Motyka et al., 2002]. Such thinning is responsible for the existence of Mendenhall Lake and also for the general terminus geometry since the 1980s, when the glacier retreated past a bedrock outcropping and ice flow was directed to the eastern side. The trend of negative mass balances and thinning has continued between 2000 and 2005. While over a long time scale, retreat may be attributed to climatically-driven thinning, on shorter (perhaps sub-decadal) time scales the rate of retreat has been strongly affected by the bed geometry. Recent thinning rates have likely accelerated the retreat already underway, since thinning to the floatation thickness left the terminus vulnerable to buoyant forcing and enhanced the potential for lacustrine calving.

Second, we consider the annual cycles of surface mass balance and lake level. Thinning of the terminus occurs largely over the melt season, which coincides with high lake levels. Both factors drive ice closer to the floatation thickness, until it eventually becomes buoyant as was the case at Mendenhall. However, if bending stresses are increased slowly and relaxed by ice creep, the terminus may undergo several annual cycles before failure occurs. At this stage, bed geometry is again important in providing lateral stability or backpressure on the calving front. The terminus of Mendenhall Glacier was locally at floatation for up

to two years, therefore we cannot consider a grounded glacier tongue affected by buoyant torque [Warren et al., 2001]. Rather we suggest that seasonal fluctuations in thinning rate and in the level of Mendenhall Lake led to a gradual upward deflection of the calving front and gradual increase in un-accommodated tensile stresses, as described further in Chapter 3.

Third, we consider short-term changes that trigger the eventual failure of the terminus. The nature of the calving events observed during Summer 2004 is strongly indicative of buoyancy-driven calving, particularly in forming large, tabular icebergs which are often associated with lacustrine calving [e.g. Warren et al., 2001; Van der Veen, 2002]. Measurements of water level and temperature in Mendenhall Lake indicate a possible link between hydrological variables and calving events. Short-term fluctuations in lake level may be important triggers for calving events, at least in cases where the terminus is already approaching instability. A slight increase in buoyant load applied over several days might not be accommodated by ice creep, especially given preexisting weakening due to buoyant upwarping and crevassing.

The ability of temperate lacustrine termini to float reflects the significant differences between lake- and tidewater-calving glaciers. Our results suggest that sublacustrine melting was not an important ablation Mendenhall Glacier during the period of our study. This may also be true at other similar lake-calving termini terminating in small, cold lakes that are predominantly fed by glacial meltwater. Overall, lacustrine termini experience fewer perturbations (e.g. tidal flexure, thermal convection leading to high subaqueous melt rates or undercutting of the ice cliff) and are therefore inherently more stable than tidewater termini. This may explain why the termini of small lake-calving glaciers such as Mendenhall are generally less weakened by crevassing. Thus it is not surprising that lake-calving rates are low, and lacustrine termini are capable of sustaining the generally unstable geometry of a floating temperate terminus in comparison to their tidewater cousins.

If current trends of recession and thinning persist, the calving rate at Mendenhall Glacier may be expected to remain high. The glacier bed remains below lake level at least 500 m behind the present terminus, and if recession continues at the 2000-2005 mean retreat rate of about 60 m a^{-1}, the terminus may recede onto land in a decade.

2.8 Acknowledgments

This work was supported by a grant from the U.S. National Science Foundation, No. OPP-0221307. Field equipment was provided by UNAVCO and VECO Polar Resources. Additional support was provided by the University of Alaska Natural Resource Fund, the Center for Global Change, the USFS Mendenhall Glacier Visitor Center, the Geophysical Institute at the University of Alaska Fairbanks, the Environmental Sciences Program at the University of Alaska Southeast, and by Northstar Helicopters, Inc of Juneau, Alaska. Ed Bueler provided invaluable help in developing the numerical model. Creation of a movie from time-lapse images was supported in part by a grant of HPC resources from the Arctic Region Supercomputing Center, with assistance from Miho Aoki. Field assistance was provided by Jason Amundson, Elsbeth Kuriger, Adam Bucki, Mike Hekkers, Matt Heavner, Eran Hood, and Cathy Connor.

2.9 References

Arendt, A., K. Echelmeyer, W. Harrison, C. Lingle, and V. Valentine (2002), Rapid wastage of Alaska glaciers and their contribution to rising sea level, Science, 297, 382–386.

Arendt, A. A., K. A. Echelmeyer, W. Harrison, C. Lingle, S. Zirnheld, V. Valentine, B. Ritchie, and M. Druckenmiller (2006), Updated estimates of glacier volume changes in the western chugach Mountains, Alaska, USA and a comparison of regional extrapolation methods, Journal of Geophysical Research, in press.

Bøggild, C. E., O. B. Olesen, A. P. Ahlstrøm, and P. Jørgensen (2004), Automatic glacier ablation measurements using pressure transducers, Journal of Glaciology, 50(169), 303–304.

Brown, C. S., M. F. Meier, and A. Post (1982), Calving speed of Alaska tidewater glaciers, with application to Columbia glacier, Tech. rep., US Geological Survey professional paper 1258-C.

Cutler, P., D. Mickelson, P. Colgan, D. MacAyeal, and B. Parizek (2001), Influence of the Great Lakes on the dynamics of the southern Laurentide ice sheet; numerical experiments, Geology, 29(11), 1039–1042.

Echelmeyer, K., W. D. Harrison, T. S. Clarke, and C. Benson (1992), Surficial glaciology of Jakobshavns Isbrae, West Greenland: Part II. Ablation, accumulation and temperature, Journal of Glaciology, 38(128), 169–181.

Echelmeyer, K. A., W. D. Harrison, C. F. Larsen, J. Sapiano, J. DeMallie, B. Rabus, G. Aðalgeirsdóttir, and L. Sombardier (1996), Airborne surface profiling of glaciers: a case-study in Alaska, Journal of Glaciology, 42(142), 538–547.

Elsberg, D., W. Harrison, K. Echelmeyer, and R. Krimmel (2001), Quantifying the effects of climate and surface change on glacier mass balance, Journal of Glaciology, 47(159), 649–658.

Funk, M., and H. Röthlisberger (1989), Forecasting the effects of a planned reservoir that will partially flood the tongue of Unteraargletscher in Switzerland, Annals of Glaciology, 13, 76–80.

Gudmundsson, G. H., G. Aðalgeirsdóttir, and H. Björnsson (2003), Observational verification of predicted increase in bedrock-to-surface amplitude transfer during a glacier surge, Annals of Glaciology, 36, 91–96.

Krimmel, R., and L. Rasmussen (1986), Using sequential photography to estimate ice velocity at the terminus of Columbia Glacier, Alaska, Annals of Glaciology, 8, 117–123.

Larsen, C. F., R. J. Motyka, A. A. Arendt, K. A. Echelmeyer, and P. E. Geissler (to be submitted), Glacier changes in southeast Alaska and contribution to sea level rise, Journal of Geophysical Research, Earth Surface Processes.

Meier, M. F., and A. Post (1987), Fast tidewater glaciers, Journal of Geophysical Research, 92(B9), 9051–9058.

Motyka, R., S. O'Neel, C. Connor, and K. Echelmeyer (2002), Twentieth century thinning of Mendenhall Glacier, Alaska, and its relationship to climate, lake calving, and glacier run-off, Global and Planetary Change, 35, 93–112.

Motyka, R., L. Hunter, K. Echelmeyer, and C. Connor (2003), Submarine melting at the terminus of a temperate tidewater glacier, LeConte Glacier, Alaska, USA, Annals of Glaciology, 36, 57–65.

Naruse, R., and P. Skvarca (2000), Dynamic features of thinning and retreating Glaciar Upsala, a lacrustine calving glacier in Southern Patagonia, Arctic and Alpine Research, 32(4), 485–491.

Nye, J. F. (1965), The flow of a glacier in a channel of rectangular, elliptic or parabolic cross-section, Journal of Glaciology, 5(41), 661–690.

O'Neel, S., K. Echelmeyer, and R. Motyka (2001), Short-term flow dynamics of a retreating tidewater glacier, LeConte Glacier, Alaska, USA, Journal of Glaciology, 47(159), 567–578.

O'Neel, S., K. Echelmeyer, and R. Motyka (2003), Short-term variations in calving of a tidewater glacier: LeConte Glacier, Alaska, USA, Journal of Glaciology, 49(167), 587–598.

Østrem, G., and M. Brugman (1991), Glacier mass-balance measurements — a manual for field and office work, Tech. rep., National Hydrology Research Institute, science Report No. 4.

Paterson, W. S. B. (1994), The Physics of Glaciers, third ed., 480 pp., Pergamon, New York.

Post, A., and R. J. Motyka (1995), Taku and LeConte Glaciers, Alaska: calving speed control of late Holocene asynchronous advances and retreats, Physical Geography, 16, 59–82.

Reeh, N., E. Christensen, C. Mayer, and O. Olesen (2003), Tidal bending of glaciers: a linear viscoelastic approach, Annals of Glaciology, 37, 83–89.

Rignot, E., D. Braaten, S. P. Gogineni, W. B. Krabill, and J. R. McConnell (2004), Rapid ice discharge from southeast Greenland glaciers, Geophysical Research Letters, 31, L10,401.

Trefethen, L. (2000), Spectral Methods in MATLAB, 165 pp., SIAM Press, Philadephia, PA.

Van der Veen, C. J. (1996), Tidewater calving, Journal of Glaciology, 42(141), 375–385.

Van der Veen, C. J. (2002), Calving glaciers, Processes in Physical Geography, 26(1), 96–122.

Venteris, E. R. (1999), Rapid tidewater glacier retreat: a comparison between Columbia Glacier, Alaska and Patagonian Calving Glaciers, Global and Planetary Change, 22, 131–138.

Warren, C., and M. Aniya (1999), The calving glaciers of southern South America, Global and Planetary Change, 22, 59–77.

Warren, C., D. Benn, V. Winchester, and S. Harrison (2001), Buoyancy-driven lacustrine calving, Glaciar Nef, Chilean Patagonia, Journal of Glaciology, 47(156), 135–146.

Warren, C. R., D. R. Greene, and N. F. Glasser (1995), Glaciar Upsala, Patagonia: rapid calving retreat in fresh water, Annals of Glaciology, 21, 311–316.

Chapter 3
Application of a 1-Dimensional Viscoelastic Bending Beam Model to the Buoyant Terminus of Mendenhall Glacier, Southeast Alaska

3.1 Introduction

The bending of a floating ice tongue is an important problem in the study of calving glaciers. Bending stresses may play a key role in the calving of ice from lacustrine and tidewater glaciers. Elastic beam theory can be used to estimate deformation and maximum stress in a floating ice tongue [Reeh, 1968]. If bending stresses exceed the tensile strength of the ice, failure (calving) occurs. Warren et al. [2001] calculated the stresses due to buoyancy using a static model in which ice was not allowed to deform upward. However, they noted that ice creep may accommodate some buoyant stresses if they increase gradually. In order to determine how quickly bending stresses are relaxed by ice creep, we use a viscoelastic beam model. Two aspects are of particular importance: first, the rheology of the ice at a particular temperature and stress state, and second, the rate at which buoyant stresses are applied.

It is thought that temperate tidewater glaciers are unable to sustain floating termini [Meier and Post, 1987]. However, temperate lacustrine termini may locally reach floatation and sustain a partially floating terminus, a situation common to polar tidewater glaciers and ice tongues. This problem may be particularly relevant to the terminus dynamics of Mendenhall Glacier, a rapidly retreating lake-calving glacier in Southeast Alaska. The purpose of this 1-dimensional model is to determine if bending was an important mechanism at Mendenhall Glacier, and to identify other circumstances where floatation of a glacier tongue may be sustained.

3.2 1-Dimensional Viscoelastic Bending Beam Model

This 1-dimensional bending beam model for viscoelastic ice deformation was developed by Reeh et al. [2003] to evaluate the tidal flexure across a floating ice tongue (transverse direction). The same basic equations and constitutive relationship are used here to evaluate the response of a floating ice tongue in the longitudinal direction. Verification of the model is performed by reproducing the results of the tidal flexure case [Reeh et al., 2003] using a different numerical method which captures transient responses as well as oscillatory

behavior.

Ice thickness and surface height may vary along a longitudinal profile. The amount by which the critical thickness (Eq. 2.1) for floatation exceeds the ice thickness will determine the buoyant force acting on the ice tongue. Beam theory is used to derive a set of coupled differential equations which describe the deflection of the ice tongue. For an elastic problem with a uniformly-applied load, these equations can be solved analytically. In the viscoelastic case, the constitutive relationship introduces some time-dependence, such that the resulting system contains 2^{nd} order spatial derivatives as well as 2^{nd} order time derivatives. The derivation of the beam equations themselves will not be addressed in detail, since it is thoroughly addressed by Reeh et al. [2003]. All partial derivatives will be denoted by subscripts: $u_x = \partial u / \partial x$.

3.2.1 Notation

The deflection (in z, the vertical direction) of a floating ice tongue along a longitudinal profile (x) is a one-dimensional problem, given the following simplifications and assumptions (discussed further in 3.3). The bending ice tongue is assumed to have infinite width in the transverse (cross-glacier) direction, y. The coordinates y and z are effectively eliminated from the model. The following notation in Table 3.1 is shown in Fig. 3.1.

Table 3.1. Model notation.

Distance (+ downglacier)	$x \in [0, L]$
Time	$t \in [0, T]$
Water depth	$d(x,t)$
Ice Thickness	$h(x,t)$
Deflection (+ up)	$u(x,t)$
Load (+ up)	$N(x,t)$
Bending Moment	$M(x,t)$
Basal Tensile Stress	σ_{xmax}
Moment of Inertia	$I = \frac{1}{12} h(x,t)^3$

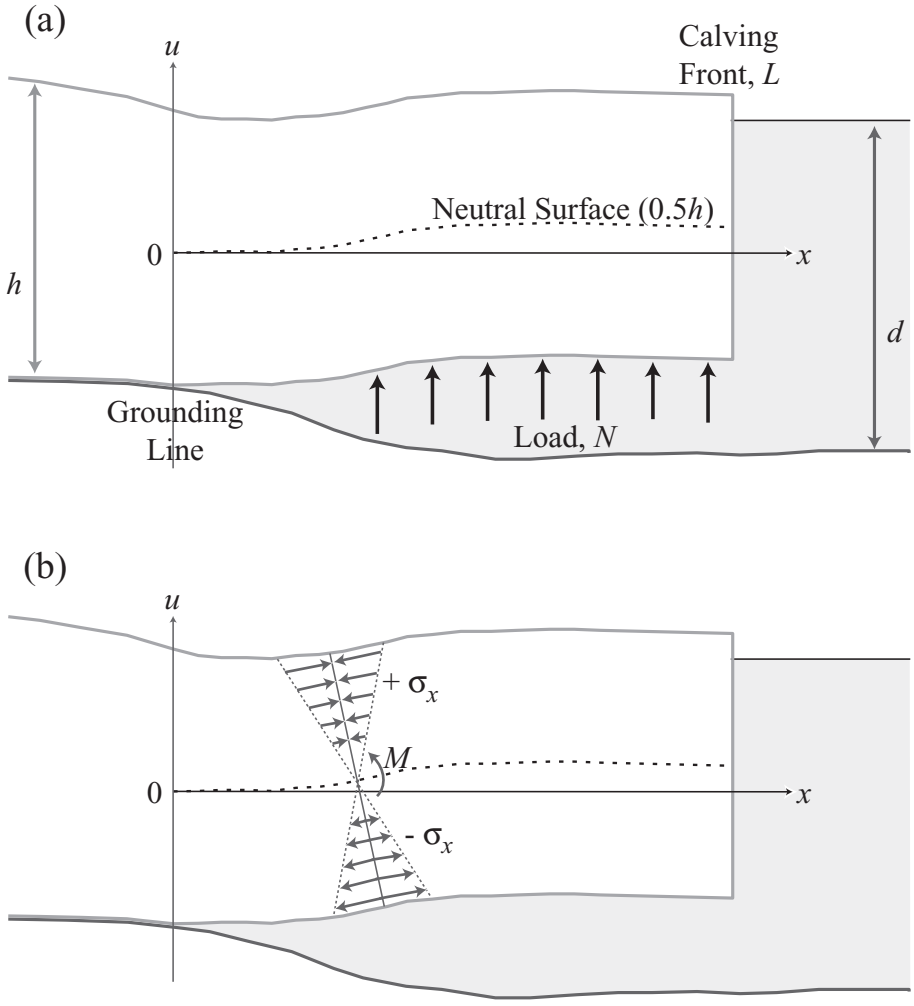

Figure 3.1. (a) Model of an upwardly deflected floating glacier terminus. (b) Torque (M) and longitudinal stresses (σ_X) due to buoyant load [adapted from Warren et al., 2001].

3.2.2 Ice Rheology

Ice is a viscoelastic material therefore strain includes elastic, primary creep, and steady creep components. The linear constitutive relationship given by Reeh et al. [2003] is the simplest rheological model incorporating all of these deformational components. Ice is treated as an incompressible four-element fluid with constant material properties. "Four-element" refers to the four material constants (μ_v, μ_m, E_v,and E_m) used to describe the elastic and viscous response of the ice to stress. The following rheological model is given by Reeh et al. [2003].

$$\varepsilon = \varepsilon_e + \varepsilon_d + \varepsilon_v = \frac{3\sigma'}{2E_m} + \frac{3\sigma'}{2E_v}\left[1 - e^{-\frac{E_v}{3\mu_v}t}\right] + \frac{\sigma'}{2\mu_m}t \tag{3.1}$$

ε is strain, σ' is deviatoric stress, E_M is Young's modulus, E_v and μ_v are elastic modulus and viscosity (associated with primary creep), and μ_M is viscosity associated with steady creep. While all four constants have some dependence on stress and temperature, Reeh et al. [2003] used fixed laboratory-measured values for the first three. According to Reeh et al. [2003] "...the viscosity for steady creep can be expressed as $\mu_M = 1/(2A\tau_e^{n-1})$, where A depends on temperature T, τ_e is effective shear stress and $n \sim 3$ [Paterson, 1994, p. 97 and 259-260]." Reeh et al. [2003, Table 2] calculate the constant μ_M using a shear strain rate derived from the surface velocity profile to estimate effective shear stress for ice at -15°C. We use the same method to obtain a reasonable value of μ_M for the terminus of a glacier such as Mendenhall. From a transverse velocity profile at Mendenhall Glacier terminus, a shear strain rate of 0.23 a^{-1} is calculated, and an effective shear stress of 81 KPa, which is significantly lower than the 250 KPa used by Reeh et al. [2003]). Using an appropriate value of the flow law parameter A [Paterson, 1994, pg.97] for ice at 0 °C yields a viscosity μ_M =11,250 GPa s, compared to 20,000-30,000 GPa s for cold ice at higher effective stress [Reeh et al., 2003]. Each test of the model is run using both sets of constants - warm ice at low effective stress and cold ice at high effective stress (Section 3.6).

Values for these constants are presented in Table 3.2, as well as the densities of water and ice (ρ_w and ρ_i) and the acceleration due to gravity (g).

Table 3.2. Constants used in model.

μ_M ("cold")	$25000 \cdot 10^9$	Pa s
μ_M ("warm")	$11250 \cdot 10^9$	Pa s
μ_v	$600 \cdot 10^9$	Pa s
E_v	$10 \cdot 10^9$	Pa s
E_M	$9.3 \cdot 10^9$	Pa s
ρ_i	917	kg m^{-3}
ρ_w	1000	kg m^{-3}
g	9.81	m s^{-2}

3.2.3 Basic Equations

For a floating beam of ice (e.g. a glacier terminus) the load, or buoyant force, on the beam depends on its deflection from hydrostatic equilibrium.

$$N = \rho_w g(f - u) \tag{3.2}$$

f is an external forcing term that may include variations in water level (such as tides or seasonal variations) or changes in ice thickness (constant thinning or an annual accumulation-ablation cycle). Different types of external forcing are discussed in 3.4.

The balance of force and torque acting on an element of the bending beam is used to derive Eq. 3.3, which relates the transverse load on the beam to the bending moment.

$$M_{xx} = N \tag{3.3}$$

Equations 3.2 and 3.3 are combined to relate the bending moment to the deflection. Note that this relationship has no time derivatives so it is a constraint at all times.

$$M_{xx} = \rho_w g(f - u) \tag{3.4}$$

The relationship between the beam curvature u_{xx} and the bending moment M depends on the constitutive equation for ice (Eq. 3.1). For a linear viscoelastic material deforming by plain strain, Reeh et al. [2003] derive the following equation.

$$I\left(\frac{3\mu_v}{E_v}u_{xxtt} + u_{xxt}\right) = \frac{2.25\mu_v}{E_v E_m}M_{tt} + 0.75\left(\frac{1}{E_v} + \frac{1}{E_m} + \frac{\mu_v}{\mu_m E_v}\right)M_t + \frac{0.25}{\mu_m}M \tag{3.5}$$

Equations 3.4 and 3.5 are coupled partial differential equations. They are solved numerically for various initial conditions, beam geometries, and boundary conditions discussed below. The result is deflection $u(x,t)$ and bending moment $M(x,t)$.

Beam theory can only calculate deflections on the neutral axis of the beam, where the assumption of zero longitudinal stress holds. For a beam of a known thickness, it is possible to estimate the longitudinal stresses at the upper and lower surfaces of the beam. Warren et al. [2001] use the torque, or bending moment M, to calculate tensile stress at the base of the bending beam of ice. Assuming a linear distribution of stress within the beam, with zero stress at the beam axis, maximum basal stress is given by Warren et al. [2001].

$$\sigma_{xmax} = \frac{hM}{2I} \tag{3.6}$$

Positive σ_{xmax} indicates tensile stresses and negative σ_{xmax} compressive stresses.

3.2.4 Boundary and Initial Conditions

The glacier is assumed to be fixed at the grounding line ($x = 0$), therefore deflection and slope are zero at that point: $u(0,t) = 0$ and $u_x(0,t) = 0$. For a vertical calving front, the transverse force acting on the front is zero: $M_x(L,t) = 0$. Applying equations (3.4) and (3.5) for a beam of uniform thickness, this corresponds to the condition on the free end of a cantilever that $u_{xxx}(L,t) = 0$. The other boundary condition for the free end of a cantilever is $u_{xx}(L,t) = 0$. For a beam of non-uniform thickness, both of these cantilever conditions must be true to result in zero transverse force at the free end. Reeh et al. [2003] state an additional condition for the front: "the bending moment of the normal stress deviations from hydrostatic stress, to first order in the deflection $u(L,t)$, equal to

$$M(L,t) = \rho_w g h(L,t)^3 \left[\frac{d_i(1-d_i)(d_i-0.5)}{6} + \frac{d_i(1-d_i)u(L,t)}{2} \right] \ldots'' \tag{3.7}$$

where $d_i = \rho_i/\rho - w$. However, for simplicity we impose the cantilever boundary conditions at the free end. Also for simplicity, initial deflection and velocity are set to zero in all tests: $u(x,0) = 0$ and $u_t(x,0) = 0$.

3.3 Model Assumptions

The model is 1-dimensional and thus cannot capture the complexity of a 3-dimensional glacier terminus. We use a simple model to study a single process in detail - the longitudi-

nal bending of a floating ice tongue under buoyant force. Reeh et al. [2003] acknowledge that modeling bending in the transition zone between grounded and ungrounded ice may be complicated, since bending may be due to buoyant forces and also to bed geometry. However, our intention is not to reproduce the surface geometry of Mendenhall Glacier terminus but to investigate the mechanism of buoyant upwarping for a hypothetical floating ice tongue, ignoring the effect of the bed and margins.

Therefore we consider a bending ice tongue of infinite width and assume plain strain, i.e. there is no deformation in the transverse direction. We solve the model in an Eulerian frame, therefore we ignore the fact that ice is moving through the beam due to regular flow of the glacier. This may introduce some error since in a real case, ice moves across the grounding line and has a finite transit time within the floating area we consider. It is also assumed that the deflection u is small compared to the thickness of the glacier, h, and that the thickness is small compared to the horizontal distance over which deflection occurs, L. This allows us to treat the ice as a thin layer. The assumption of plane strain (from which the Eq. 3.4 is derived) requires this "thin beam" assumption. We also assume ice to be homogeneous, and ignore basal and surface crevassing which may reduce the effective thickness of the bending beam.

3.4 Application of Buoyant Stresses

This viscoelastic model was originally used to determine the response of a floating ice tongue to tides [Reeh et al., 2003]. To approximate the behavior of semi-diurnal tides, the external forcing function takes the form $f = a \sin \omega t$, where a is the tidal amplitude and ω is the tidal frequency. Values of a =0.5 m and $\omega = 2\pi/(12 \text{ hrs})$ were chosen to approximately reproduce the results of the original study.

Our goal was to investigate factors affecting lake-calving termini which do not typically experience tidal-frequency perturbations. We used data from Mendenhall Glacier to create representative forcing functions for a lacustrine system. The floating terminus is considered to have zero deflection in the initial case of hydrostatic equilibrium. Perturbations from equilibrium include:

1. Changes in the water level over time.

2. Changes in the ice thickness over time.

3. Changes in the length of the glacier tongue over time.

We only consider the first two types of perturbations here. Tidal oscillations are obviously an example of changes in water level over time; for a lacustrine system the highest amplitude changes in water level tend to occur on a seasonal time scale. Water level data from Mendenhall Lake (Section 2.4.6) are used to derive the forcing term $f_b = 0.75\cos(2\pi(t + 7/52 \text{ yrs})) + 1.063$, for t in years and f_b in meters. (Fig. 3.2(a)). Water levels are referenced to 0 m on the USGS lake gauge.

Second we consider changes in the ice thickness. Comparison of the ice surface along a laser altimetry profile of Mendenhall Glacier indicated an average thinning of 6 m a^{-1} between 2000 and 2005 (Section 2.5.6). Therefore one test of the model assumes a constant thinning rate of 6 m a^{-1}. Next we consider seasonal variations in the thinning rate which are due to annual accumulation and ablation. An approximate sinusoidal fit to balance rate data is $f_a' = 14\cos(2\pi(t + 2/52)) - 11$, for t in years and f_a' in m a^{-1} (Fig. 3.2(b)). Since this fit to balance data implies an annual surface loss of 11 m, we make a 5 m correction in order to match the actual surface change measured along the altimetry profile. We realize that the profile is not representative of total thinning of the lower glacier, but to test the model we only use changes along a longitudinal transect of the eastern terminus. f_a' is integrated to give the actual forcing term f_a, surface height (in meters) over time. In tests of the model for seasonal variation in load, f_a and f_b are inserted into Eq. 3.4 such that a lowering of lake level ($-f_b$) causes a downward load ($-N$), and thinning of the ice ($-f_a$) causes upward load ($+N$).

3.5 Numerical Solution of the Model

Reeh et al. [2003] assume that the deflection and bending moment will have the same time-dependent behavior as the tidal forcing $a\sin\omega t$, that is, $u = u_S(x)\sin\omega t + u_C(x)\cos\omega t$ and $M = M_S(x)\sin\omega t + M_C(x)\cos\omega t$. They rewrite the problem as a system of ordinary linear differential equations which can be solved by standard numerical integration techniques. We choose to use a different numerical method, one that does not need to presuppose oscillatory solutions at the same frequency as the forcing function.

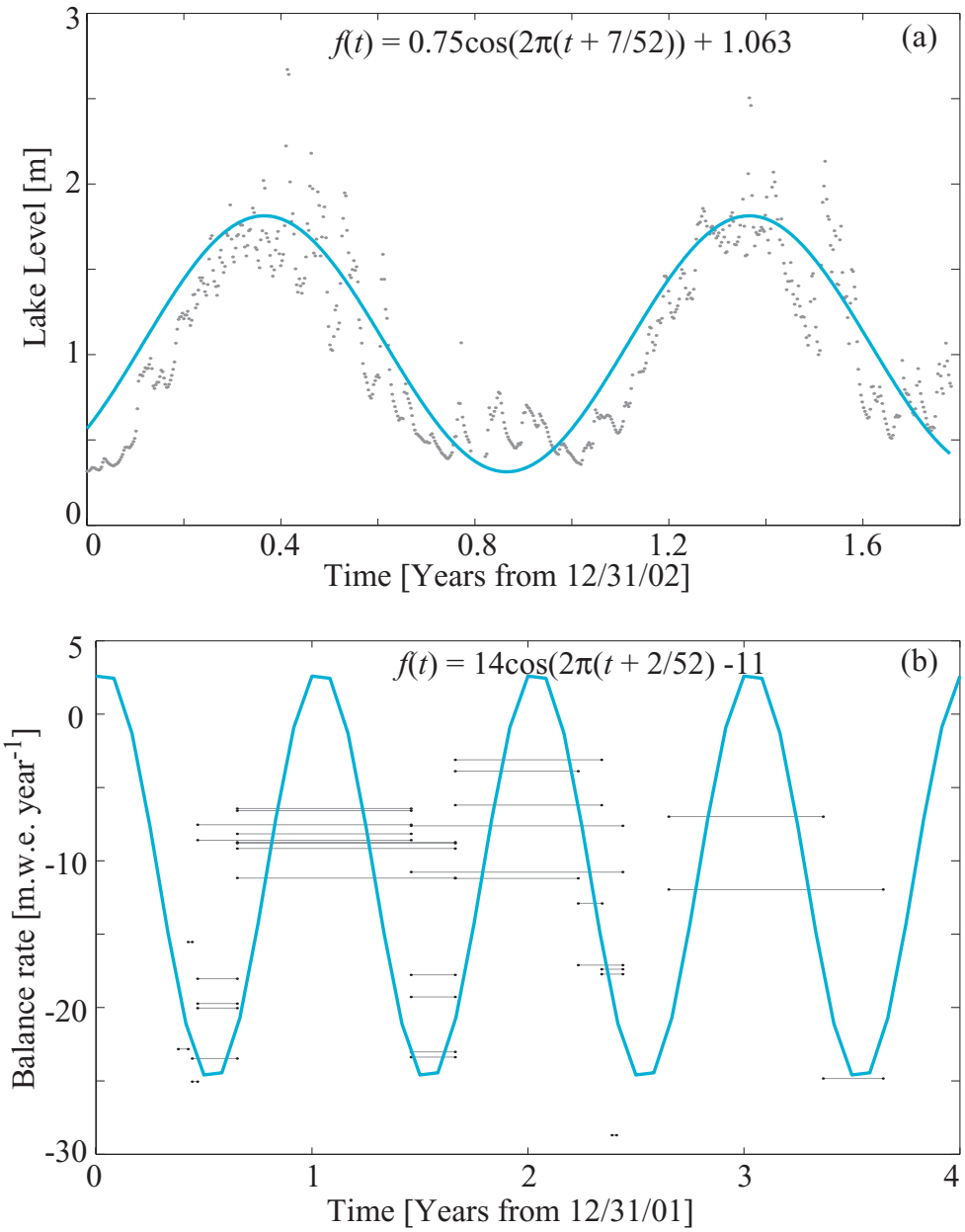

Figure 3.2. Forcing functions for seasonally-varying ice thickness and water level. (a) Approximate fit (blue line) to daily mean lake level (grey dots) over a ~ 2 year period. (b) Balance rates measured at the terminus of Mendenhall Glacier between 2002 and 2005 (grey lines indicate mean balance rate over measurement period), and approximate sinusoidal fit (blue line).

First, Eq. 3.4 and Eq. 3.5 are semi-discretized in time using centered finite difference approximations. A Chebyshev spectral method is used to calculate differentiation matrices in space [Trefethen, 2000, pg.51]. A system of equations is set up, making the appropriate substitutions for boundary conditions and known external forcing. We step forward in time from a known initial condition, solving the system of equations at each time step using MATLAB® built-in matrix inversion. Scripts for the numerical solution are given in Appendix B. Since spectral methods converge quite quickly, we can use a relatively small spatial grid of less than 40 points. The length of the time step is 1 minute for all model tests. This method finds both the transient response and long-term oscillations if such behavior exists. Ice thickness is allowed to vary longitudinally and temporally: $h = h(x,t)$.

3.6 Model Results and Discussion

We present only a few examples of model results. These were chosen for the purpose of showing that the numerical method is accurate and also to illustrate the different types of perturbations discussed above (3.4). In the test cases, we consider a floating ice tongue between the grounding line and a freely floating calving front, with the boundary conditions discussed above (3.2.4). In each case the model will be run twice: once using an appropriate μ_M for "cold" ice at higher effective stress, and one for "warm" ice at lower effective stress (Section 3.2.2). The test geometry is a beam 1000 m in length and a constant 200 m thick, initially at equilibrium. The resulting deflection (u) and maximum basal tensional stress (σ_{xmax}, from Eq. 3.6) are plotted at characteristic times in order to show the long-term surface deformation and accommodation of stress in different parts of the beam. In the assumption of plane strain, surface tensional stress will always be equal and opposite to the basal stress, but we will show only the basal stress.

3.6.1 Tidal Bending

First, we demonstrate that our numerical method is capable of reproducing the results of the tidal flexure case [Reeh et al., 2003]. For an ice tongue 20 km long and 200 m thick, we use only 40 spatial grid points in the numerical approximation. Since the forcing is a semi-diurnal tide, we only run the model for a few tidal cycles in order to see the long-term oscillatory behavior. The results (Fig. 3.3) match those of Figs. 3(a,b) and 4 in Reeh et al.

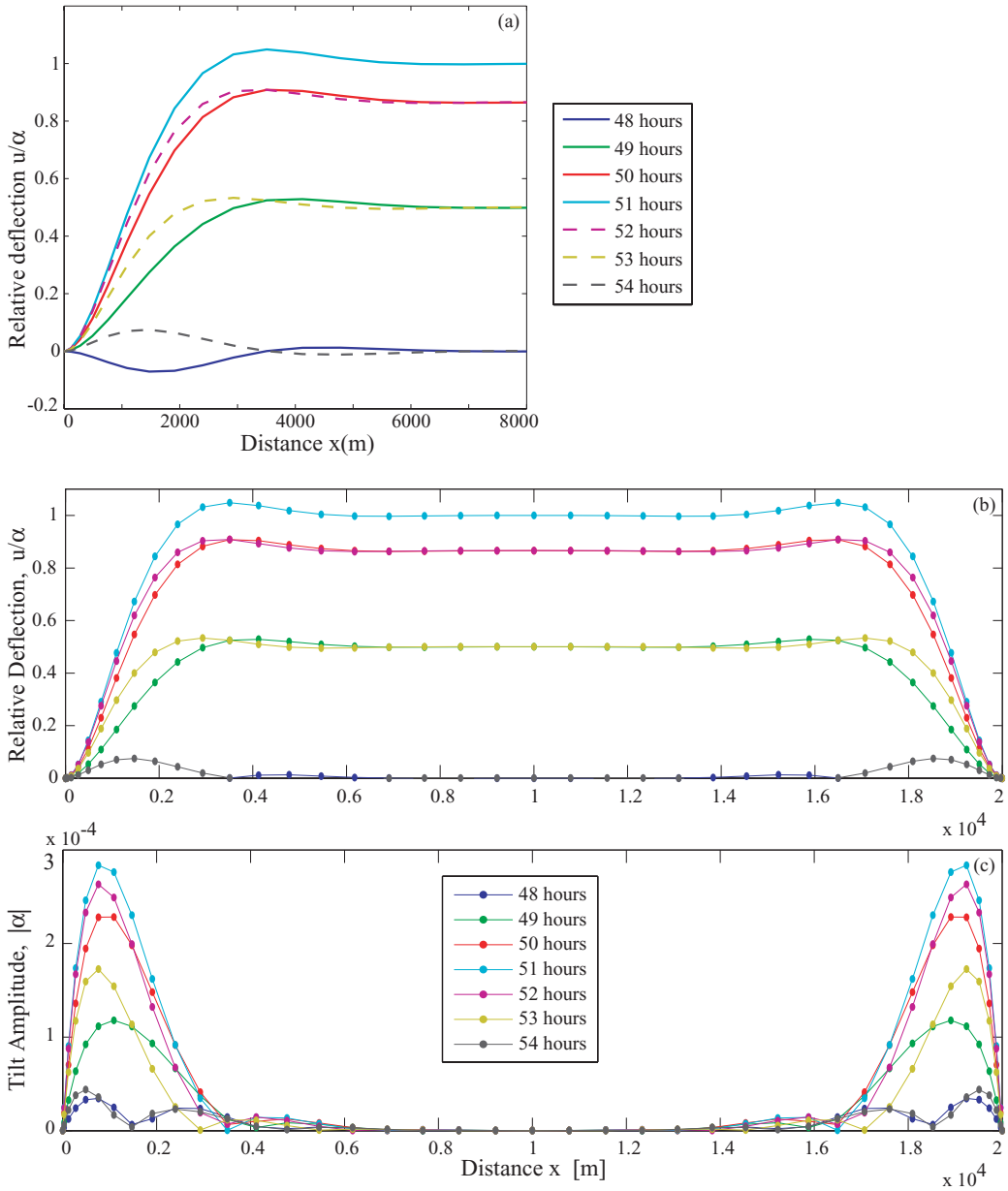

Figure 3.3. Tidal forcing case. (a)Reproduction of Fig. 4 in Reeh et al. [2003]. Tidal deflection curves from the northernmost 8000 m of the transverse profile of the glacier during a half tidal cycle. Rising tide is shown by solid lines and falling tide by dashed lines. (b,c) Reproduction of Fig. 3(a,b) in Reeh et al. [2003]. Tidal deflection and absolute tilt on the transverse profile of Nioghalvfjerdsfjorden glacier. Only results from the viscoelastic model are shown here.

[2003]. Unlike the rest of the model tests, this case has two pinned boundaries with zero deflection and tilt.

3.6.2 Constant Thinning

The first test (Figs. 3.4 and 3.5) uses a constant thinning rate of 6 m a^{-1} as the external forcing term. In both cases, the maximum deflection of just over 12 m (after 2 years) occurs at $\sim$ 400 m, or $\sim$2 ice thicknesses from the grounding line. Maximum basal tensile stress is located at the grounding line in both the "cold" and "warm" cases. The magnitude of the tensile stress in the "cold" beam is greater, while stress is relaxed more quickly in the "warm" beam. Basal compressional stresses are found approximately one ice thickness from the grounding line.

3.6.3 Seasonal Variations

The second test (Figs. 3.6 and 3.7) has two external forcing functions (Fig. 3.2). The water level has an annual cycle, peaking in late summer and dropping over the winter to a minimum between December and March. Thickness changes also undergoes an annual cycle with mass gain in winter and greater mass loss over the melt season, with a net thinning of 6 m a^{-1}, the same amount used in the constant thinning test. The tests are started in January, therefore their initial response is to rising lake level during the first several months. The elevated water level negates the effect of ice thickening during the early part of the year. Through the summer water levels drop and ablation causes thinning, producing peak deflections of 10 m during the first summer and 28 m during the second summer. The deflection curves for "cold" and "warm" ice are again very similar, as in the constant thinning case. During the winter (t =1.0, 2.0 years) low water levels and increased ice thickness cause negative deflections. These are lower in amplitude than the positive peaks. It should be noted that in the case of a real glacier tongue which is barely at floatation, these negative deflections would not be possible since ice would become grounded. However for the theoretical model test we allow all possible deflections.

During the first summer, positive deflections correspond to maximum basal tensile stresses of around 350 KPa in the "cold" ice and around 250 KPa, in the "warm" ice. The

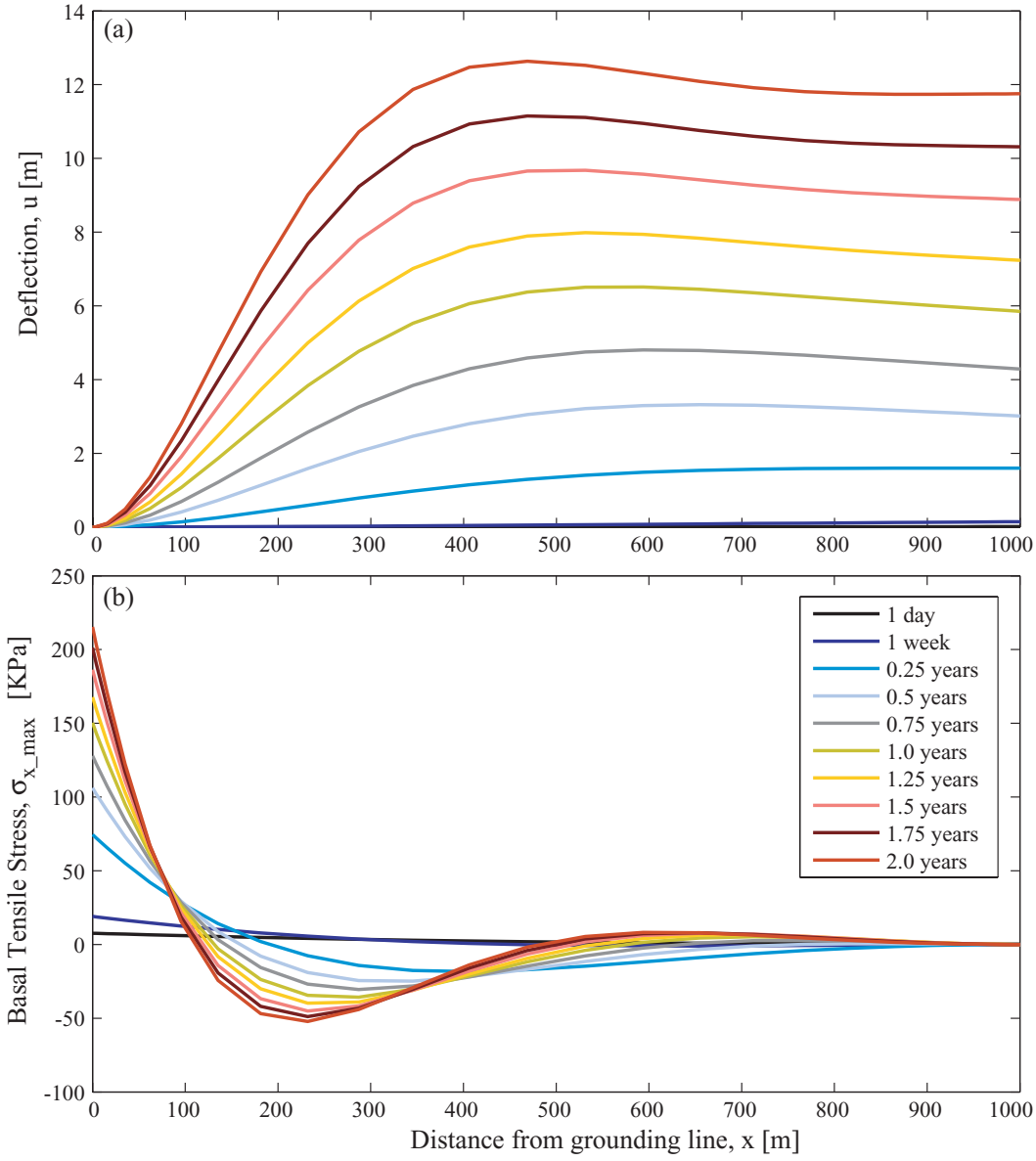

Figure 3.4. Constant thinning of a "cold" beam of ice. (a) Deflection over a two year period. (b) Basal tensile stress over a two year period.

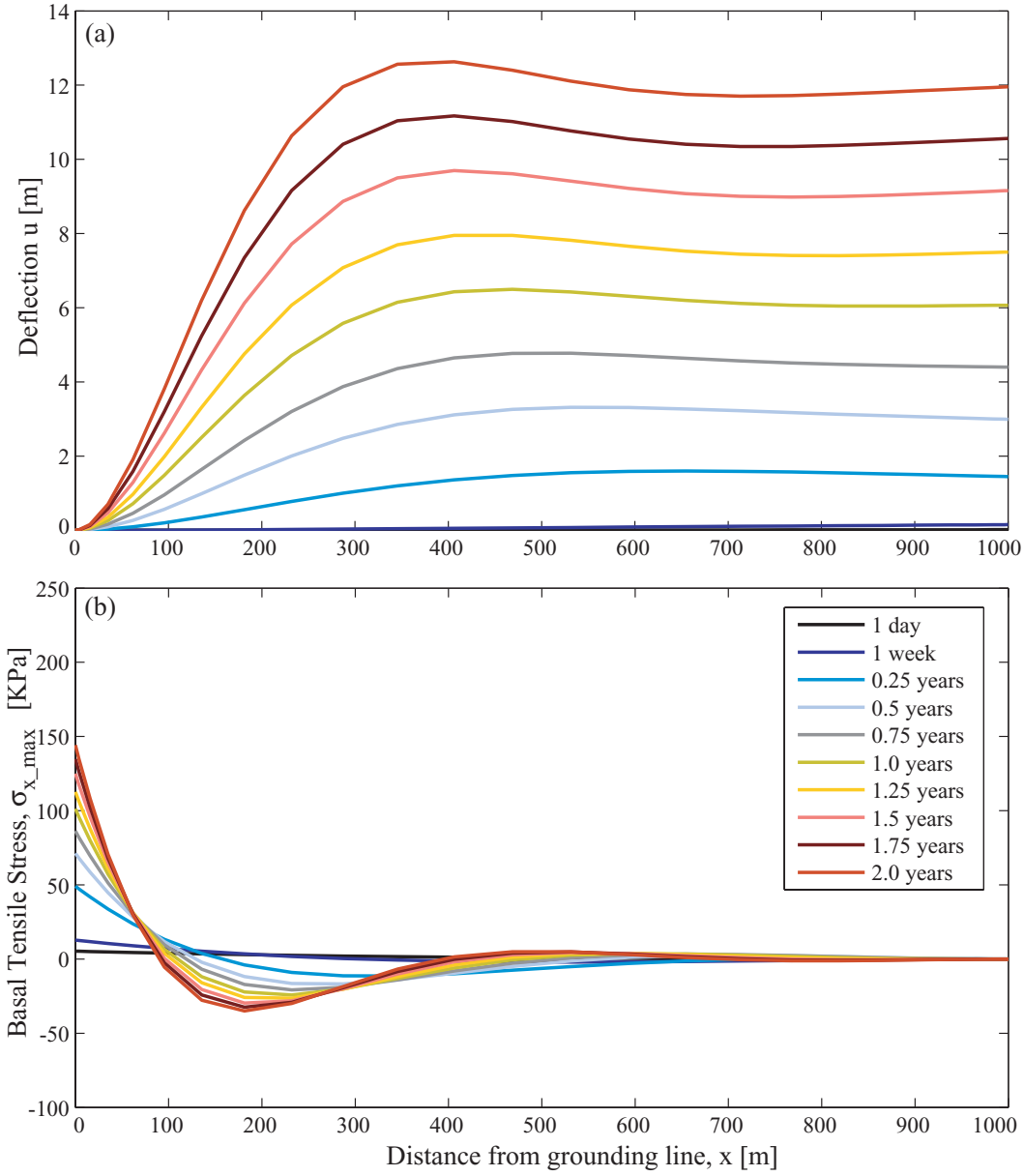

Figure 3.5. Constant thinning of a "warm" beam of ice. (a) Deflection over a two year period. (b) Basal tensile stress over a two year period.

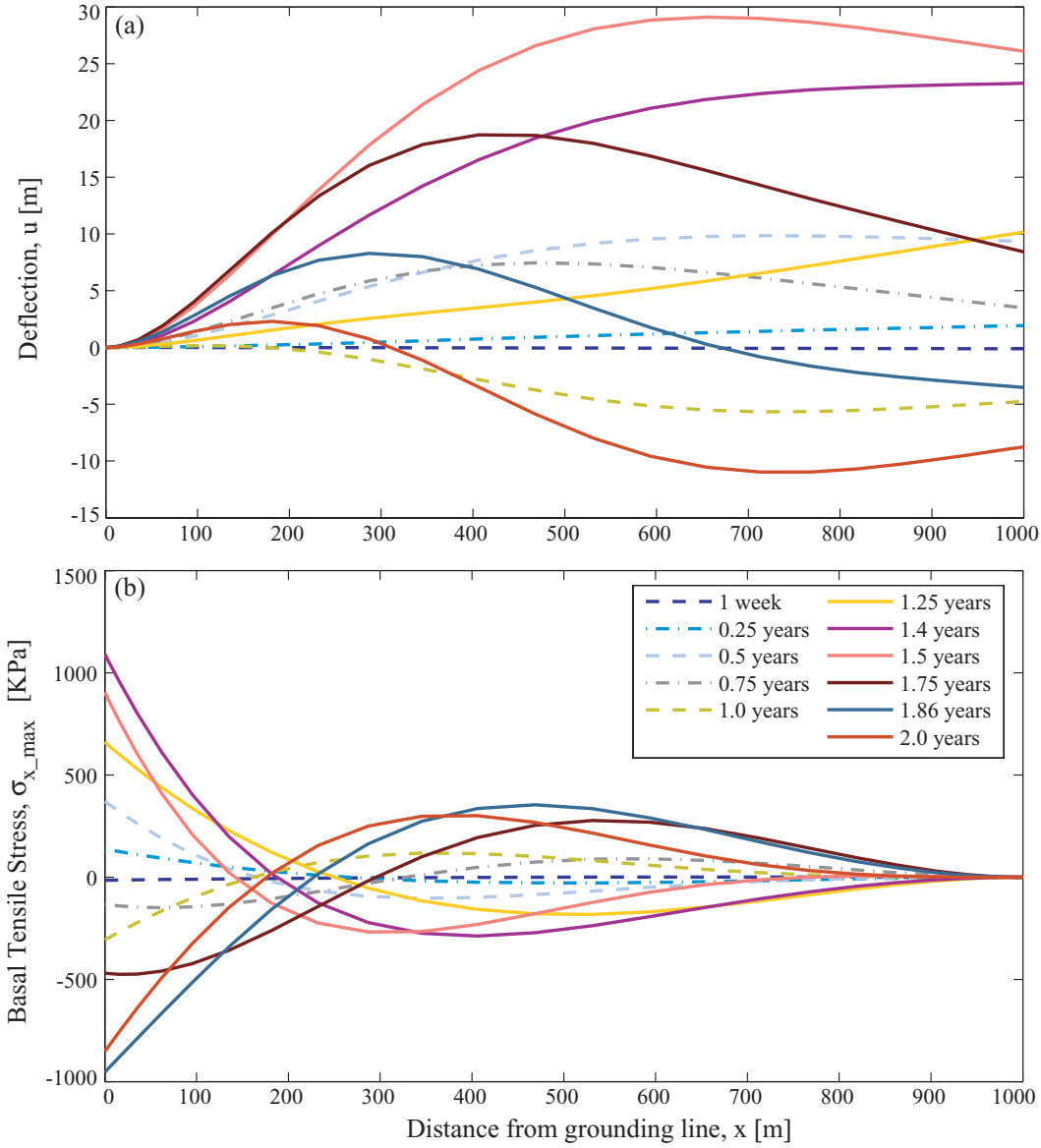

Figure 3.6. Seasonally-variable thinning and water level, "cold" ice. Dashed lines indicate the first year, solid lines the second year. (a) Deflection over a two year period. (b) Basal tensile stress over a two year period.

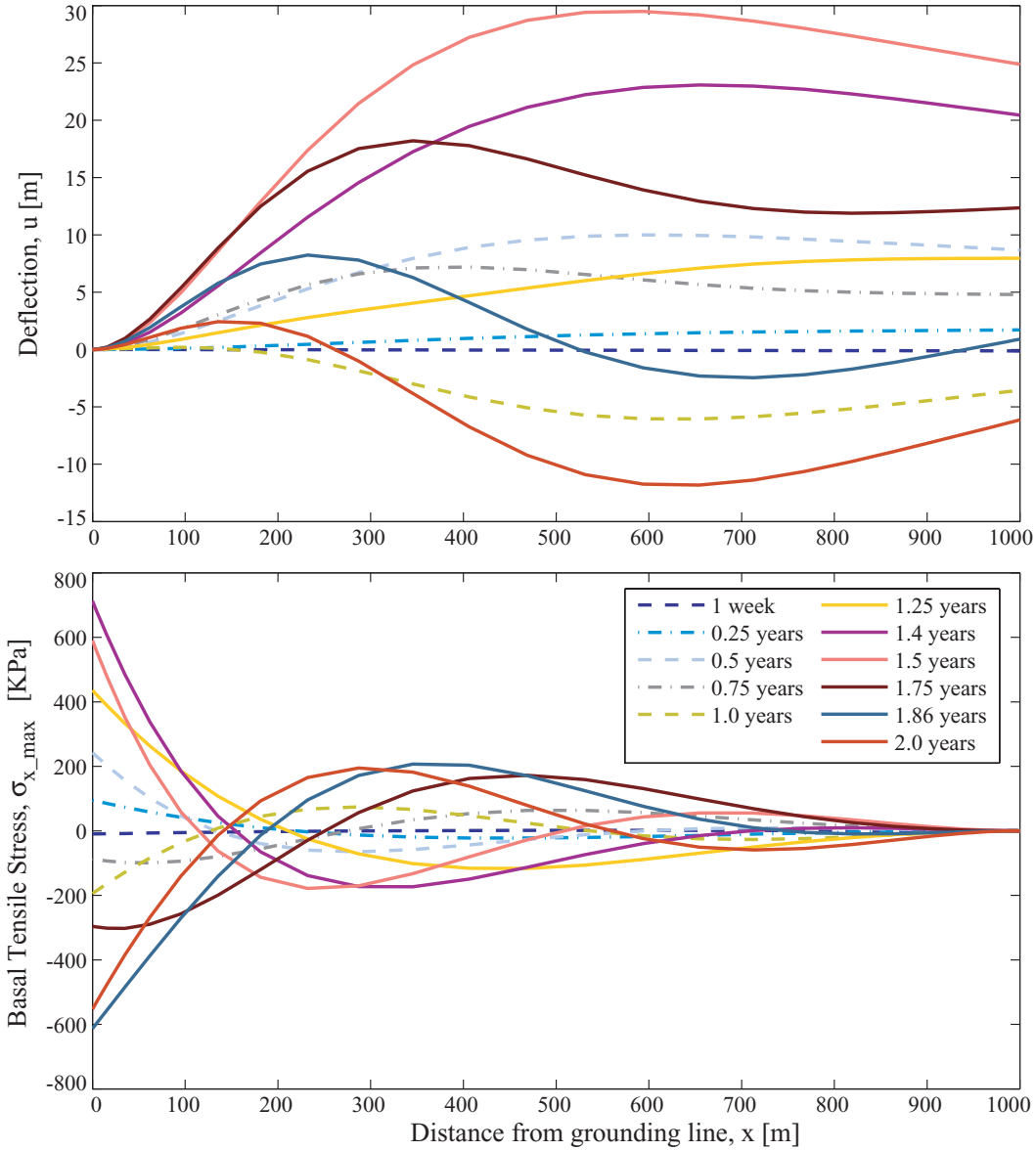

Figure 3.7. Seasonally variable thinning and water level, "warm" ice. Dashed lines indicate the first year, solid lines the second year. (a) Deflection over a two year period. (b) Basal tensile stress over a two year period.

location of the maximum tensile stress is always at the grounding line. However, it is at the base of the beam during periods of upward deflection (between the start of the model run and mid July during the first year, and between mid-January and mid-July in subsequent years) and at the surface of the beam during periods of negative deflection (between mid-July and mid-January). The greater amplitude stresses are always found in the "cold" beam and are approximately 1.5$\times$ those in the "warm" beam. Over the second summer, thinning and high lake levels cause even greater upward deflection than in the first year. Maximum tensile stresses are approximately 3$\times$ greater at 1.5 years (second summer) than at 0.5 years (first summer).

3.6.4 Seasonal Variations of a Short Terminus

The third test shows the results of the bending beam model when applied to a Mendenhall-like geometry (Figs. 3.8 and 3.9). The geometry uses actual bathymetric data from Mendenhall Lake and assumes an ice surface barely at floatation. Length is $\sim 3\times$ ice thickness, therefore the "thin" beam approximations do not hold. While the behavior is similar to the seasonally varying test discussed above (3.6.3), the model greatly over-estimates the deflections and stresses that could actually occur in a real glacier terminus. Even for "cold" ice, the model predicts that basal tensile stresses will exceed overburden stress within two years. In the "warm" case, even though stresses are lower the model predicts deflections on the scale of the ice thickness (which also violates this small deflection assumption). We can clearly see why the model results cannot be compared to the actual geometry of Mendenhall Glacier terminus.

3.7 Conclusions

The results of the model tests indicate conditions under which floating temperate glacier termini may be stable. First, thinning rates must not be too high. For a net thinning of 6 m a^{-1}, unresolved stresses could exceed the tensile stress after two years. Also, it is important that water levels only fluctuate within a small range, and do so over seasonal time scales. Short-term variations in water level may increase bending stresses too quickly to be accommodated by ice creep.

We have developed a useful tool for investigating the effect that thinning may have

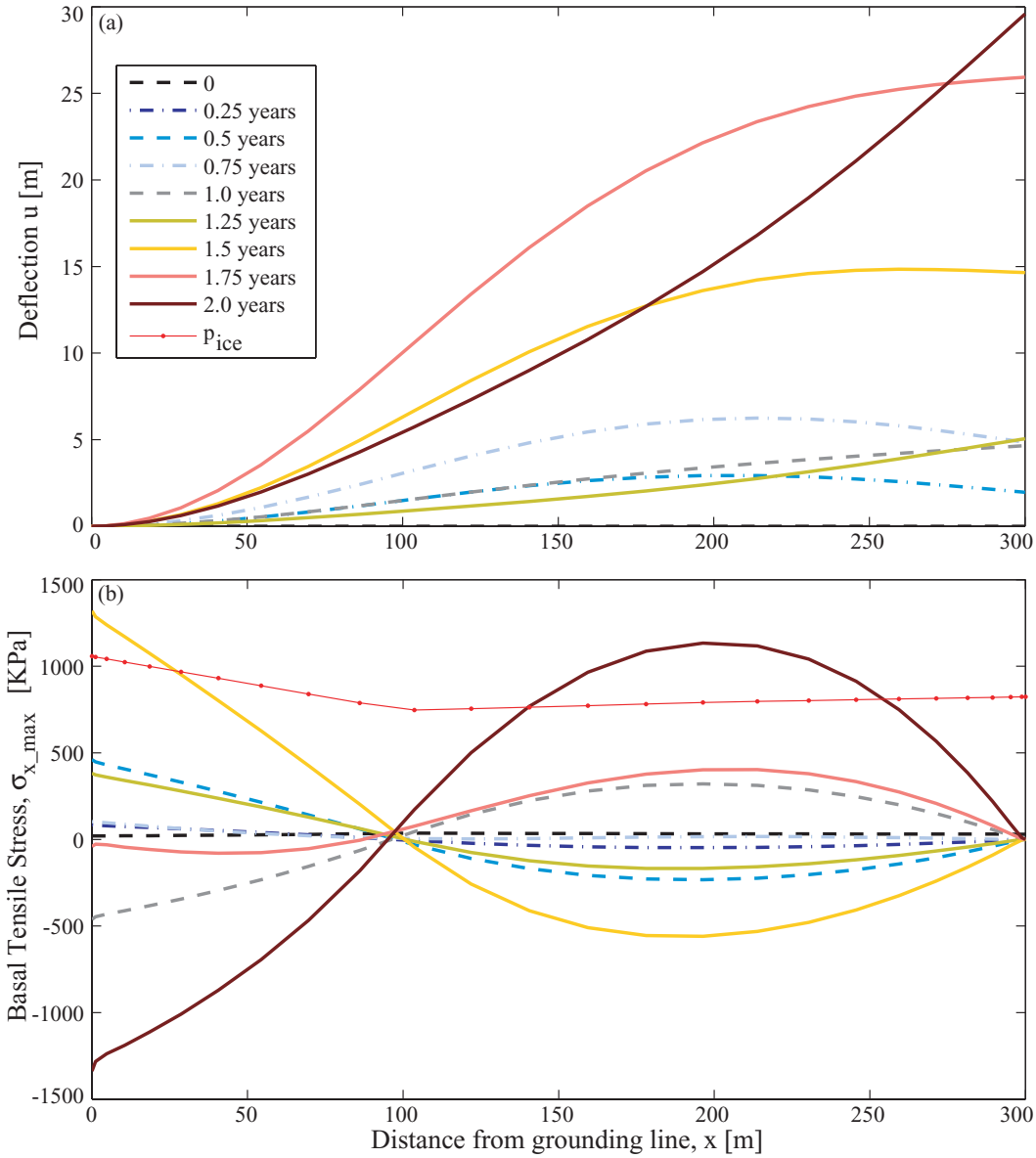

Figure 3.8. Seasonally variable thinning and water level, "cold" ice with Mendenhall-like geometry. (a) Deflection over a two year period. (b) Basal tensile stress over a two year period.

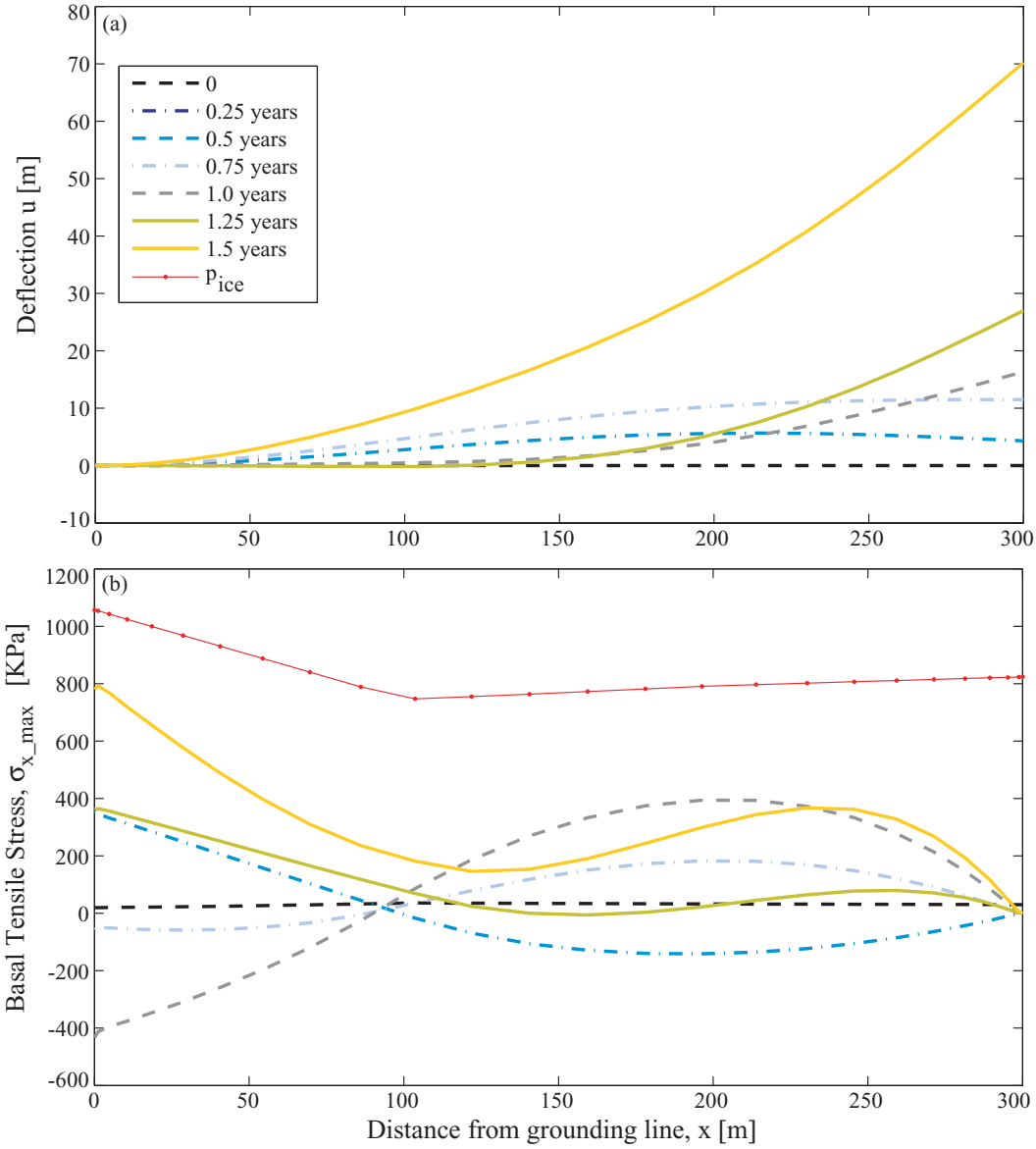

Figure 3.9. Seasonally variable thinning and water level, "warm" ice with Mendenhall-like geometry. (a) Deflection over a two year period. (b) Basal tensile stress over a two year period.

on a glacier tongue that is close to floatation. However, we can see from the results that care must be taken in selecting an appropriate initial geometry when a bending beam type model is applied. The model was found to be unsuited to small calving termini such as Mendenhall Glacier, because we cannot make the "thin ice" assumption. At Mendenhall Glacier, the length of the terminus which reached floatation was at most $1.5\times$ the ice thickness and terminus behavior varies greatly across its width. Still the model is useful in explaining the underlying physical processes which may affect the terminus.

The ideal application would be to a large lake-calving glacier that achieves floatation across most of its width and has a less complicated bed geometry than Mendenhall (e.g. Glaciar Nef, Glacier Upsala, Bering Glacier/Vitus Lake). The model could also be applied to outlet glaciers and polar tidewater glaciers to investigate tidal flexure, response to basal melting, or response to rapid thinning. It could also be used as a verification tool for more complicated models in their thin beam limits.

3.8 References

Meier, M. F., and A. Post (1987), Fast tidewater glaciers, Journal of Geophysical Research, 92(B9), 9051–9058.

Paterson, W. S. B. (1994), The Physics of Glaciers, third ed., 480 pp., Pergamon, New York.

Reeh, N. (1968), On the calving of ice from floating glaciers and ice shelves, Journal of Glaciology, 7(50), 215–232.

Reeh, N., E. Christensen, C. Mayer, and O. Olesen (2003), Tidal bending of glaciers: a linear viscoelastic approach, Annals of Glaciology, 37, 83–89.

Trefethen, L. (2000), Spectral Methods in MATLAB, 165 pp., SIAM Press, Philadephia, PA.

Warren, C., D. Benn, V. Winchester, and S. Harrison (2001), Buoyancy-driven lacustrine calving, Glaciar Nef, Chilean Patagonia, Journal of Glaciology, 47(156), 135–146.

Chapter 4
Conclusions

As the title suggests, this thesis has discussed the instability of a retreating lake-calving glacier. However, although there are factors that may lead to instability at a lacustrine terminus, there is also a period of surprising stability. How was the glacier able to sustain a terminus so close to floatation for so long? In the case of Mendenhall Glacier it seems very likely that the margins and glacier bed provide additional backpressure on the terminus. This supports previous ideas, such as the suggestion by A. Post that temporary floatation of lake-calving glaciers may occur while lateral or bottom topography provides stability [pers. comm. to Warren et al., 2001]. This thesis concentrates on a different potential stabilizing factor, namely, that viscoelastic deformation is capable of accommodating buoyant stresses before they induce calving - but only to a point. Eventually, the threshold of instability is reached, and small perturbations cause large-scale calving.

4.1 Summary of Results

At Mendenhall Glacier, long-term thinning caused narrowing and retreat of the terminus. By 2000, the terminus was poised to retreat into an overdeepening. Continued thinning and retreat left the eastern part of the terminus vulnerable to buoyant forces by 2002. Between 2002 and early 2004, partial floatation of the terminus caused dramatic changes in terminus geometry. The retreat rate decreased, possibly due to stabilization by bed topography increased backpressure as ice flow was directed toward the eastern margin. During this period, viscoelastic deformation may have played a strong role in accommodating seasonal fluctuations in buoyant forces.

By spring 2004, the eastern terminus had reached some threshold for instability. Perhaps accumulated damage and crevassing had weakened the ice, or the upward deflection of the terminus finally caused bending stresses to exceed the tensile strength of the ice. At that point, only slight additional deflections from equilibrium were required to cause failure. It seems likely that small, rapid rises in lake level were the final trigger for calving events during summer 2004. In a more stable geometry, the terminus might not have been affected by small rises in water level, indeed it seems it was not strongly affected during 2002 or 2003.

The model of viscoelastic bending shows that if buoyant load is continuously increased at a low rate, ice creep will accommodate much of the bending stress. As ice becomes thinner and deflections are greater, unresolved stresses increase. This buildup of unresolved stress would eventually result in an unstable terminus. Steady creep cannot quickly accommodate sudden increases in the buoyant load and calving will occur. In an idealized model of a glacier tongue, the basal tensile stress first exceeds the tensile strength; therefore basal crevassing could be the mechanism by which the ice tongue finally breaks. Actual glacier tongues have preexisting zones of weakness, and these may act as both hinge lines and fracture lines. While calving events at Mendenhall Glacier often occur at existing transverse crevasses, it is not clear whether these crevasses were formed under the same stress field as the upward deflection of the calving front.

The numerical model is included not for the purpose of comparing exact model results to Mendenhall Glacier. As stated in the text, it should be viewed as a conceptual model that helps explain the underlying mechanism of deformation and failure of a floating ice tongue under bending stress.

As stated in the introduction, this is a case study of a lake-calving glacier. The results clearly show that while the retreat of Mendenhall Glacier is the result of long-term thinning, recent acceleration of the retreat is not indicative of short-term changes in climate. Rather it is due to increased calving rates as the glacier retreats into a deeper basin in Mendenhall Lake. If current trends of recession and thinning persist (at the 2000-2005 rates), the terminus may recede onto land within one decade.

Mendenhall Glacier is popular destination for Alaskans and tourists alike - according to the US Forest Service Visitor Center, the glacier is viewed by more than a quarter million people every year. It is also one of the most accessible glaciers in southeast Alaska for glaciological research. This thesis contributes up-to-date knowledge on the current state and recent behavior of Mendenhall Glacier. It also continues a long history of research on the glacier, and lays groundwork for future studies.

4.2 Future Research Questions

I believe the most important direction for future research is a continued long-term monitoring program of Mendenhall Glacier. There are opportunities for more detailed studies

of ice dynamics, microclimate, mass balance, and glacier hydrology. For the next ten years or so, continued studies of the lacustrine terminus could greatly contribute to knowledge of lake-calving and how it differs from tidewater calving. This may be a small calving glacier in Alaska, but a good explanation of the mechanisms responsible for its behavior can be applied to other lake-calving glaciers as well as tidewater glaciers, polar ice streams, and even the retreat of continental ice sheets.

The 1-dimensional viscoelastic bending beam model could be applied to other floating termini, such as polar tidewater glaciers and ice tongues, or the large lake-calving glaciers of Patagonia. Here in Alaska, it has potential applications at Bering Glacier, which exhibits a similar style of terminus breakup albeit on a much larger scale than Mendenhall Glacier.

4.3 References

Warren, C., D. Benn, V. Winchester, and S. Harrison (2001), Buoyancy-driven lacustrine calving, Glaciar Nef, Chilean Patagonia, Journal of Glaciology, 47(156), 135–146.

Appendix A

Appendix: Survey data

Poles, wires, magnets and other temporary markers have been used to measure velocity and mass balance on Mendenhall Glacier. These markers are surveyed one or more times per year using differentially-corrected GPS. Data are post-processed for increased accuracy. Wire and velocity marker positions from 2002-2003 have an estimated accuracy of $\pm$10cm. Positions from 2004-2005 have an estimated accuracy of $\pm$5cm. Magnet positions are only accurate to within $\pm$1m for all years. Positions are given in Table A.1, and these data were used to calculate the velocities given in Tables A.2 and A.3.

Table A.1: Ablation poles, wires, magnets, and velocity marker positions on Mendenhall Glacier from 2002-2005. All times are given in local time (Alaska Standard Time or Alaska Daylight Time). Horizontal and vertical positions are referenced to the WGS-84 ellipsoid. W=ablation wire, P=mass balance pole, M=magnet, V=velocity marker

Site	Date	Type	Northing	Easting	HAE
AblMet	5/8/04 20:04	W	6477592.84	526290.20	120.56
AblMet	6/10/04 11:02	W	6477582.25	526288.53	116.94
CL2_04	5/9/04 18:28	W	6478825.78	526947.64	328.18
CL2_04	8/24/04 14:12	W	6478864.61	526998.94	317.78
CL2_04	5/16/05 19:16	W	6478773.45	527006.45	312.47
CL2_04	8/24/05 16:25	W	6478737.30	527008.57	302.19
CL2_05	5/16/05 19:34	W	6478772.27	527009.88	312.09
CL2_05	8/24/05 16:44	W	6478735.82	527012.03	301.65
FG1	5/10/04 13:04	V	6483890.11	526670.91	695.09
FG1	8/24/04 15:27	V	6483851.28	526698.33	685.48
FG-1	5/10/04 10:46	V	6483657.71	526276.45	707.97
FG-1	8/24/04 17:17	V	6483619.18	526303.08	699.76
FG2	5/10/04 13:10	V	6484016.12	526888.35	689.03
FG2	8/24/04 15:52	V	6483980.56	526914.42	680.57
FG-2	5/10/04 11:13	V	6483523.01	526051.78	706.80
FG-2	8/24/04 17:40	V	6483493.16	526071.98	698.66
FG3	5/10/04 12:46	V	6484200.86	527208.34	695.18
FG3	8/24/04 16:18	V	6484181.55	527222.74	688.67
FG-3	5/10/04 11:46	V	6483468.22	525658.30	714.87

Table A.1: Continued

Site	Date	Type	Northing	Easting	HAE
FGCL_04	8/24/04 16:54	W	6483739.35	526512.74	694.59
SB1_2003	8/25/04 14:33	M	6487457.67	535424.57	1357.07
SB1_2004	8/25/04 14:03	M	6487682.91	535458.31	1373.27
SB1B_04	8/25/04 15:28	W	6487019.88	533745.63	1250.48
Bench_02	4/7/02 11:39	W	6477471.34	526356.13	126.93
Bench_02	5/19/02 14:51	W	6477456.51	526355.35	125.86
Bench_02	6/5/02 13:15	W	6477450.89	526354.75	124.64
Bench_02	6/21/02 13:25	W	6477446.14	526354.02	122.43
Bench_02	8/27/02 14:54	W	6477424.44	526353.64	116.51
Bench_02	6/17/03 16:46	W	6477342.15	526360.58	108.07
Bench_03	3/8/03 15:33	W	6477372.03	526357.34	112.41
Bench_03	6/17/03 16:55	W	6477340.76	526360.98	108.14
Bench_03	9/5/03 16:07	W	6477317.70	526363.80	100.82
Bench_03	5/8/04 14:28	W	6477253.18	526373.66	96.97
Bench_04	5/8/04 16:10	W	6477575.42	526416.63	124.51
Bench_04	6/10/04 12:02	W	6477564.52	526414.62	120.84
Bench_04	8/26/04 15:28	W	6477541.23	526410.57	108.28
Bench_04	5/15/05 12:41	W	6477471.69	526405.31	97.77
Bench_05	5/15/05 13:35	W	6477581.70	526335.46	112.00
Bench_05	8/23/05 12:29	W	6477553.81	526331.73	98.79
Bob_02	8/28/02 14:44	W	6480652.37	526887.75	454.37
Bob_02	6/17/03 17:59	W	6480606.57	526825.41	452.53
Bob_02	8/31/03 9:08	W	6480594.56	526809.97	447.40
Bob_03	8/31/03 9:42	W	6480637.44	526856.40	451.19
Bob_03	8/24/04 11:21	W	6480583.93	526783.71	442.62
Bob_04	5/9/04 17:03	W	6480600.39	526806.26	451.53
Bob_04	8/24/04 12:18	W	6480657.72	526924.87	449.09
Bob_04	5/16/05 17:46	W	6480617.53	526871.83	448.40
Bob_05	5/16/05 18:27	W	6480620.61	526872.30	448.79
Bob_05	8/26/05 12:46	W	6480604.53	526851.14	441.65
Bob_05b	8/26/05 13:14	W	6480729.07	527001.25	448.18
Cairn02	3/24/02 12:13	V	6476786.68	526573.14	27.44
Cairn02	6/21/02 11:18	V	6476789.43	526752.73	33.90
Cairn02	8/27/02 13:36	V	6476780.70	526757.67	32.54
Cairn02	3/8/03 14:38	V	6476761.85	526767.59	35.02

Table A.1: Continued

Site	Date	Type	Northing	Easting	HAE
Cairn03	3/8/03 15:16	V	6476761.90	526767.57	35.00
CL1_02	8/28/02 16:30	P	6483631.25	526620.25	695.67
CL1_02-03	8/31/03 11:10	P	6483499.80	526709.84	686.06
CL1_03	8/24/04 18:39	W	6483371.30	526792.77	677.61
CL1_04	8/24/04 18:09	W	6483743.55	526508.02	695.33
CL1_04	8/24/05 18:10	W	6483615.50	526597.15	686.12
CL1_05	8/24/05 19:18	W	6483620.21	526597.67	686.52
CL2_02	8/28/02 17:44	P	6478889.92	526916.15	334.44
CL2_02	8/31/03 13:06	P	6478747.83	526924.49	320.13
CL2_03	8/31/03 13:54	P	6478915.97	526940.08	332.07
CL2_03	8/24/04 12:54	W	6478784.31	526951.32	316.05
CL2_05b	8/24/05 17:20	W	6478739.96	527000.13	303.35
Divide04	5/6/04 9:41	W	6491027.31	534513.61	1569.52
Divide05	5/13/05 14:02	W	6491028.27	534478.72	1568.44
Divide05	9/3/05 11:03	W	6491017.51	534476.01	1562.67
Divide2002	9/2/02 12:57	M	6491113.35	534507.88	1569.06
Divide2002	8/25/04 12:15	M	6491053.27	534493.65	1564.41
Divide2003	8/25/03 12:02	M	6491109.89	534503.37	1568.66
Divide2004	8/25/04 8:46	M	6491017.15	534510.89	1562.85
Divide2004	8/25/04 12:38	M	6491080.66	534495.29	1565.33
Divide2004	9/3/05 11:30	M	6490985.07	534502.19	1561.30
Divide2005	9/3/05 11:17	M	6491014.34	534511.49	1562.58
FGCL_02	8/28/02 15:31	V	6483651.11	527124.40	680.98
FGCL_04	5/10/04 13:29	V	6483778.96	526485.21	703.17
LkEast02	6/21/02 10:41	W	6476869.75	526775.76	32.54
LkEast02	8/27/02 16:03	W	6476861.59	526779.82	29.98
LkEast02	3/8/03 13:48	V	6476843.84	526788.24	29.52
LkEast02	6/17/03 11:07	W	6476835.32	526792.25	27.83
LkEast03	3/8/03 13:55	V	6476844.82	526787.65	30.44
LkEast03	6/17/03 11:19	W	6476836.04	526791.28	27.86
LkEast03	8/31/03 8:56	W	6476826.10	526797.61	26.06
LkEast03	3/25/04 17:20	W	6476808.46	526809.72	23.15
LkEast03	5/4/04 16:16	W	6476804.93	526812.23	21.59
LkEast03	6/9/04 16:57	W	6476803.54	526815.18	20.56
LkLow02	5/19/02 16:01	V	6476740.21	526768.62	38.30

Table A.1: Continued

Site	Date	Type	Northing	Easting	HAE
LkLow02	6/5/02 12:04	V	6476738.88	526769.33	36.56
LkLow02	6/12/02 15:34	V	6476737.88	526770.41	36.29
LkLow02	6/21/02 11:55	V	6476736.75	526769.64	36.88
LkUpp02	5/19/02 16:28	V	6476934.17	526765.96	43.02
LkUpp02	6/5/02 12:45	V	6476931.94	526766.27	41.63
LkUpp02	6/12/02 15:52	V	6476930.35	526766.50	40.61
LkUpp02	6/21/02 12:47	V	6476930.27	526765.65	39.88
LkUpp02	6/21/02 10:06	V	6476930.30	526765.64	39.92
LkUpp02	8/27/02 16:37	W	6476921.65	526768.53	35.79
LkUpp02	3/8/03 14:14	V	6476903.78	526775.16	34.16
LkUpp02b	8/27/02 0:00	W	6476921.65	526768.53	35.79
LkUpp02b	3/8/03 15:42	V	6476903.82	526775.23	34.15
LkUpp02b	6/17/03 11:33	W	6476894.01	526780.39	29.90
LkUpp02b	8/31/03 9:33	W	6476885.59	526788.43	27.27
LkUpp03	6/17/03 14:17	W	6476893.26	526781.16	29.93
LkUpp03	8/31/03 10:41	W	6476885.53	526788.46	27.20
LkUpp03	3/25/04 16:46	W	6476866.51	526810.59	25.29
LkUpp03	6/9/04 16:26	W	6476861.63	526815.21	22.43
LkWest02	6/21/02 11:45	W	6476927.59	526686.75	32.28
LkWest02	8/27/02 16:20	W	6476916.27	526691.41	27.94
LkWest03	8/31/03 10:21	W	6476871.47	526709.46	20.81
LkWest03	3/25/04 16:05	W	6476845.42	526729.04	21.69
LkWest03	5/4/04 15:47	W	6476840.01	526733.56	20.97
LkWest03	6/9/04 13:35	W	6476835.45	526737.55	20.98
LkWest04	5/5/04 13:34	W	6476852.66	526746.56	21.52
LkWest04	6/9/04 13:35	W	6476848.23	526750.95	20.50
NB1_04	5/6/04 17:53	W	6489767.11	531749.41	1211.48
NB1_04	8/25/04 16:19	M	6489765.37	531722.59	1203.26
NB1_05	5/13/05 11:13	W	6489690.26	531761.66	1208.31
NB1_05	9/3/05 13:29	W	6489688.20	531734.24	1201.01
NB1_2002	9/2/02 15:43	M	6489676.26	531715.75	1206.51
NB1_2002	8/25/04 17:41	M	6489659.47	531552.52	1194.02
NB1_2004	9/3/05 14:35	M	6489759.28	531639.47	1198.75
NB1_2005	9/3/05 14:14	M	6489761.09	531723.33	1202.12
NB2_02	9/2/02 15:26	P	6489482.73	527147.60	1006.38

Table A.1: Continued

Site	Date	Type	Northing	Easting	HAE
NB2_04	5/6/04 19:19	W	6489668.25	527502.15	1020.80
NewLk02	3/31/02 16:20	V	6476841.46	526730.43	35.77
NewLk02	5/19/02 15:24	W	6476837.21	526731.48	34.12
NewLk02b	5/19/02 15:36	V	6476834.39	526731.74	34.78
NewLk02b	6/5/02 12:26	W	6476833.25	526732.19	31.81
NewLk02b	6/12/02 15:10	W	6476831.92	526732.82	32.62
NewLk02b	6/21/02 11:02	W	6476831.06	526732.07	32.73
NewLk02b	8/27/02 13:05	W	6476821.72	526736.71	30.62
NewLk02c	8/27/02 15:32	W	6476828.21	526737.59	30.28
NewLk02c	3/8/03 14:19	V	6476803.02	526745.54	32.39
NewLk02c	6/17/03 12:31	W	6476797.46	526752.17	30.22
NewLk02c	8/31/03 11:35	W	6476784.40	526760.40	29.97
NewLk03	6/17/03 12:44	W	6476800.02	526753.58	29.98
NewLk03	3/25/04 17:49	W	6476761.74	526778.67	29.61
NewLk03	5/5/04 12:21	W	6476756.57	526782.68	28.09
NL1_02	6/21/02 13:44	V	6476789.86	526789.92	34.43
NL1_02	8/27/02 13:50	V	6476781.72	526794.70	33.04
NL1_02	3/8/03 14:36	V	6476764.31	526804.20	34.72
NL1_03	3/8/03 15:00	V	6476764.31	526804.20	34.72
NL1_03	8/31/03 11:56	V	6476742.30	526819.85	31.91
NL3_02	6/21/02 14:34	V	6476864.91	526689.53	30.18
NL3_02	8/27/02 17:02	V	6476854.50	526695.41	26.29
NL3_02	3/8/03 14:49	V	6476832.85	526703.12	28.35
NL3_02-03	8/31/03 11:17	V	6476807.17	526717.04	26.61
NL3_02-03	3/25/04 18:07	V	6476783.68	526735.54	30.45
NL3_02-03	5/5/04 11:44	V	6476778.79	526739.95	30.05
NL3_02-03	6/9/04 15:04	V	6476773.78	526745.18	29.29
NL4_02	6/21/02 15:07	V	6476902.66	526635.25	30.82
NL4_02	8/27/02 16:45	V	6476891.13	526641.52	25.93
NL4_02-03	3/8/03 15:02	V	6476864.34	526649.66	26.47
NL4_02-03	3/25/04 15:54	V	6476839.61	526685.10	24.38
NL4_02-03	5/4/04 15:03	W	6476833.87	526689.02	24.16
NL4_02-03	5/5/04 11:09	W	6476834.19	526688.92	23.98
SB1_04	8/25/04 13:31	W	6487425.72	535410.06	1354.88
SB1_05	5/13/05 15:09	W	6487660.31	535367.61	1378.04

Table A.1: Continued

Site	Date	Type	Northing	Easting	HAE
SB1_05	9/3/05 16:09	W	6487648.13	535366.33	1370.90
SB1_2002	9/2/02 14:25	P	6487490.65	535441.08	1364.50
SB1_2003	8/25/03 17:41	M	6487490.85	535440.96	1362.71
SB1_2004	5/6/04 11:41	W	6487696.31	535458.56	1382.34
SB1_2005	9/3/05 16:29	M	6487684.58	535461.67	1372.08
SB1_2004	9/3/05 16:45	M	6487644.73	535456.54	1369.20
SB1B_04	5/6/04 15:46	W	6487019.17	533755.11	1256.92
SB2_02	9/2/02 11:43	W	6485917.49	529399.89	997.31
SB2_02	9/5/03 16:39	W	6485911.58	529287.74	987.79
SB2_03	8/25/04 13:44	W	6485904.11	529182.75	978.62
SB2_04	8/25/04 15:03	W	6485909.40	529285.39	985.24
SB2_04	8/26/05 13:58	W	6485901.33	529176.34	976.49
SB2_98	9/2/02 12:20	P	6485917.13	529324.79	993.73
Term_04	4/23/09 12:13	W	6477115.23	526708.28	44.01
Term_04	5/14/05 14:07	W	6477091.28	526721.00	41.53
Term_05	5/14/05 14:39	W	6477100.09	526738.13	36.97
Term_05	8/23/05 15:22	W	6477092.35	526741.47	30.73
UAS1	5/5/04 11:21	V	6476798.79	526735.86	31.44
UAS1	5/9/04 9:40	V	6476798.39	526736.42	31.41
UAS1	6/9/04 14:36	V	6476794.74	526741.17	30.80
UAS2	5/5/04 11:57	V	6476890.10	526773.19	27.40
UAS2	5/9/04 10:07	V	6476889.48	526773.42	27.13
UAS2	6/9/04 15:33	V	6476884.65	526775.13	25.84
UAS3	5/5/04 12:26	V	6476939.66	526717.59	25.45
UAS3	5/9/04 10:32	V	6476939.13	526717.86	25.34
UAS3	6/9/04 16:03	V	6476935.16	526719.68	24.00
UAS4	5/5/04 12:45	V	6476927.60	526670.56	25.56
UAS4	5/9/04 10:55	V	6476926.98	526670.93	25.38
UAS4	6/9/04 13:11	V	6476921.52	526673.47	23.17
UAS5	5/9/04 11:19	V	6476956.73	526576.94	34.89
UAS5	6/9/04 12:43	V	6476949.27	526582.84	31.35
UAS6	5/5/04 13:13	V	6476960.87	526519.17	37.62
UAS6	5/9/04 11:36	V	6476959.78	526519.76	37.24
UAS6	6/9/04 12:13	V	6476952.28	526523.61	33.90
UAS6	8/26/04 11:21	V	6476935.23	526538.98	22.99

Table A.1: Continued

Site	Date	Type	Northing	Easting	HAE
VEL1	5/6/04 10:32	V	6477454.20	526336.31	112.79
VEL1	5/9/04 10:07	V	6477453.23	526336.25	112.63
VEL1	6/10/04 14:16	V	6477442.28	526335.70	109.48
VEL1	8/26/04 14:10	V	6477421.44	526337.42	99.47
VEL2	5/6/04 11:24	V	6477460.01	526477.23	110.60
VEL2	5/9/04 10:32	V	6477458.93	526477.26	110.38
VEL2	6/10/04 13:44	V	6477447.84	526478.35	107.08
VEL2	8/26/04 15:02	V	6477428.64	526483.35	95.53
VEL3	5/6/04 11:59	V	6477248.26	526467.03	95.41
VEL3	6/10/04 13:18	V	6477238.55	526471.81	91.81

Table A.2: Glacier-wide annual velocities. All times are given in local time (Alaska Standard Time or Alaska Daylight Time). t_0 and t_F indicate the initial and final time of survey, respectively. Horizontal positions are referenced to the WGS-84 ellipsoid and elevations are referenced to Geoid96 (Alaska). Velocities are given in m a^{-1} with direction measured in degrees from true north.

Marker	t_0	t_f	Easting	Northing	MSL	Speed	Azimuth
Bench	Aug-02	Sep-03	526363.80	6477317.70	97.17	104.3	174
Bench	Sep-03	Aug-04	526410.57	6477541.23	104.62	106.1	181
Bench	Aug-04	Aug-05	526331.73	6477553.81	95.13	100.1	186
Bobs	Aug-03	Aug-04	526783.71	6480583.93	438.70	91.8	234
Bobs	Aug-02	Aug-03	526809.97	6480594.56	443.48	96.2	233
Cairn	Aug-99	Aug-00	526706.91	6476824.56	35.46	46.9	163
CL_1	Aug-03	Aug-04	526792.77	6483371.30	673.48	155.5	147
CL_1	Aug-02	Aug-03	526709.84	6483499.80	681.92	158.0	146
CL_1	Aug-04	Aug-05	526552.59	6483679.52	686.57	156.1	145
CL_2	May-04	May-05	527006.45	6478773.45	308.71	134.2	175
CL_2	Aug-03	Aug-04	526951.32	6478784.31	312.28	134.5	175
CL_2	Aug-02	Aug-03	526924.49	6478747.83	316.36	141.3	177
CL_2	Aug-04	Aug-05	527003.75	6478800.96	306.21	127.7	176
Divide	Sep-02	Aug-04	534493.65	6491053.27	1559.81	31.1	193
Divide	Aug-03	Aug-04	534495.29	6491080.66	1560.73	30.3	195

Table A.2: Continued

Marker	t_0	t_f	Easting	Northing	MSL	Speed	Azimuth
Lake	Jul-98	Aug-00	526613.11	6476715.21	23.94	86.6	171
LakeEast	Aug-02	Aug-03	526797.61	6476826.10	22.44	46.8	151
LakeEast	Jun-03	Jun-04	526815.18	6476803.54	16.95	42.8	136
LakeUpper	Aug-02	Aug-03	526788.43	6476885.59	23.66	40.7	151
LakeUpper	Mar-03	Mar-04	526810.59	6476866.51	21.67	49.0	137
LakeUpper	Jun-03	Jun-04	526815.21	6476861.63	18.81	47.4	133
LakeWest	Aug-02	Aug-03	526709.46	6476871.47	17.19	47.9	158
LakeWest	Aug-03	Jun-04	526750.95	6476848.23	16.89	61.8	139
NB_1	Sep-02	Aug-04	531552.52	6489659.47	1189.44	82.9	264
NL_1	Aug-02	Aug-03	526819.85	6476742.30	28.30	46.8	148
NL_2	Aug-02	Aug-03	526760.40	6476784.40	26.36	48.9	152
NL_3	Aug-02	Aug-03	526717.04	6476807.17	23.00	52.1	156
NL_3	Aug-03	Jun-04	526745.18	6476773.78	25.68	59.6	139
NL_4	Mar-03	Mar-04	526685.10	6476839.61	20.76	41.2	125
SB_1	Sep-02	Aug-04	535410.06	6487425.72	1350.50	36.4	206
SB_1	Aug-03	Aug-04	535424.57	6487457.67	1352.68	37.0	206
SB_2	Sep-02	Sep-03	529182.75	6485904.11	974.27	111.4	267
SB_2	Sep-03	Aug-04	529285.39	6485909.40	980.89	108.3	266
Term	Aug-04	Aug-05	526741.47	6477092.35	27.10	34.2	154

Table A.3: Glacier-wide summer velocities. All times are given in local time (Alaska Standard Time or Alaska Daylight Time). t_0 and t_F indicate the initial and final time of survey, respectively. Horizontal positions are referenced to the WGS-84 ellipsoid and elevations are referenced to Geoid96 (Alaska). Velocities are given in m a^{-1} with direction measured in degrees from true north.

Marker	t_0	t_f	Easting	Northing	MSL	Speed	Azimuth
AblMet	May-04	Jun-04	526288.53	6477582.25	113.28	120.0	189
Bench	Jun-02	Aug-02	526353.64	6477424.44	112.85	118.2	181
Bench	May-02	Aug-02	526353.64	6477424.44	112.85	117.3	183
Bench	May-02	Jun-02	526354.75	6477450.89	120.98	122.0	186
Bench	Jun-03	Sep-03	526363.80	6477317.70	97.17	106.1	173
Bench	Jun-04	Aug-04	526410.57	6477541.23	104.62	111.9	190

Table A.3: Continued

Marker	t_0	t_f	Easting	Northing	MSL	Speed	Azimuth
Bench	May-04	Aug-04	526410.57	6477541.23	104.62	115.3	190
Bench	May-04	Jun-04	526414.62	6477564.52	117.18	123.3	190
Bench	May-05	Aug-05	526331.73	6477553.81	95.13	102.8	188
Bench_E1	May-04	Jun-04	526534.75	6477614.61	137.71	123.5	198
Bench_E2	May-04	Jun-04	526520.90	6477471.99	109.98	109.9	177
Bench_W1	May-04	Jun-04	526288.03	6477583.09	113.42	121.0	189
Bench_W1	May-04	Jun-04	526288.03	6477583.09	113.42	120.5	189
Bobs	May-04	Aug-04	526783.71	6480583.93	438.70	95.5	234
Bobs	Jun-03	Aug-03	526809.97	6480594.56	443.48	95.7	232
Cairn	Jun-02	Aug-02	526757.67	6476780.70	28.93	54.6	150
Cairn	May-00	Aug-00	526706.91	6476824.56	35.46	58.7	159
Cairn	May-00	Aug-00	526702.42	6476869.37	35.46	46.4	194
CL_1	May-04	Aug-04	526512.74	6483739.35	690.44	166.0	145
CL_2	May-04	Aug-04	526951.32	6478784.31	312.28	142.4	175
CL_2	May-05	Aug-05	527010.96	6478754.05	303.11	133.5	177
Divide	May-04	Aug-04	534510.89	6491017.15	1558.25	34.6	195
Lake	May-00	Aug-00	526610.86	6476680.12	23.94	82.6	168
LakeEast	Jun-02	Aug-02	526779.82	6476861.59	26.37	49.5	154
LakeEast	Jun-03	Aug-03	526797.61	6476826.10	22.44	57.5	148
LakeEast	Aug-03	May-04	526812.23	6476804.93	17.98	38.0	145
LakeEast	May-04	Jun-04	526815.18	6476803.54	16.95	33.0	115
LakeUpper	Jun-03	Aug-03	526788.43	6476885.59	23.66	56.8	136
LakeUpper	Jun-03	Aug-03	526788.46	6476885.53	23.58	51.9	137
LakeUpper	Jun-02	Aug-02	526768.53	6476921.65	32.17	49.4	162
LakeUpper	May-02	Jun-02	526765.65	6476930.27	36.26	43.5	176
LakeWest	Jun-02	Aug-02	526691.41	6476916.27	24.32	66.5	158
LakeWest	May-04	Jun-04	526737.55	6476835.45	17.36	61.7	139
LakeWest	May-04	Jun-04	526750.95	6476848.23	16.89	65.1	135
NB_1	May-04	Aug-04	531722.59	6489765.37	1198.67	88.5	266
NL_1	Jun-02	Aug-02	526794.70	6476781.72	29.43	51.5	150
NL_2	Jun-02	Aug-02	526736.71	6476821.72	27.01	56.8	154
NL_2	May-02	Jun-02	526732.07	6476831.06	29.12	37.2	174
NL_3	Jun-02	Aug-02	526695.41	6476854.50	22.68	65.1	151
NL_3	May-04	Jun-04	526745.18	6476773.78	25.68	75.3	134
NL_4	Jun-02	Aug-02	526641.52	6476891.13	22.31	71.5	151

Table A.3: Continued

Marker	t_0	t_f	Easting	Northing	MSL	Speed	Azimuth
SB_1	May-04	Aug-04	535458.31	6487682.91	1368.88	44.1	181
SB_1.5	May-04	Aug-04	533745.63	6487019.88	1246.08	31.3	274
Term	May-05	Aug-05	526741.47	6477092.35	27.10	30.5	157
UAS1	May-04	Jun-04	526741.17	6476794.74	27.19	70.1	128
UAS2	May-04	Jun-04	526775.13	6476884.65	22.22	59.9	161
UAS3	May-04	Jun-04	526719.68	6476935.16	20.38	51.1	155
UAS4	May-04	Jun-04	526673.47	6476921.52	19.55	70.7	155
UAS5	May-04	Jun-04	526582.84	6476949.27	27.73	111.9	142
UAS6	Jun-04	Aug-04	526538.98	6476935.23	19.38	97.7	138
UAS6	May-04	Jun-04	526523.61	6476952.28	30.28	99.2	153
VEL1	Jun-04	Aug-04	526337.42	6477421.44	95.82	99.2	175
VEL1	May-04	Jun-04	526335.70	6477442.28	105.82	124.5	183
VEL2	Jun-04	Aug-04	526483.35	6477428.64	91.88	93.0	168
VEL2	May-04	Jun-04	526478.35	6477447.84	103.42	126.7	174
VEL3	May-04	Jun-04	526471.81	6477238.55	88.17	112.8	154

Appendix B

Appendix: Model Code

The following MATLAB® scripts were used to run the 1-dimensional viscoelastic bending beam model.

B.1 constants.m

```
function [g rhow rhoi di eF c1 c2 c3 c4 omega amp tau maxU...
 p1 p2]=constants;
% physical constants; units are MKS
g=9.81;  % m s^{-2};  acceleration of gravity
rhow=1000;  % kg m^{-3}; density of liquid water
rhoi=917;  % kg m^{-3}; density of polycrystalline ice
di=rhoi/rhow;
eF=0.5;
% material constants for viscoelastic beam
% see Reeh et al for linearization which explains the constants
muM=25000*10^9;  % Pa s - for polar ice(-15 C), Tau_e~250 kPa
% muM=11250*10^9; % Pa s - for temperate ice(0 C), Tau_e~80.85 kPa
EM=9.3*10^9;  % Pa s
muV=600*10^9;  % Pa s
EV=10*10^9;  % Pa s
% derived constants
c1=3*muV/EV;
c2=2.25*muV/(EV*EM);
c3=(3/4)*( (1/EV) + (1/EM) + muV/(muM*EV) );
c4=0.25/muM;
p1=(-c3+sqrt(c3^2-4*c2*c4))/(2*c2);
p2=(-c3-sqrt(c3^2-4*c2*c4))/(2*c2);
% parameters for tidal case
per=12;                              % tidal period in hours
omega=2*pi/(per*3600);  % s^{-1};  radian frequency of tidal...
 oscillation
amp=0.5;                              % amplitude of tidal...
 oscillation in [m]
```

B.2 chebdif.m

```
function [x, DM] = chebdif(J,M)
%  The function [x,DM]=chebdif(J,M) computes the differentiation
%  matrices D1,D2,...,DM on Chebyshev nodes.
%  Input:
%   J:  Size of differentiation matrix.
%   M:  Number of derivatives required (integer).
%  Note:     0<M<=J-1.
%  Output:
%   DM: DM(1:J,1:J,ell) contains ell-th derivative matrix,...
 ell=1..M.
%
%  The code implements two strategies for enhanced
%  accuracy suggested by W. Don and S. Solomonoff in
%  SIAM J. Sci. Comp. Vol. 6, pp. 1253--1268 (1994).
%  The two strategies are (a) the use of trigonometric
%  identities to avoid the computation of differences
%  x(k)-x(j) and (b) the use of the "flipping trick"
%  which is necessary since sin t can be computed to high
%  relative precision when t is small whereas sin (pi-t) cannot.
%  Note added May 2003:  It may, in fact, be slightly better not
%  to implement the strategies (a) and (b).   Please consult the
%  following paper for details:   "Spectral Differencing with a
%  Twist", by R. Baltensperger and M.R. Trummer, to appear in
%  SIAM J. Sci. Comp.
%
%  J.A.C. Weideman, S.C. Reddy 1998.  Help notes modified by
%  JACW, May 2003.
I=eye(J);                     % Identity matrix.
L=logical(I);                 % Logical identity matrix.
j1=floor(J/2); j2=ceil(J/2);  % Indices used for flipping trick.
k=[0:J-1]';                   % Compute theta vector.
th=k*pi/(J-1);
x=sin(pi*[J-1:-2:1-J]'/(2*(J-1)));% Compute Chebyshev points.
T=repmat(th/2,1,J);
DX=2*sin(T'+T).*sin(T'-T);    % Trigonometric identity.
DX=[DX(1:j1,:); -flipud(fliplr(DX(1:j2,:)))];  % Flipping trick.
DX(L)=ones(J,1);           % Put 1's on the main diagonal of DX.

C=toeplitz((-1).^k);          % C is the matrix with
C(1,:)=C(1,:)*2; C(J,:)=C(J,:)*2;            % entries c(k)/c(j)
```

```
C(:,1)=C(:,1)/2; C(:,J)=C(:,J)/2;
Z=1./DX;                        % Z contains entries 1/(x(k)-x(j))
Z(L)=zeros(J,1);                % with zeros on the diagonal.
D=eye(J);                       % D contains diff. matrices.
for ell=1:M
    D=ell*Z.*(C.*repmat(diag(D),1,J)-D);     % Off-diagonals
    D(L)=-sum(D');              % Correct main diagonal of D
    DM(:,:,ell)=D;              % Store current D in DM
end
```

B.3 initialM.m

```
function M0=initialM(u0,h,di,rhow,g,J,D1,D2);
% subfunction to calculate a self-consistent
% set of initial conditions for
% M(x,0) using the constraint M_xx(x,0)=-rhow*g*u(x,0) and
% the boundary condition: M_x(L,0)=0
% M(L,0)=rhow*g*h(L)^3*(di*(1-di)*(di-1/2)/6-di*(di-1)*u(L,0)/2)
% the BVP is solved using the chebyshev spectral method F*M=f

%build spectral operator F
F=zeros(J+1,J+1);
F(2:J,:)=D2(2:J,:);
F(1,:)=D1(J+1,:);
F(J+1,J+1)=1;
%build vector f;
f=zeros(J+1,1);
f(2:J)=-rhow*g*u0(2:J);
f(J+1)=rhow*g*h(J+1)^3*(di*(1-di)*(di-1/2)/6-di*(di-1)*u0(J+1)/2);
%solve
M0=F\f;
```

B.4 model_Reeh.m

```
function [alloutputs]=model_Reeh(J,dt,tt)
% MODEL_REEH runs the bending beam model for the numerical
% solution of Reeh's model.
% author: ESB, 10/10/05, revised 11/05
% The case is: 1. Reeh's tidal flexure model, with
% sinusoidal forcing
%
% The basic format is as follows:
%
% Notation
%       t=time, 0<t<T
%       x=horizontal coordinate, 0<x<L
%       u(x,t)=vertical deflection, +up, from equilibrium
%       M(x,t)=bending moment
%       f(t)=forcing equation
% Equations
%           M_xx=rhow*g*(f(x,t)-u)
%               f(x,t)=amp*sin(omega*t)
%           I*O{u_xx}=P{M}
%               where O, P are time derivative operators
%               O=c1*d^2/dt^2+d/dt
%               P=c2*d^2/dt^2+c3*d/dt+c4.
% Boundary Conditions
%           BC1   u(0,t)=0
%           BC2   u_x(0,t)=0
%           BC3_1 u(L,t)=0
%           BC4_1 u_x(L,t)=0
% Initial Conditions
%           u(x,0)=u0(x)
%           u_t(x,0)=u0_t(x)
%           M(x,0)=consistent with u0
%           M_t(x,0)=consistent with u0_t
%               1. assume no initial deflection or motion
% Calls functions: chebdif, constants, initialM
% Includes subfunctions: plotting


clear all, close all
dbstop if error
```

```
tt=48:1:54;  % a half-tidal cycle, after transients die away
dt=1/60; %(hours)
J=40;

[g rhow rhoi di eF c1 c2 c3 c4 omega amp tau maxU p1 p2]=...
constants;
% time-stepping
tt=tt*3600;  dt=dt*3600;  % convert to seconds
T=max(tt); N=length(tt);
% preallocate output vars
tout=zeros(size(tt));
u=zeros(J+1,N); alpha=u;
M=u; sig_xmax=zeros(J+1,N);

L=20000; h=200*ones(J+1,1); %beam length and thickness

% space-spectral grid
[x,DM]=chebdif(J+1,3);
x=(L/2)*(1-x); % recall order: x_1=0, x_{J+1}=L; this scales x
D1=(2/L)*DM(:,:,1);     % first differentiation matrix, scaled
D2=(2/L)^2*DM(:,:,2);   % second diff. matrix, scaled
D3=(2/L)^3*DM(:,:,3);   % third diff. matrix, scaled

% initial conditions (u_a,M contain values for _all_ x)
I=1/12*h.^3;
uold_a=zeros(size(x)); Mold=zeros(size(x));
ucur_a=uold_a; Mcur=Mold;
uold=uold_a(2:J); ucur=ucur_a(2:J);
u0old=uold_a(1); uLold=uold_a(J+1);
u0cur=ucur_a(1); uLcur=ucur_a(J+1);

% spectral operator A - main blocks all the same
K=(J-1)+(J+1); A=zeros(K,K);
A(2:J-2,2:J-2)=rhow*g*eye(J-3); %upper left
A(2:J-2,J:K)=D2(3:J-1,:); %upper right
for r=1:J+1
    A(r+J-1,1:J-1)=(c1+dt/2)*I(r)*D2(r,2:J); %lower left
end
A(J:K,J:K)=(-c2-c3*dt/2)*eye(J+1); %lower right
% BC rows
A(1,1:J-1)=D1(1,2:J); % BC2
A(J-1,1:J-1)=D1(J+1,2:J); % BC3
```

```
% precondition by heuristic: scale columns for M variables
PC=diag([ones(1,J-1) repmat(1e9,1,J+1)]); APC=A*PC;

% build known vector b
b=zeros(K,1);
b(1)=0; % BC2
b(J-1)=0; % BC3

t=0; nt=1;
while t<=T
    % store current values if at appropriate time
    if t>=tt(nt)
        tout(nt)=t;
        u(:,nt)=[u0cur;ucur;uLcur];
        M(:,nt)=Mcur;
        alpha(:,nt)=D1*u(:,nt);  % alpha=du/dx
        nt=nt+1;
    end
    if t+dt>T, break, end
    % continue to build known vector b from cur and old values
    ucur_a=[u0cur;ucur;uLcur]; uold_a=[u0old;uold;uLold];
    for r=1:J+1
        b(r+J-1)=(2*c1)*I(r)*D2(r,:)*ucur_a+...
             (-c1+dt/2)*I(r)*D2(r,:)*uold_a+...
             (-2*c2+c4*dt^2)*Mcur(r)+(c2-c3*dt/2)*Mold(r);
    end
    b(2:J-2)=rhow*g*amp*sin(omega*(t+dt))*ones(J-3,1); % f(x,t)

    uMnew=PC*((APC)\b);  % A\b preconditioned by PC
    u0new=0; % BC1
    uLnew=0; % BC4
    uold=ucur; Mold=Mcur; % values at t_{l}   -> t_{l-1}
    ucur=uMnew(1:J-1); Mcur=uMnew(J:K);
    u0old=u0cur; uLold=uLcur;
    u0cur=u0new; uLcur=uLnew;
    t=t+dt;      % time corresponding to most recent "new"
end
tout=tout/3600; % back to hours
plotting1(x,tout,u,M,alpha,sig_xmax,L,amp)
```

```
function plotting1(x,tout,u,M,alpha,sig_xmax,L,amp)
s='';   % build tags for legend
for j=1:length(tout)
    s=strvcat(s,[num2str(tout(j)) ' hours']);
end
figure(1)
maxj=4; % tt(maxj)=51 is time of max deflection
subplot(2,1,1), plot(x,u(:,:)/amp,'.-','MarkerSize',12)
axis([0 L 0 1.1])
title('Model 1: Reeh tidal forcing')
xlabel('distance x(m)'), ylabel('relative deflection u/amp')
subplot(2,1,2), plot(x,abs(alpha(:,:)),'.-','MarkerSize',12)
xlabel('distance x(m)')
ylabel('tilt amplitude |\alpha| (dimensionless)')
legend(s,'Location','SouthOutside','Orientation','Horizontal')

figure(2)
plot(x,u(:,1:maxj)/amp,'-',x,u(:,maxj+1:end)/amp,'--')
axis([0 8000 -0.2 1.2])
xlabel('distance x(m)')
ylabel('relative deflection u/amp')
legend(s,'Location','SouthOutside','Orientation','Horizontal')
```

B.5 model_const.m

```
function [tout u M sig_xmax alpha]=model_const;
% MODEL_CONST runs the bending beam model for the buoyant
% case with constant ice thinning
% author: ESB, 11/15/05
% The case is:
%       2. Buoyant forcing model, with different free end BC's
% the model is adapted from model2 in the last version
% (all_models_v5.m) to include an initial situation of
% ice at equilibrium, imposing some constant thinning
% rate at each time step, and seeing how the shape and
% stress state of the ice evolve
% The basic format is as follows:
%
% Notation
%       t=time, 0<t<T
%       x=horizontal coordinate, 0<x<L
%       u(x,t)=vertical deflection, +up, from equilibrium
%       M(x,t)=bending moment
%       f(t)=forcing equation
%       a=dh/dt, thinning rate
%       h(x,t)=ice thickness
%       d(x,t)=water depth
% Equations
%           M_xx=rhow*g*(f(x,t)-u)
%               f(x,t)=-a*t
%           I*O{u_xx}=P{M}
%               where O, P are time derivative operators
%               O=c1*d^2/dt^2+d/dt
%               P=c2*d^2/dt^2+c3*d/dt+c4.
% Boundary Conditions
%           BC1   u(0,t)=0
%           BC2   u_x(0,t)=0
%           BC3   M_x(L,t)=0
%           BC4   u_xx(L,t)=0
% (cantilever BC's are u_xx=0 and u_xxx=0 at the free end;
%  if I=~I(x) then u_xxx=0 corresponds to M_x=0, so
%    I impose the condition M_x=0 and u_xx=0 at the free end)
% Initial Conditions
%           u(x,0)=u0(x)
%           u_t(x,0)=u0_t(x)
```

```
%           M(x,0)=consistent with u0
%           M_t(x,0)=consistent with u0_t
%           For thinning test, let:
%               u0=zeros(size(h));
%               M0=initialM(u0,h,di,rhow,g,J,D1,D2);
% Calls functions: chebdif, constants, initialM
% Includes subfunctions: plotting
% Example:  tt=0:2:12; %(hours)
%           dt=1/60; %(hours)
%           J=25; %(grid spacing)


dbstop if error
dbstop if naninf
warning off
tic
s='';
% constant thinning rate
byear=-6; %m year^{-1} thinning rate

bday=byear/365.25; %m day^{-1} thinning rate
a=bday/24/60/60; % average thinning/second

%                 tt=0:24:24*7; %1 week
dt=1/60; %(hours)
J=25;
% tt=[0:24*7:51*24*7  52*24*7]; %1 years
tt=[0:24:24*7 24*7:2*24*7:2*52*24*7]; %2 years

[g rhow rhoi di eF c1 c2 c3 c4 omega amp tau maxU p1 p2]=...
constants;
% time-stepping
tt=tt*3600;  dt=dt*3600;  % convert to seconds
T=max(tt); N=length(tt);
% preallocate output vars
tout=zeros(size(tt));
u=zeros(J+1,N); alpha=u;
M=u; sig_xmax=zeros(J+1,N);
L=1000;
% space-spectral grid
[x,DM]=chebdif(J+1,3);
x=(L/2)*(1-x); % recall order: x_1=0, x_{J+1}=L; this scales x
```

```
D1=(2/L)*DM(:,:,1);     % first differentiation matrix, scaled
D2=(2/L)^2*DM(:,:,2);   % second diff. matrix, scaled
D3=(2/L)^3*DM(:,:,3);   % third diff. matrix, scaled

% initial geometry
h0=200*ones(size(x));
ucur_a=zeros(size(x));
uold_a=zeros(size(x));
Mcur=initialM(ucur_a,h0,di,rhow,g,J,D1,D2);
Mold=Mcur;
uold=uold_a(2:J+1); ucur=ucur_a(2:J+1);
u0old=uold_a(1);
u0cur=ucur_a(1);


% start building known vector b
K=(J)+(J+1);
b=zeros(K,1);
b(1)=0; % BC2 u_x(0)=0
b(J-1)=0; % BC3b u_xx(L)=0
b(J)=0; % BC3 M_x(L)=0

% start time stepping
t=0; nt=1;
while t<=T
    h=h0+a*t;
    sig_h=rhow*g*h/1e3; % hydrostatic stress at base, KPa
    I=1/12*h.^3;
    if t>=tt(nt)
        t
        tout(nt)=t;
        u(:,nt)=[u0cur;ucur];
        M(:,nt)=Mcur;
        sig_xmax(:,nt)=0.5*h.*Mcur./I/1e3;
        alpha(:,nt)=D1*u(:,nt);  % alpha=du/dx
        nt=nt+1;
    end
    if t+dt>T, break, end

    % spectral operator A - main blocks all the same
    A=zeros(K,K);
    A(2:J-2,2:J-2)=rhow*g*eye(J-3); %upper left
```

```
    A(2:J-2,J+1:K)=D2(3:J-1,:); %upper right
    for r=1:J+1
    A(r+J,1:J)=(c1+dt/2)*I(r)*D2(r,2:J+1); %lower left
    end
    A(J+1:K,J+1:K)=(-c2-c3*dt/2)*eye(J+1); %lower right
    % BC rows
    A(1,1:J)=D1(1,2:J+1); % BC2 u_x(0)=0
    A(J-1,1:J)=D2(J+1,2:J+1); % BC3b u_xx(L)=0
    A(J,J+1:K)=D1(J+1,:); % BC3 M_x(L)=0

    % precondition by heuristic
    PC=diag([ones(1,J)  repmat(1e9,1,J+1)]); APC=A*PC;
    % finish building known vector b from cur and old values,...
    %  adding ablation forcing
    ucur_a=[u0cur;ucur]; uold_a=[u0old;uold];
    for r=1:J+1
        b(r+J)=(2*c1)*I(r)*D2(r,:)*ucur_a+...
             (-c1+dt/2)*I(r)*D2(r,:)*uold_a+...
             (-2*c2+c4*dt^2)*Mcur(r)+(c2-c3*dt/2)*Mold(r);
    end

    b(2:J-2)=-rhow*g*a*(t+dt)*ones(J-3,1);
    uMnew=PC*((APC)\b);  % A\b preconditioned by PC
    u0new=0; % BC1
    uold=ucur; Mold=Mcur;
    ucur=uMnew(1:J); Mcur=uMnew(J+1:K);
    u0old=u0cur;
    u0cur=u0new;
    t=t+dt;      % time corresponding to most recent "new"
% end former time loop
end
tout=tout/3600; % back to hours
plottingm2(x,tout,u,M,alpha,sig_xmax,sig_h,L,amp,s)
toc

function plottingm2(x,tout,u,M,alpha,sig_xmax,sig_h,L,amp,s)
% subfunction to plot results of different runs
for j=1:length(tout)
    s=strvcat(s,[num2str(tout(j)) ' hours']);
end
    figure(4)
    hold on
```

```
subplot(2,1,1), plot(x,u(:,1:end),'--')
ylabel('deflection u (m)')
title('Model 2: Bouyant')
subplot(2,1,2), plot(x,abs(alpha(:,1:end)),'--')
ylabel('tilt amplitude |\alpha| (dimensionless)')
legend(s)

figure(5)
hold on
subplot(2,1,1), plot(x,M(:,:),'--')
ylabel('bending moment M')
title('Model 2: Bouyant')
subplot(2,1,2), plot(x,sig_xmax(:,:),'--',x,sig_h,'r.-')
ylabel('\sigma _{x max} Basal Tens Stress, KPa')
xlabel('distance x from grounding line (m)')
legend(s)
```

B.6 model_seasvar.m

```
function [tout u M sig_xmax alpha]=model_seasvar;
% MODEL_SEASVAR runs the bending beam model for the buoyant
% case with seasonally varying forcing functions
% author: ESB, 11/15/05
% The case is:
%       2. Buoyant forcing model, with different free end BC's
% the model is adapted from model2 in the last version
% (all_models_v5.m) to include an initial situation of zero
% deflection from equilibrium, imposing a seasonally varying
% thinning rate and lake level at each time step, and seeing
% how the shape and stress state of the ice evolve
%
% The basic format is as follows:
%
% Notation
%       t=time, 0<t<T
%       x=horizontal coordinate, 0<x<L
%       u(x,t)=vertical deflection, +up, from equilibrium
%       M(x,t)=bending moment
%       fa(t)=thinning forcing equation
%       fb(t)=lake level forcing equation
%       h(x,t)=ice thickness
%       d(x,t)=water depth
% Equations
%           M_xx=rhow*g*(f(x,t)-u)
%               f(x,t)=fb-fa
%               fa=rhow/rhoi*(-6*s2y*t+...
% 14/2/pi*(sin(2*pi*(s2y*t-2/52))-sin(2*pi*(-2/52))))
%               fb=-3/4*cos(2*pi*(s2y*t+7/52))+1.063;
%                 (-thickness change causes +forcing,
%  +deeper water causes +forcing)
%                 (-deflection causes +forcing)
%           I*O{u_xx}=P{M}
%               where O, P are time derivative operators
%               O=c1*d^2/dt^2+d/dt
%               P=c2*d^2/dt^2+c3*d/dt+c4.
% Boundary Conditions - same as model_const boundary conditions
% Initial Conditions
%           u(x,0)=u0(x)
%           u_t(x,0)=u0_t(x)
```

```
%           M(x,0)=consistent with u0
%           M_t(x,0)=consistent with u0_t
%               For ablation test, let:
%               u0=zeros(size(h)); % note: NO initial deflection
%               M0=initialM(u0,h,di,rhow,g,J,D1,D2);
%               and also u_1=u0, Mold=Mcur (No initial velocity)
% Calls functions: chebdif, constants, initialM
% Includes subfunctions: plotting, forceratea, forcerateb
% Example:  tt=0:2:12; %(hours)
%           dt=1/60; %(hours)
%           J=25; %(grid spacing)


% dbstop if error
% dbstop if naninf
warning off
tic
s='';
tt=[0:24:24*7 24*7:2*24*7:2*52*24*7]; %2 years
dt=1/60; %(hours)
J=25; %number of spatial steps along beam

[g rhow rhoi di eF c1 c2 c3 c4 omega amp tau maxU p1 p2]=...
constants;
% time-stepping
tt=tt*3600;  dt=dt*3600;  % convert to seconds
T=max(tt); N=length(tt);
% preallocate output vars
tout=zeros(size(tt));
u=zeros(J+1,N); alpha=u;
M=u; sig_xmax=zeros(J+1,N);

L=1000;
h=200*ones(size(x)); %length and thickness of beam

% space-spectral grid
[x,DM]=chebdif(J+1,3);
x=(L/2)*(1-x); % recall order: x_1=0, x_{J+1}=L; this scales x
D1=(2/L)*DM(:,:,1);     % first differentiation matrix, scaled
D2=(2/L)^2*DM(:,:,2);   % second diff. matrix, scaled
D3=(2/L)^3*DM(:,:,3);   % third diff. matrix, scaled
```

```
% interpolate initial thickness and deflection
b=forcerateb(0);
a=forceratea(0);
ucur_a=zeros(size(x));
uold_a=zeros(size(x));
Mcur=initialM(ucur_a,h,di,rhow,g,J,D1,D2);
Mold=Mcur;
uold_a=ucur_a-a*dt; uold_a(1)=0; h_1=h-a*dt;
Mold=initialM(uold_a,h_1,di,rhow,g,J,D1,D2);

uold=uold_a(2:J+1);
ucur=ucur_a(2:J+1);
u0old=uold_a(1);
u0cur=ucur_a(1);
% start building known vector b
K=(J)+(J+1);
b=zeros(K,1);
b(1)=0; % BC2 u_x(0)=0
b(J-1)=0; % BC3b u_xx(L)=0
b(J)=0; % BC3 M_x(L)=0

% start time stepping
t=0; nt=1;
while t<=T
    fa=forceratea(t);
    h=h+fa*dt;
    fb=forcerateb(t);
    sig_h=rhow*g*h/1e3; % hydrostatic stress at base, KPa
    I=1/12*h.^3;

    % store current values if at appropriate time
    if t>=tt(nt)
        tout(nt)=t;
        u(:,nt)=[u0cur;ucur];
        M(:,nt)=Mcur;
        sig_xmax(:,nt)=0.5*h.*Mcur./I/1e3;
        alpha(:,nt)=D1*u(:,nt);  % alpha=du/dx
        nt=nt+1;
% fa, fb
    end
    if t+dt>T, break, end
```

```
    % spectral operator A - main blocks all the same
    A=zeros(K,K);
    A(2:J-2,2:J-2)=rhow*g*eye(J-3); %upper left
    A(2:J-2,J+1:K)=D2(3:J-1,:); %upper right
    for r=1:J+1
    A(r+J,1:J)=(c1+dt/2)*I(r)*D2(r,2:J+1); %lower left
    end
    A(J+1:K,J+1:K)=(-c2-c3*dt/2)*eye(J+1); %lower right
    % BC rows
    A(1,1:J)=D1(1,2:J+1); % BC2 u_x(0)=0
    A(J-1,1:J)=D2(J+1,2:J+1); % BC4 u_xx(L)=0
    A(J,J+1:K)=D1(J+1,:); % BC3 M_x(L)=0

     % precondition by heuristic
    PC=diag([ones(1,J)  repmat(1e9,1,J+1)]); APC=A*PC;

    % finish building known vector b from cur and old values,
    %  adding ablation forcing
    ucur_a=[u0cur;ucur]; uold_a=[u0old;uold];
    for r=1:J+1
        b(r+J)=(2*c1)*I(r)*D2(r,:)*ucur_a+...
             (-c1+dt/2)*I(r)*D2(r,:)*uold_a+...
             (-2*c2+c4*dt^2)*Mcur(r)+(c2-c3*dt/2)*Mold(r);
    end
    fa=forceratea(t+dt); % thinning rate
    fb=forcerateb(t+dt); % water level variation
    b(2:J-2)=rhow*g*(fb*(t+dt)-fa*(t+dt));

    uMnew=PC*((APC)\b);  % A\b preconditioned by PC
    u0new=0; % BC1
    uold=ucur; Mold=Mcur;
    ucur=uMnew(1:J); Mcur=uMnew(J+1:K);
    u0old=u0cur;
    u0cur=u0new;
    t=t+dt;      % time corresponding to most recent "new"
% end former time loop
end
tout=tout/3600; % back to hours
plottingm2(x,tout,u,M,alpha,sig_xmax,sig_h,L,s)

toc
```

```
% subfunction plottingm2 same as model_const

function fa=forceratea(t2);
t=t2/60/60/24/365.25;
fa=1000/917*(-6+14*cos(2*pi*(t-2/52))); % in m/a
fa=fa/365.25/24/60/60; %in m/s
function fb=forcerateb(t2);
t=t2/60/60/24/365.25;
fb=2*pi*3/4*sin(2*pi*(t+7/52)); % in m/a
fb=fb/365.25/24/60/60; %in m/s
```

B.7 model_mend.m

```
function [tout u M sig_xmax alpha]=model_MEND;
% MODEL_MEND runs the bending beam model for the buoyant case
% with seasonally varying forcing and a geometry similar to
% Mendenhall (The model is virtually identical to model_seasvar
% except for the initial geometry.  For explanatory text, see
% model_seasvar.)
% author: ESB, 11/15/05


dbstop if error
dbstop if naninf
warning off
tic
s='';
tt=[0:24:24*7 24*7:2*24*7:2*52*24*7]; %2 years
dt=1/60; %(hours)
J=25;

[g rhow rhoi di eF c1 c2 c3 c4 omega amp tau maxU p1 p2]=...
constants;
% time-stepping
tt=tt*3600;  dt=dt*3600;  % convert to seconds
T=max(tt); N=length(tt);
% preallocate output vars
tout=zeros(size(tt));
u=zeros(J+1,N); alpha=u;
M=u; sig_xmax=zeros(J+1,N);

fid='d-Mend.txt'; dp=load(fid);  % depth  [xd,depth], +up
fis='s-Mend.txt'; sp=load(fis);  % surface  +up
x0=6477000; % upglacier limit of area considered
xxd=x0-dp(:,1); xxs=x0-sp(:,1);
L=max(xxd); % terminus position, x=0 at 6476749 N

% space-spectral grid
[x,DM]=chebdif(J+1,3);
x=(L/2)*(1-x); % recall order: x_1=0, x_{J+1}=L; this scales x
D1=(2/L)*DM(:,:,1);     % first differentiation matrix, scaled
D2=(2/L)^2*DM(:,:,2);   % second diff. matrix, scaled
D3=(2/L)^3*DM(:,:,3);   % third diff. matrix, scaled
```

```
% interpolate initial thickness and deflection data
dd=interp1(xxd,dp(:,2),x);
dd=dd-1.063; % constant term in lake level variation
ss=interp1(xxs,sp(:,2),x);
b=forcerateb(0);
a=forceratea(0);
h=ss-dd; % account for initial thickness change (should be 0)
h_c=-dd/di; % calculated equilibrium thickness based on depth
i=find(h<=h_c);
% initial conditions (u_a,M contain values for _all_ x)
ucur_a=zeros(size(x));
ucur_a(i)=-h(i)+h_c(i); % initial deflection
ucur_a(1)=0;
uold_a=ucur_a-a*dt-b*dt; uold_a(1)=0; h_1=h-a*dt;
Mcur=initialM(ucur_a,h,di,rhow,g,J,D1,D2);
Mold=initialM(uold_a,h_1,di,rhow,g,J,D1,D2);

uold=uold_a(2:J+1);
ucur=ucur_a(2:J+1);
u0old=uold_a(1);
u0cur=ucur_a(1);
% start building known vector b
K=(J)+(J+1);
b=zeros(K,1);
b(1)=0; % BC2 u_x(0)=0
b(J-1)=0; % BC3b u_xx(L)=0
b(J)=0; % BC3 M_x(L)=0

% start time stepping
t=0; nt=1;
while t<=T
    fa=forceratea(t);
    h=h+fa*dt;
    fb=forcerateb(t);
    sig_h=rhow*g*h/1e3; % hydrostatic stress at base, KPa
    I=1/12*h.^3;

    % store current values if at appropriate time
    if t>=tt(nt)
        t
        tout(nt)=t;
```

```
    u(:,nt)=[u0cur;ucur];
    M(:,nt)=Mcur;
    sig_xmax(:,nt)=0.5*h.*Mcur./I/1e3;
    alpha(:,nt)=D1*u(:,nt);  % alpha=du/dx
    nt=nt+1;
    fa, fb
end
if t+dt>T, break, end

% spectral operator A - main blocks all the same
A=zeros(K,K);
A(2:J-2,2:J-2)=rhow*g*eye(J-3); %upper left
A(2:J-2,J+1:K)=D2(3:J-1,:); %upper right
for r=1:J+1
A(r+J,1:J)=(c1+dt/2)*I(r)*D2(r,2:J+1); %lower left
end
A(J+1:K,J+1:K)=(-c2-c3*dt/2)*eye(J+1); %lower right
% BC rows
A(1,1:J)=D1(1,2:J+1); % BC2 u_x(0)=0
A(J-1,1:J)=D2(J+1,2:J+1); % BC4 u_xx(L)=0
A(J,J+1:K)=D1(J+1,:); % BC3 M_x(L)=0

 % precondition by heuristic
PC=diag([ones(1,J)  repmat(1e9,1,J+1)]); APC=A*PC;
% finish building known vector b
ucur_a=[u0cur;ucur]; uold_a=[u0old;uold];
for r=1:J+1
    b(r+J)=(2*c1)*I(r)*D2(r,:)*ucur_a+...
         (-c1+dt/2)*I(r)*D2(r,:)*uold_a+...
         (-2*c2+c4*dt^2)*Mcur(r)+(c2-c3*dt/2)*Mold(r);
end
fa=forceratea(t+dt); % thinning rate
fb=forcerateb(t+dt); % water level variation
b(2:J-2)=rhow*g*(fb*(t+dt)-fa*(t+dt));

uMnew=PC*((APC)\b);  % A\b preconditioned by PC
u0new=0; % BC1
uold=ucur; Mold=Mcur;
ucur=uMnew(1:J); Mcur=uMnew(J+1:K);
u0old=u0cur;
u0cur=u0new;
t=t+dt;      % time corresponding to most recent "new"
```

```
% end former time loop
end
tout=tout/3600; % back to hours
plottingm2(x,tout,u,M,alpha,sig_xmax,sig_h,L,s)
toc


% subfunction plottingm2 same as in model_const
% subfunctions forceratea, forcerateb same as in model_seasvar
```

Appendix C
Appendix: Supplemental Material

The following material is included on the pocket CD enclosed in this thesis. This supplementary data was not incorporated into the written part of the thesis for space considerations. Included are survey and mass balance data, half-hourly positions from the continuous GPS station, air temperature and precipitation data, lake level and water temperature data, daily terminus positions derived from time-lapse photography, movies created from time-lapse photography, and MATLAB® scripts for the model (Chapter 3). The contents of the CD are described in detail below.

C.1 Directory of CD Contents

Mass Balance Data >		
	AblationMeter_2004.xls	*EXCEL spreadsheet*
	MassBalance_1998-2005.xls	*EXCEL spreadsheet*
Mendenhall Lake Data >		
	LakeTemp_2004-2005.xls	*EXCEL spreadsheet*
	USGSgauge_2003-2004.xls	*EXCEL spreadsheet*
Model Codes >		
	chebdif.m	*MATLAB function*
	initialM.m	*MATLAB function*
	model_const.m	*MATLAB function*
	model_mend.m	*MATLAB function*
	model_reeh.m	*MATLAB function*
	model_seasvar.m	*MATLAB function*
	d.txt	*tab-delimited model input*
	s.txt	*tab-delimited model input*
Survey Data >		
	Continuous GPS Data >	
	GLAC_EpochA.txt	*tab-delimited text file*
	GLAC_EpochB.txt	*tab-delimited text file*
	GLAC_EpochC.txt	*tab-delimited text file*
	Positions_2002-2005.xls	*EXCEL spreadsheet*
	Termini_and_Boundaries.xls	*EXCEL spreadsheet*
	Velocities.xls	*EXCEL spreadsheet*
Thesis >		
	ESB_MSthesis.pdf	*PDF*
Time-Lapse Photography >		
	Movies >	
	Terminus_breakup.avi	*AVI movie file*
	Terminus_Feb-Aug2004.avi	*AVI movie file*
	Terminus Positions 2004 >	
	term*mmdd*.avg	*tab-delimited text file*
Weather Station Data >		
	TermWeather_2002-2005.xls	*EXCEL spreadsheet*

C.2 Mass Balance Data

The file "AblationMeter_2004.xls" contains raw and calibrated data from the pressure gauge ablation meter installed at "Bench" in summer 2004. Cumulative ablation, ablation rate, and 12-hour and 24-hour running means are also calculated.

The file "MassBalance_1998-2005.xls" contains specific mass balance data available for Mendenhall Glacier. The sheet "Specific Balances" lists the elevation, initial and final time of measurement period, specific balance, specific balance rate, and balance year for each site visited. Some screening of the raw data has been performed to remove measurements of dubious quality. The sheet "Balance Curves" summarizes the data in the form of specific balance rate vs. elevation for each balance year in which data was collected. The sheet "A-z bins, b-z interps, volume" contains the area elevation bins used to estimate surface mass balance, the interpolated balance within each elevation bin, and an estimated total volume change for balance years 1998, 2000, and 2003-2005. The sheet "ELA estimates" contains visually estimated altitudes of the equilibrium line for various years between 1998 and 2004.

C.3 Mendenhall Lake Data

The file "LakeTemp_2004-2005.xls" contains calibrated water temperatures from three temperature sensors located on a mooring adjacent to the terminus of Mendenhall Glacier during the summer of 2004 and 2005. The depth of each sensor is given in the file. Time is given in decimal day of year for 2004 and Day/Time for 2005.

The file "USGSgauge_2003-2004.xls" contains water level data for Mendenhall Lake. "RawData" contains preliminary data obtained from USGS Water Resources of Alaska (http://nwis.waterdata.usgs.gov/ak/nwis/dv/?site_no=15052500&agency_cd=USGS). The sheet "CleanedData" contains lake level data between June 2002 and December 2004, with data gaps removed.

C.4 Model Codes

The section contains the MATLAB® codes for the 1-dimensional viscoelastic bending beam model discussed in Chapter 3 and printed in Appendix B. Th additional text files are water depth (d.txt) and ice surface (s.txt) to be used for the model test case given in model_mend.m.

C.5 Survey Data

The file "Positions_2002-2005.xls" is a summary of all points surveyed (and documented by field notes) on Mendenhall Glacier. Most sheets contains data from one study site (e.g. mass balance marker), with the exception of "Bench," "UAS," and "Vels" which contain data from multiple velocity markers. The sheet "LakeLevel" includes DGPS surveys of lake ice and water level as well as important locations on the eastern terminus. The sheet "Camera" contains camera control points and the location of the time-lapse camera shown in Fig. 2.2.

The file "Termini_and_Boundaries.xls" contains terminus positions and glacier boundaries from surveys or derived from aerial photographs. All data are given in UTM 8N and referenced to WGS-84.

The file "Velocities.xls" contains annual and summer surface ice velocities for the entire glacier. Initial and final survey times are given for each calculated velocity. Positions are given in WGS8-84 and elevations referenced to Geoid96 (Alaska). Speeds are in m $^{a-1}$ and directions are measured from true north.

C.5.1 Continuous GPS data

The continuous GPS station "GLAC" was installed on the terminus of Mendenhall Glacier in January 2004. It collected data intermittently through May 2004. A base station "MENG" located near the USFS Mendenhall Visitor Center, across Mendenhall Lake, was simultaneously recording. Data were collected at 30 second intervals and stored in 24 hour files. A conversion script written in MATLAB® was used to chop daily files into 30 minute rinex files for processing. Differential correction was performed in Trimble Geomatics Office® using daily IGS ephemeris files. Poor baseline solutions were immediately discarded. The exported positions were then sorted in EXCEL, and additional outlying points were removed. Epoch A (see below) positions were corrected for antenna tilt as the station began to melt out of the ice. Data are exported in local time (Alaska Standard Time and Alaska Daylight Time), horizontal and vertical positions are referenced to the WGS-84 ellipsoid.

Table C.1. Different phases of continuous GPS data. The data are divided according to the status of the glacier GPS.

Epoch A	Jan 13 - Apr 10	Drilled into ice. Corrected for antenna tilt near end of epoch.
Epoch B	Apr 17 - May 1	Not drilled into ice. Elevation is affected by ablation.
Epoch C	May 5 - May 24	Drilled into ice. No antenna tilt.

C.6 Thesis

A copy of this thesis is included in PDF format.

C.7 Time-Lapse Photography

The acquisition and processing of oblique photographs from a time-lapse camera stationed on bedrock adjacent to the glacier terminus is discussed in Section 2.4.1. The reduction process will be briefly summarized here. After digitizing, each photo is individually adjusted (in Adobe Photoshop® or a similar image processing software) to a suitable brightness and contrast. It is important that both bedrock control points and the waterline at the calving front are easily discernible. (Identifiable control points located on the eastern margin of the glacier have known coordinates from DGPS surveys.) Each adjusted image is opened in SCION Image software, and a file of image coordinates is created. The digitized points include at least two control point as well as a sufficient number of points along the calving front. The waterline is chosen as a surface of known elevation, since daily lake levels are approximately known from the USGS lake gauge. MATLAB® scripts, written by Martin Truffer for photogrammetric work at LeConte Glacier, have been adapted for use at Mendenhall Glacier by Ellie Boyce. The file of image coordinates is reduced using the method described by Krimmel and Rasmussen [1986]. The output is a list of geographic coordinates for the digitized points along the terminus. Thus each daily photograph (that is of sufficient quality) can be reduced to a geographic terminus position.

C.7.1 Movies

Additionally, the digitized time-lapse images can be assembled and processed to make a movie of glacier movement and terminus change. The CD contains preliminary versions of a movie covering the spring and summer of 2004. This movie will be made available to the US Forest Service Mendenhall Glacier Visitor Center.

C.7.2 Terminus Positions 2004

This folder contains the output geographic terminus positions from February 29, 2004 through August 6, 2004. Some days are missing as low quality images were not digitized. Each file is labeled "term*mmdd*.avg," where *mm* and *dd* indicate the month and day of the image, respectively. These files are tab-delimited ASCII.

C.8 Weather Station Data

The file "TermWeather_2002-2005.xls" contains air temperature and precipitation event data from a weather station located at the terminus of Mendenhall Glacier. An hourly record air temperature exists from June 2002 - March 2003 and September 2003 - August 2005. Precipitation is recorded in 0.2 mm events from August 2003 - March 2005 and May - August 2005.

C.9 References

Krimmel, R., and L. Rasmussen (1986), Using sequential photography to estimate ice velocity at the terminus of Columbia Glacier, Alaska, Annals of Glaciology, 8, 117–123.